Aleksander Olvik Thorbergsen

In-depth assessment on the structural geological and engineering geological condition of the weakness zone at Svandalsflona HPP

Master's thesis in Geotechnology
Supervisor: Krishna Kanta Panthi
May 2019

Master's thesis

NTNU
Norwegian University of
Science and Technology

Aleksander Olvik Thorbergsen

In-depth assessment on the structural geological and engineering geological condition of the weakness zone at Svandalsflona HPP

NTNU
Norwegian University of
Science and Technology

GEOL Master Thesis
for
GeoReal student Aleksander Olvik Thorbergsen

In-depth assessment on the structural geological and engineering geological condition of the weakness zone at Svandalflona HPP

Background

Most of the waterway system in Norwegian hydropower plants consists of low-, medium-, and high-pressure headrace tunnels, high-pressure shafts, and tailrace tunnels. More than 90% of these plants were built before the 1990s and these water tunnels have been in operation at full hydrostatic pressure for over 30 years. More importantly, these tunnels are built typically in very old (older than 400 MA) hard rock consisting mostly of high quality rock mass. The design philosophy of waterway system in these plants considers the rock mass as capable of absorbing the water pressure exerted on the tunnel wall. Hence, no rock support is applied in these tunnels apart from in critical areas where fractured rock mass, faults, and weakness zones exist. In recent years, some of the high-pressure shafts and tunnels have experienced partial collapses, which forced the stoppage of the power plant and required comprehensive repair work to be carried out to bring the plant in operation once again. One such incidences took place at the Stutakvelven inclined shaft at Svandalflona Hydropower Project where the undersigned here involved in the inspection and evaluation of the collapse in 2009. A brief engineering geological conditions along the shaft and headrace tunnel and a comprehensive discussions on the chronology of the event can be found in Panthi (2014).

MSc Project Task

The FME HydroCen has among others one PhD research, which relates on the study on the effect of frequent start-stop sequences on the long-term stability of waterway system. This master thesis is also closely related to this theme of the research and will include on the study on:

- Theoretical review of the design principal of Norwegian hydropower projects
- Review on the regional structural geological conditions of the area
- Detail structural geological and engineering geological surface mapping of the project area with more focus on weakness zone area of the Stutakvelven inclined shaft
- Collect rock samples from the weakness zone area and carry out engineering geological laboratory testing at IGP.

- Present structural geological and engineering geological conditions of the project area and the weakness zone.
- Carry out stability assessment of the weakness zone area and analyse the potential reasons for the collapse.
- Discuss and conclude the work.

Relevant computer software packages

Arc GIS, rockscience package and relevant as per the need.

Background information for the study

- Relevant information about the project such as reports, maps, information received from the supervisors and data collected by the candidate from field work.
- The information and scientific papers and books provided by the supervisors.
- Scientific papers, reports and books related to rock engineering, hydropower engineering and structural geology.

Cooperating partner

Norsk Hydro Energi is the co-operating partner. PhD fellow Bibek Neupane will be co-supervisor from for this project, with whom the candidate will work very closely.

MSc thesis work starts in 5th September 2018 and should be completed by 15th May 2019.

The Norwegian University of Science and Technology (NTNU)
Department of Geology and Mineral Resources Engineering

5th September 2018

Krishna Panthi

Krishna K. Panthi
Associate Professor of geological engineering, main supervisor

Abstract

Stutakvelven inclined shaft functions as both an inlet tunnel and a pressure shaft. It is part of the Svandalsflona hydropower project which is located in an area characterised by highly deformed Caledonian thrust nappes. The shaft is intersected by a steep weakness zone. Excavating through the zone proved challenging and it was therefore constructed a rectangular cast concrete lining to secure the zone, leaving an empty space above the support roof.

In 2008, after 30 years of operation, a cave-in occurred. This was discovered by abnormal high-water level in the Stutakvelven lake and a sinkhole in the topography near the gatehouse. Further investigations confirmed that the shaft was blocked. Six month later, in an attempt to clear the slide deposits, a sudden burst flood took place killing two workers. This necessitated thorough investigations including a brief study by Panthi (2014) which is the basis for this thesis.

Stability assessments are conducted based on field investigations and rock mechanical laboratory testing. The numerical analysis indicates that the applied concrete support should have been adequate to prevent a collapse, despite the potential challenges with the empty space in the crown. Investigations of the failure indicates that insufficient lining allowed erosion of the rock mass behind the lining progressively increasing the support pressure which ultimately led to partially failed lining resulting in the cave-in. This was also indicated in the investigations post-failure.

This master thesis is a part of the ongoing FME HydroCen research project on long-term stability, including the study on the effect of water transients from frequent start-stop sequences following the change in operational regime towards demand-driven hydropower plants. In light of this, it is possible that the applied support was not dimensioned to withstand the frequent change in the water level following the increased start-stop sequences and varying production.

The case study conducted reveals commonalities between failures in weakness zones in recent time indicating insufficient rock support in these zones. This is especially true for how extensively the rock support is covering sensitive areas thereby securing contact between the

Abstract

support and the surrounding rocks of higher quality, thus, keeping water from eroding. Therefore, it should be aspired to gain more accurate knowledge on securing weakness zones.

Sammendrag

Stutakvelven er en sjakt med 45 graders helning som fungerer både som innløpstunnel og svingesjakt. Den er en del av Svandalsflona vannkraftverk som er lokalisert i et område preget av deformerte kaledonske skyvedekker. Sjakten krysses av en steil svakhetssone. Driving gjennom denne sonen viste seg å være utfordrende og det ble derfor konstruert et støp i rektangulær form for å sikre sonen, som etterlot et tomrom mellom konstruksjonen og hengen.

I 2008, etter 30 år med drift, oppstod et ras i sjakten. Dette ble oppdaget ved unormalt høy vannstand i innsjøen Stutakvelven samt ved observasjon av et synkehull i topografien nært lukehuset. Nærmere undersøkelser bekreftet at sjakten var blokkert. Seks måneder senere, under et forsøk på å rydde unna massene, oppstod et plutselig vannutløst ras som førte til at to arbeidere mistet livet. Dette nødvendiggjorde grundige undersøkelser, inkludert en undersøkelse utført av Panthi (2014) som har lagt grunnlaget for denne masteroppgaven.

Stabilitetsvurderinger er utført basert på feltundersøkelser og bergmekanisk laboratorietesting. Den numeriske analysen indikerer at den anvendte sikringen i utgangspunktet skulle være tilstrekkelig for å hindre et større ras, på tross av stabilitetsutfordringer med tomrommet i hengen. Undersøkelser av kollapsen indikerer at utilstrekkelig sikring tillot erosjon av bergmassen bak sikringsstøpet som førte til en gradvis økende belastning på sikringen. Dette førte igjen til delvis brudd i sikringsstøpet som resulterte i kollapsen. Dette ble også indikert i undersøkelsene i etterkant av raset.

Denne masteroppgaven er en del av det pågående forskningsprosjektet til FME HydroCen vedrørende langtidsstabilitet, som inkluderer forskning på effekten av vanntransienter indusert av hyppige start-stopp sekvenser etter endringen i operasjonsregime til etterspørselsstyrte vannkraftverk. I lys av dette er det mulig at sikringen ved Stutakvelven ikke var tilstrekkelig dimensjonert for å motstå hyppigere endringer i vannivået som en følge av de økte start-stop-sekvensene og varierende strømproduksjon.

Case-studiet avdekker et fellestrekk mellom flere ras i svakhetssoner i nyere tid, nemlig at disse sonene ikke er tilstrekkelig sikret. Dette gjelder særlig hvor omhyggelig sensitive soner dekkes og sikres i godt sideberg for å holde vann borte og dermed forhindre erosjon. Det bør derfor etterstrebes mer presis kunnskap om sikring av svakhetssoner med hensyn til dette.

Sammendrag

Acknowledgements

I want to thank Associate Professor Krishna Kanta Panthi for being very accommodating and inspiring during initial talks about a possible subject for my thesis. I want to thank him for good guidance during my initial master year in Trondheim with regards to selecting subjects, and for encouraging me to participate in the engineering geological advanced field and laboratory methods course during my last year, which he also lectures very well in. I want to thank him for the opportunity presented to me with this thesis, which suited my interests very well.

I want to thank PhD fellow Bibek Neupane, my co-supervisor, for constructive discussions and great teamwork during the field mapping at Stutakvelven. I want to thank Senior Engineer Gunnar Vistnes for interesting discussions and for assisting me in my work at the NTNU/SINTEF laboratory. I want to thank Norsk Hydro Energy for presenting this master's thesis and sharing information regarding the Stutakvelven case.

I also want to thank my friends and close family for discussions and support during my studies.

Above all, I want to thank my dearest Synne for the love and huge support during my studies and writing. You gave me motivation when I needed it most, and you endured my absence when I had to stay in Trondheim. Our discussions throughout my studies has undoubtedly made me a better geologist, and it has made you what I love to call a mini-geologist. I am deeply thankful to have you in my life, by my side.

Lastly, I want to thank our dearest knøtty (tiny) for introducing me to a new deadline, and thriving my work forwards – I greet you, my son, welcome to this world, and I expect to meet you for the first time 15 May 2019.

With love,

Aleksander Olvik Thorbergsen

Trondheim, 14 May 2019

Acknowledgements

Table of contents

Table of contents

Table of contents

Table of contents

1 Introduction

1.1 Background

In 2008, a cave-in occurred in Stutakvelven inclined shaft at Svandalsflona hydropower project (HPP) followed by a sudden burst flood in 2009 killing two people. This thesis is an in-depth assessment on the structural geological and engineering geological condition of the weakness zone intersecting the shaft, with the purpose of analysing the cave-in.

In Norway there exist more than 4000 km unlined hydropower tunnels and 200 underground powerhouses (Broch, 2016). The Norwegian reservoir capacity constitutes almost 50 percent of the European marked (Bråtveit et al., 2016). Generally, favourable rock conditions in Norway have led to a design philosophy which utilises the rocks without any support, however, weakness zones can lead to severe stability problems. In addition, over the last decades the hydroelectrical power production has changed towards a dynamic operation controlled by the demands of the marked. This has led to frequent start-stop sequences which may have an influence on the long-term stability of the rock mass.

FME HydroCen has an ongoing research project on the long-term stability with respect to the dynamic operational regime. This thesis is a part of this research, focusing on the case of Stutakvelven inclined shaft.

A brief engineering geological review on the failure at Stutakvelven inclined shaft is carried out in Panthi (2014) and is the basis for the assessments in this thesis. To aid in the understanding of the failure in the shaft a theoretical review of Norwegian hydropower design principals is carried out as well as a case study of similar failures, followed by a regional structural geological study. The stability assessments carried out are based on engineering geological field investigations as well as rock mechanical and rock engineering laboratory testing of collected field samples. Finally, potential reasons for the collapse are discussed.

1.2 Project task

The project tasks are defined by main supervisor Dr. Krishna Kanta Panthi as follows:

- Theoretical review of the design principal of Norwegian hydropower projects
- Review on the regional structural geological conditions of the area

- Detailed structural geological and engineering geological surface mapping of the project area with more focus on the weakness zone area of Stutakvelven inclined shaft
- Collect rock samples from the weakness zone area and carry out engineering geological laboratory testing at IGP
- Present structural geological and engineering geological conditions of the project area and the weakness zone
- Carry out stability assessments of the weakness zone area and analyse the potential reasons for the collapse
- Discuss and conclude the work

1.3 Limitations

Keeping in mind the comprehensive nature of investigating a failure in rock mass, the master thesis has naturally been limited by the scope of the thesis and the time available, in particular the time before and in the field. A further limitation is that the shaft was unavailable for investigations. In addition, it is a recognition that this kind of investigations requires a considerable engineering geological experience to understand and evaluate all factors of significance. Lastly, it is very limited knowledge available regarding the in-situ rock stresses.

The topics of fluid mechanics and material weakening in concrete and steel are omitted from the thesis.

2 Norwegian hydropower design principles

2.1 Development of Norwegian hydropower

The Stutakvelven inclined shaft is part of Svandalsflona hydropower scheme built in late 1970, and functions as both an inlet tunnel and a surge shaft. Understanding its function and design is an important basis for the stability assessments carried out in this thesis. In Norway, the principles of hydropower tunnelling has developed over the last century based on more than 4000 km unlined tunnels and 200 underground powerhouses (Broch, 2016).
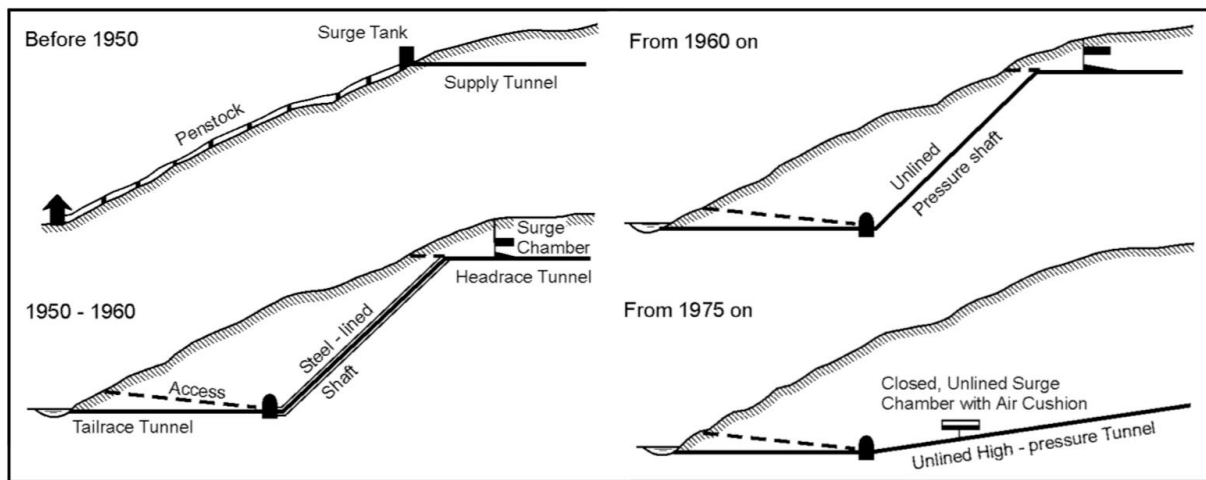
Figure 1. The general development of Norwegian hydropower design principles (Palmstrøm and Broch, 2017).

Figure 1 found in Palmstrøm and Broch (2017) illustrates the development of Norwegian hydropower design principles. Before 1950 the conventional building design was a surface powerhouse and steel-penstock. In the 1950s the hydropower constructions were placed underground normally with a steel-lined shaft. The 1960s represents a change in the design philosophy where unlined tunnels were utilised and became the conventional design. In the 1970s the simple calculation method called "rule-of-thumb" was introduced, based on that the rock overburden should be significant enough to induce rock stresses counteracting the water pressure in tunnels. The rule-of-thumb were updated after some cases of instability, and a new rule-of-thumb was presented. Despite of this, the criterion still has its weaknesses, and is today only used as a quick preliminary design estimate. One of the weaknesses is that the criterion does not account for low rock stresses. From 1975 and onwards the preferred design is unlined high-pressure tunnels with a closed surge chamber with air cushion to reduce water hammer (Nilsen and Thidemann, 1993). As an alternative to the surge chamber, surge shafts may be

used, such as the Stutakvelven shaft. Also, computerised methods have been developed since the 1970s regarding rock stresses and have been of significant help in planning. The general idea is that the water pressure nowhere in the tunnel shall overstep the rock stresses causing leakage and instability. Today the common practice is to conduct in-situ stress measurements since analytical methods of estimating rock stress often deviates from the actual rock stresses (Palmstrøm and Broch, 2017).

The modern design philosophy in hydropower rock engineering is to take advantage of the bearing capacity of the rock mass itself (Nilsen and Thidemann, 1993). This design principle is possible because of the generally favourable geology in Norway, and because the design allows some block fall in the head- and tailrace tunnel (Panthi, 2014). This design improves cost-efficiency and reduces building time.

2.2 Functions and challenges of the modern design

According to Palmstrøm and Broch (2017), the two main challenges of building hydropower tunnels are hydro-jacking and collapses blocking the water flow. Hydro-jacking may occur if the hydrostatic pressure oversteps the minor principle stress acting on a discontinuity causing instability. A method for avoiding hydro-jacking is to build the access tunnel first, and at arrival of the planned location of the power house, hydraulic splitting is conducted with a pressure overstepping the calculated hydrostatic pressure (with a safety margin). If jacking occurs in existing discontinuities, the location must be moved deeper into the mountain where the confining pressure is sufficient. It is important to conduct the testing in three directions normal on each other in order to test all possible discontinuities. The critical point for unlined hydropower tunnels is where the hydrostatic pressure is at its largest, normally where the tunnel ends upstream the powerhouse or where the penstock starts. Alternatively to the hydraulic splitting, rock stress measurements may be conducted (Palmstrøm and Broch, 2017).

In Norway, the production pattern of hydroelectrical energy has changed in the last decades (Neupane and Panthi, 2018). The production pattern is driven by demand in the marked, meaning, a high production at high energy prices, and low production at low energy prices. As a consequence, the start-stop sequences and varying load of the hydropower plants has significantly increased leading to changes in the water flow. This causes a pressure change in the water which propagates as a pressure wave upstream the turbine towards the nearest free

surface where it reflects back towards the turbine. The amplitude of the pressure wave is mainly dependent on the tunnel length and the closing or opening time of the valve at the powerhouse. The magnitude of this wave can cause serious damage to both the tunnel and the turbine. Normally, it is not possible to always keep a certain closing or opening rate, thus, shortening the length between the nearest free surface and the turbine is the only viable option. This is achieved by using surge tanks such as closed air chambers and shafts with open surface to the atmosphere, illustrated in Figure 2 (Chaudhry, 1979).

This pressure wave which travels back and forth between the turbine and the nearest free surface, is a rapid transient known as water hammer. When implementing two free surfaces in the system, another phenomenon known as slow transients or mass oscillation occurs between these two free surfaces due to the inertia of the moving water during change in the flow rate. This means, for instance, when stopping the production, a rise of the water level occurs in the surge tank until the kinetic energy is transformed to potential followed by a backwards movement of the water from the surge tank to the reservoir. The water level in the surge tank is dependent on the water level in the reservoir, and the change in water level due to mass oscillation is dependent on the load variation. The upsurge and down surge water level in the surge tank can vary greatly since the water surface in the surge tank is significantly lesser than in the reservoir (Chaudhry, 1979).
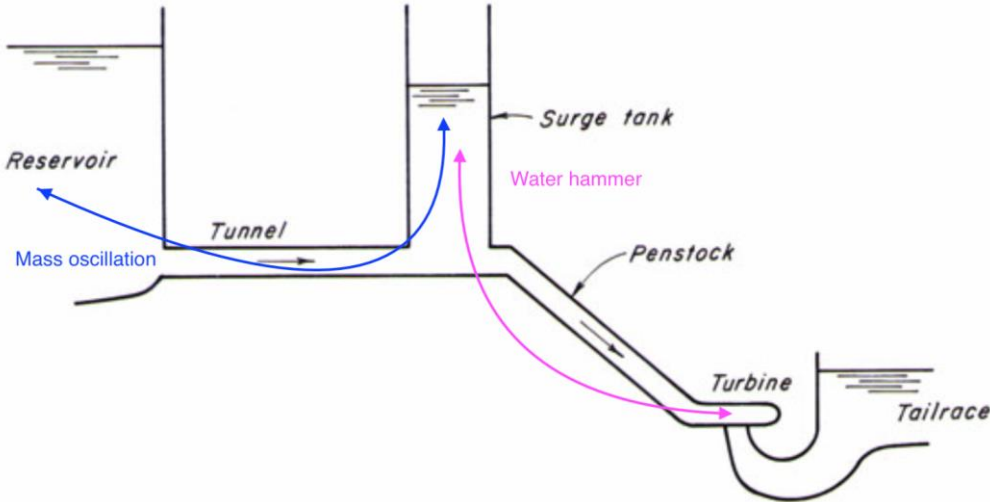
Figure 2. Illustration of a set-up using surge tank with water transients indicated. Figure modified from Chaudhry (1979).

The increase in frequent start-stop sequences and in the load variation (flow rate) increases the occurrence of water hammer and mass oscillation in hydropower waterway systems (Neupane and Panthi, 2018).

2.3 Case study

2.3.1 Rock fall and cave-ins in Norwegian hydropower tunnels

Palmstrøm (2003) has reviewed the study from 1991 by Bruland and Thidemann of rock fall and cave-ins in Norwegian hydropower tunnels. Bruland and Thidemann inspected 330 km tunnels at 29 hydropower projects which had been operational for 5 to 70 years. The cross-section of the tunnels varied from 6 m^2 to 70 m^2. Two main conclusions can be highlighted, firstly that most of the tunnels were without noticeable rock fall when excluding blocks smaller than 50 dm^3, and secondly that most of the cases of instability are related to weakness zones. Bråtveit et al referred in Neupane and Panthi (2018) has found that tunnels subjected to frequent start-stop-sequences have an increase in rock fall of 3 to 4 times compared to the study of Bruland and Thidemann.

Bruland and Thidemann (1991) found that the number of rock slides in Norwegian hydropower tunnels with significant impact on the operation was 6 fully blocked and 2 nearly blocked. Despite that the inspection was based on 330 km tunnel, the authors states that findings of these blockings should be related to the entire Norwegian hydropower tunnels of 3300 km because that the inspection were also based on reports from all of the Norwegian tunnels at that time. Most of these blockages were caused by swelling clay and occurred equally in unlined areas and areas mainly supported with only shotcrete. Aagaard referred in Brende et al. (2018) described in 2005 six blockages in addition to the ones described by Bruland and Thidemann.

Bruland and Thidemann (1991) also studied the rock support used and the condition of these. In the inspected tunnels it was found 76 occasions of damaged support mostly due to bad execution. Of these 17 were related to casted concrete.

The study shows that the rock falls and slides are predominantly time-independent in the way that the amount of rock falls and slides is the same either the inspection takes place shortly after the start-up or after several years of operation. From this the authors conclude that the rock falls and slides occurs at start-up in relation to water-filling of the tunnels, since the water affects

the rock mass properties (Bruland and Thidemann, 1991). This coincides well with the occurrence of swelling clay in most of the tunnels, since swelling clay reacts in contact with water.

Two exceptions from this are highlighted, namely zones of joint infill material which over time dissolves and washes out, and areas where the support safety margins are low and weakens over time. Examples of the latter are too low-density bolting, too short section of cast concrete and bad execution of the initially adequate support.

The cases presented in **Feil! Fant ikke referansekilden.** are based on the study conducted by Palmstrøm (2003) on instability cases in tunnels, and are complemented with examples from Palmstrøm (2018) and Brende et al. (2018). Some of the instability-cases presented in **Feil! Fant ikke referansekilden.** are briefly elaborated on in the following in an attempt to reveal commonalities between these cases and the case of Stutakvelven.

Table 1. This table is based on the cases presented in Palmstrøm (2003), Brende et al. (2018) and examples from Palmstrøm (2018).

HPP	Description (year)	Time after filling	Cause
Matre Haugsdal	Slide (2017)	6 months	Swelling clay in weakness zone
Nedre Vinstra	Large slide (2015), large slide (1991)	25 years, 2 years	Weakness zone in 2015. Gradually outwash in 1991 in unsupported parts
Trollheimen	Large slide (2000)	35 years	Jointed rock with infill. Sink-hole at terrain topography
Mauranger	Large slide (2000)	25 years	Clay-rich weakness zone secured with a too short section of cast concrete
Songa	Slide (1999)	25 years	Weakness zone
Sundsbarm	Large slide (1995)	24 years	Clay-rich weakness zone secured with a too short section of cast concrete

2.3.2 Matre Haugsdal HPP

Matre Haugsdal hydropower plant is located in Hordaland county, and was operational in 2016 after a major renewal. The powerplant has averagely produced 637 GWh annually with a

capacity of 180 MW, and utilises a gross head of approximately 529 m (NVE, Undated). In 2017, after six months of operation a slide took place in the headrace tunnel forcing a shutdown of the powerplant to prevent damages to the turbines (Brende et al., 2018). This slide was estimated to 20-30 m^3 and occurred in a weakness zone supported with reinforced ribs of sprayed concrete. Sampling and testing of the weakness zone material indicated an active swelling material (0,7 MPa), identified as montmorillonite. After excavation and installation of the rock support the situation was considered stable. The problem first arose when water entered the system. This water in contact with clay caused stability problems and led to swelling and increase of support pressure. This caused the reinforced ribs of sprayed concrete to fail, as shown in Figure 3. The authors (Brende et al., 2018) states that this case illustrates the limitations of reinforced ribs, as this support is not as strong as the more heavy-duty cast concrete constructions. The cost for the repair is estimated to 40 million NOK (2017).

Figure 3. Failure of the reinforced ribs of sprayed concrete and slide in the Matre Haugsdal tunnel in 2017 Brende et al. (2018).

2.3.3 Nedre Vinstra HPP

Nedre Vinstra HPP is located in Oppland county and was operational in 1953. The powerplant has averagely produced 1264 GWh annually with a capacity of 308 MW, and utilises a gross

head of 443 m (NVE, Undated). In 1991, a cave-in in a two-year-old pressure shaft occurred and blocked the headrace tunnel. The volume of the deposits was estimated to 7000-10 000 m^3 including blocks of 6-7 tons. This cave-in occurred most likely due to gradually outwash in the invert and lower part of the walls. During construction the roof and walls were supported with rock bolts and shotcrete before removing the blasted muck used on the construction road. This led to the invert and lower part of the walls being left unsupported. The development of the cave-in is illustrated on Figure 4 (Palmstrøm, 2018).

This collapse caused 3 ½ months of continuously tunnel-work, as it was necessary to excavate a bypass-tunnel through the weakness zone. This new tunnel was secured with reinforced ribs of sprayed concrete and 50 cm cast concrete in the invert.
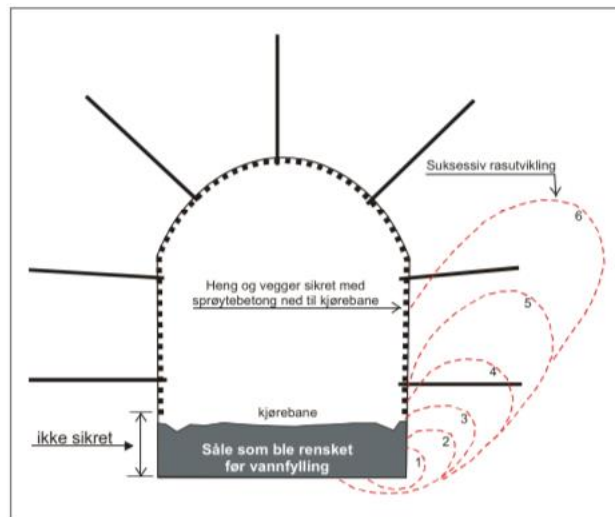
Figure 4. Illustration of the development of the cave-in in 1991 at Nedre Vinstra HPP. This could most likely occur due to the unlined invert and lower part of the walls (Palmstrøm, 2018).

Nedre Vinstra HPP was once again hit by a serious cave-in of almost 2500 m^3 as late as in 2015, referred to in Brende et al. (2018) as one of the most known cave-in related to hydropower in recent times. The cave-in occurred in relation to a weakness zone and had similarities to the cave-in at Matre Haugsdal HPP.

2.3.4 Trollheim HPP

Trollheim HPP is located in Møre og Romsdal county and was operational in 1968. The powerplant has averagely produced 893 GWh annually with a capacity of 127 MW, and utilises a gross head of 400 m (NVE, Undated). In 2000, a sink hole in the topography was discovered

after 35 years of operation. This was caused by a cave-in which filled the tunnel with deposits of more than 300 m Figure 5. The geology consists of mica schist and mica gneiss with several distinct joint sets. At the cave-in, a 40-50 cm thick inclined clay zone above the tunnel was observed. This zone was commented by workers during construction, noting that minor rock falls occurred. The tunnel was left unsupported allowing the cave-in to gradually develop (Palmstrøm, 2018).
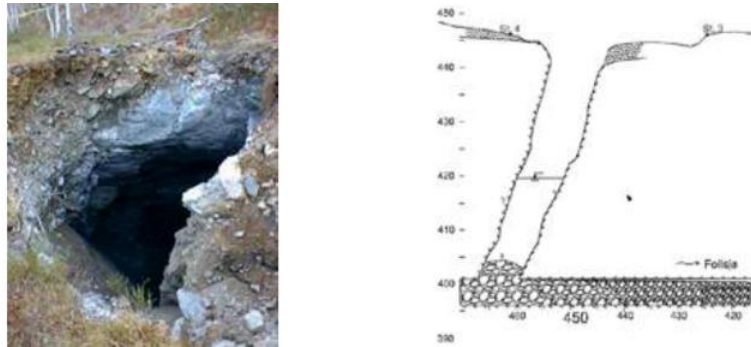
Figure 5.The cave-in at Trollheim HPP where a sink hole appeared at the surface (Palmstrøm, 2018).

2.3.5 Mauranger HPP

Mauranger HPP is located in Hordaland county and was operational in 1974. The powerplant has averagely produced 1146 GWh annually with a capacity of 250 MW, and utilises a gross head of 830 m (NVE, Undated).
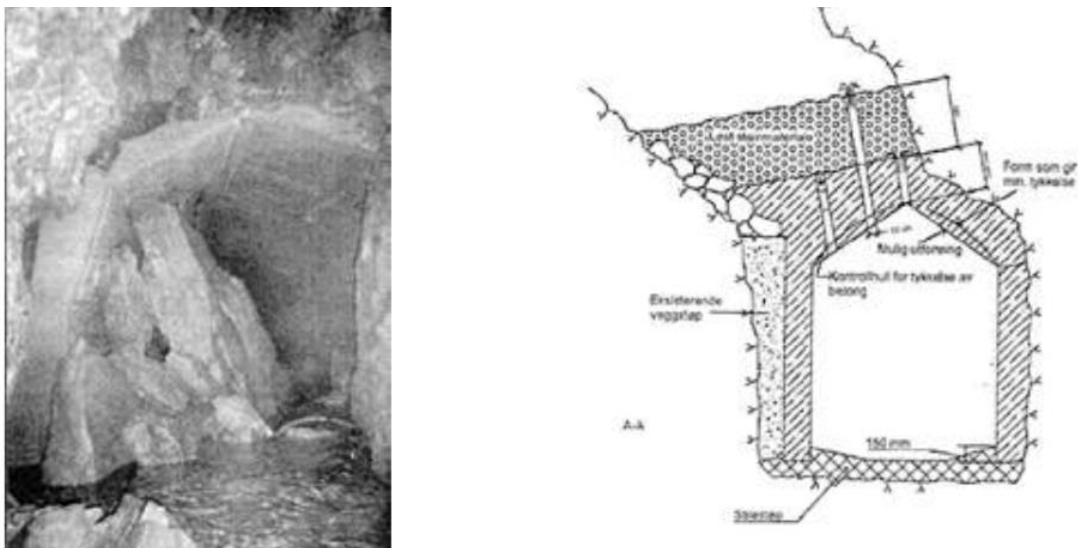
Figure 6. The cave-in at Mauranger HPP with old failed concrete support. Here it was constructed a new support with dampening masses on the roof of the support construction (Palmstrøm, 2018).

In a transfer tunnel, a cave-in occurred caused by failed cast concrete lining. Figure 6 shows the old concrete, which was used again during the new support design. It was discovered that the weakness zone was not entirely covered by the old cast concrete which consequently led to the development of the cave-in near and over the cast concrete support (Palmstrøm, 2018).

2.3.6 Final remarks on the cases

The case study shows commonalities between the different collapses. Firstly, most of the cases have occurred after several years of operation, and all of the cases are in relation to weakness zones. The general impression is that major cave-ins occur where lining is executed insufficiently in either length or quality. In both Mauranger, Sundsbarm and Nedre Vinstra (1991), the cave-ins were due to the rock support not covering the crucial areas of sensitive rock mass. The water undoubtedly played an important role as triggering factor, since in most of the cases clay or swelling clay were present. Lastly, it is important to emphasise that all the slides causing cave-ins have led to significant repair cost and income losses.

3 Rock mass properties and considerations

3.1 Introduction

Rock engineering is about building in rock masses. Understanding the building material is essential for every underground project. Rock samples can be brought from the field and tested in a laboratory for properties such as deformability and rock strength. However, a rock sample does not reflect the rock mass with all its variations and the stability condition. It is therefore important to consider the in-situ rock mass which consist of intact rock, joints and all other discontinuities (Nilsen and Thidemann, 1993).

Panthi (2006) defines underground stability as a function of rock mass quality and mechanical processes acting on the rock mass. The rock mass quality is characterised by the rock mass strength, rock mass deformability, rock mass anisotropy, discontinuities, weathering and alternation. The mechanical processes acting on the rock mass are linked to rock stresses and ground water. In addition, the stability is affected by the orientation of the underground cavern or tunnel with respect to the in-situ geology (Panthi, 2006).

The intention of this chapter is to elaborate on the theoretical principals of rock properties and rock behaviour.

3.2 Rock mass strength

3.2.1 Strength of intact rock specimen

The rock mass strength is defined by Panthi (2006) as the ability of the rock mass to withstand stress and deformation. The intact rock strength is commonly obtained by uniaxial compressive strength (UCS) test (Nilsen and Thidemann, 1993). This is typically done by applying axial load on a cylindrical test specimen in a stiff hydraulic testing machine until failure occurs in the specimen. The intact rock strength (σ_{ci}) of the specimen is considered in terms of stress applied on the sample, where stress is defined by the maximum possible applied load (P) on the test specimen's cross-section (A).

$$\sigma_{ci} = \frac{P}{A}$$

Rock mass properties and considerations

By measuring the inflicted load and the axial shortening of the specimen, a stress-strain curve can be obtained (Figure 7). The axial strain (ϵ_z) is defined by the change in the length of the specimen (Δl) divided by its initial length (l) (Li, 2018).

$$\epsilon_z = \frac{\Delta l}{l}$$

From the stress-strain curve, rock properties such as the peak-strength (σ_{ci}), intact deformation modulus (E_i) and post-failure behaviour can be determined (Hudson and Harrison, 2000).
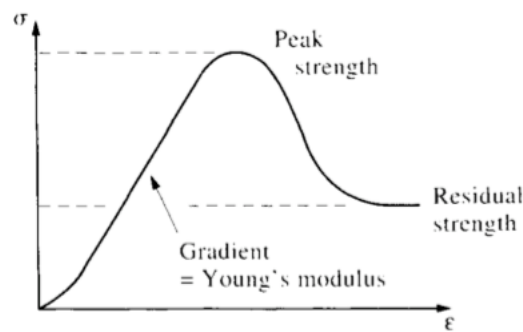
Figure 7. Stress-strain curve obtained by measuring the axial stress (σ) and the axial strain (ε) in uniaxial compressive testing (Hudson and Harrison, 2000).

The peak-strength is normally given in megapascal (MPa). Rocks usually have UCS in the range of just a few to well above 200 MPa (Nilsen and Thidemann, 1993). The deformation modulus, also known as Youngs modulus (E_{ci} for intact rocks, E_m for rock mass), is defined by the ratio of stress (σ) to strain (ε), which reflects the stiffness of the test specimen. A high E-value reflects a stiff rock sample.

$$E = \sigma / \varepsilon$$

In addition, by measuring the diametric strain (ε_x) , the Poisson's ratio (ν) may be calculated from the slope of the diametric stress-strain curve divided on the slope of the axial stress-strain curve, in the elastic regions of both curves, normally at 50 percent of the peak strength (Hudson and Harrison, 2000, Bieniawski and Bernede, 1979). The Poisson's ratio of rock samples is the constant for the elastic behaviour describing the radial expansion, that is, expansion perpendicular to the load, due to the axial loading for cylindrical test specimen. As the radial

Rock mass properties and considerations

(diametric) strain is considered negative, a negative sign is used to make the Poisson's expression positive (Li, 2018).

$$\nu = -\frac{\varepsilon_x}{\varepsilon_z}$$

Other methods for measuring the UCS is the triaxial compressive strength test and the point-load test.

The intact rock strength of rock samples is dependent on the diameter (*d*) of the specimen. Hoek and Brown (1997) defines the uniaxial compressive strength by the strength of 50 mm cores (σ_{50} or σ_{ci}) and have therefore suggested a correlation formula for cores of varying diameters (σ_{cd}). This equation (*Eq. 1*) shows that in samples smaller than 50 mm, the strength is overestimated and therefore reduced, and that in samples larger than 50 mm, the strength is underestimated and therefore increased. Hoek and Brown (1997) explains this by that a larger sample includes more grains which increases the possibility of failure, as the failure occurs through and around grains. However, this is only valid to a certain point where the strength becomes constant.

This correlation is useful since empirical formulas are based on the strength of 50 mm cores (Panthi, 2006):

$$\sigma_{cd} = \sigma_{c50} \left(\frac{50}{d}\right)^{0.18} \hspace{3cm} \textit{Eq. 1}$$

3.2.2 Correlation of intact rock strength and rock mass strength

The rock mass strength with its intact rock, joints and other discontinuities is difficult to measure directly in the field and by laboratory methods. This has led to the suggestion of a numerous empirical relationships for estimating the rock mass strength (Panthi, 2006). The Hoek-Brown relation and the Q-value correlation are presented in Table 2, in addition to an empirical relationship suggested by Panthi (2006). These equations should be used as an approximation for weaker, schistose rocks. For more solid, crystalline rocks, a reduction in the range of 50 percent of the intact rock strength is suitable for estimation of the rock mass strength (Panthi, 2006). However, this correlation is simplified by utilizing rock mass classification systems such as the GSI, discussed in section 3.7. These equations are used for comparative purposes.

Rock mass properties and considerations

Table 2. Empirical formulas for estimating the rock mass strength found in Panthi (2006).

Author	Empirical equation
Panthi (2006)	$$\sigma_{cm} = \frac{\sigma_{ci}^{1.50}}{60}$$
Barton (2002)	$$\sigma_{cm} = 5\gamma \times Q_c^{\frac{1}{3}}$$ $$where \; Q_c = \left(\frac{\sigma_{ci}}{100} \times Q\right) \; and \; \gamma = t/m^3$$
Hoek (2000)	$$\sigma_{cm} = \sigma_{ci} \times s^a$$ $$where \; s = \left[exp\left(\frac{GSI-100}{9-3D}\right)\right] \; and \; a = \frac{1}{2} + \frac{1}{6}(e^{-GSI/15} - e^{-20/3}$$

3.2.3 Strength anisotropy

In general, rocks are anisotropic, especially sedimentary and metamorphic rocks, but also crystalline rocks that appear homogeneous have anisotropic properties (Broch, 1983). Thus, the measurable properties within a rock or a rock mass vary with respect to direction. This is explained by several reasons such as difference in mineral sizes and composition and discontinuities in the rock masses. The grade of anisotropy also varies within inhomogeneous rock masses (Hudson and Harrison, 2000).

Panthi (2006) found that phyllites, slates and schists had a significant strength anisotropy, that is, a large difference in the lowest and highest measured strength. The weakest loading direction was found to be approximately 30 degrees to the schistosity planes, and the strongest loading direction perpendicular to the schistosity planes. Thus, to obtain the weakest direction in UCS test, the test cores must be drilled approximately at 30 degrees oblique on the weakness/schistosity plane.

To establish the strength anisotropy, the point load test is a superior way compared to the directional uniaxial compressive strength test with respect to both preparation, requirements and testing procedures. The point load test may be conducted on all sorts of specimens, such as irregular ones as well as cylindrical cores drilled normal and perpendicular to the schistosity planes. In general, rocks have the lowest tensile strength parallel to the weakness planes (i.e. foliation, bedding, schistosity planes), and the highest strength normal to the weakness planes (Broch, 1983).

Rock mass properties and considerations

The International Society of Rock Mechanics (ISRM, 1985) has suggested a method for determining the strength anisotropy by using the Point Load Strength Anisotropy Index (I_a). The Index is based on the Point Load Strength Index (I_s) of cores with 50 mm ($I_{s(50)}$). The I_a is the ratio between the highest and the lowest mean values obtained from the point load test. Based on the I_a and the foliation index after Tsidzi referred in Panthi (2006) the rocks can be classified according to Table 3.

Table 3. Classification of rock strength anisotropy after Panthi (2006) and Tsidzi and Palmstrøm referred in Panthi (2006).

Class	Descriptive class	Strength anisotropy index (I_a)	Typical rock types
I	Isotropic or close to isotropic	1.0 – 1.2	*Most of igneous rocks and very high-grade metamorphic rocks, i.e. diorite, granite, gabbro, quartzite granitic gneiss, granulite etc.).* Rocks with < 10 % platy/prismatic minerals, randomly oriented.
II	Slightly anisotropic	1.2 – 1.5	*High-grade metamorphic rocks and some strong sedimentary rocks, i.e. quartz-feldspatic gneiss, marble, migmatite, sandstone etc.* Rocks with 10-20 % platy/prismatic minerals in compositional layering.
III	Moderately anisotropic	1.5 – 2.5	*Medium- to high-grade metamorphic rocks, i.e. mica gneiss, quartzitic schist, mica schist, biotite schist etc.* Rocks with 20-40 % platy/prismatic minerals with distinctly visible foliation planes
IV	Highly anisotropic	2.5 – 4.0	*Low to medium-grade metamorphic rocks i.e. phyllite, silty slate etc.*
V	Extremely anisotropic	> 4.0	*Low-grade metamorphic and argillaceous sedimentary rock, i.e. slate, carbonaceous phyllite, shale etc.*

3.2.4 The influence of physical properties

The physical properties of intact rock have a direct impact on the rock mass strength (σ_{cm}). In addition to the influence from anisotropy and inhomogeneity, factors such as density, porosity and wave velocity affect the rock mass strength. Rocks normally have a density in the range of 2.5 and 3.2 g/cm^3, where the upper values consist of magmatic rocks such as gabbros and basalts, and the lower values consist of porous sandstones (Nilsen and Thidemann, 1993). The density and porosity often correlates in rocks, and presence of pores influences the strength negatively and enhances the deformability (ISRM, 1979). Rock strength reduces when the

specimens are saturated, even old, crystalline rocks with effective porosity below 1 percent had a significant strength reduction when saturated (Nilsen and Thidemann, 1993). Hence, the laboratory testing of rock specimen should be conducted saturated. The wave velocity gives general information about the rock quality. Measuring primary waves is quick and easy, and the test is non-destructive. This allows for the wave velocity tests to be conducted before conducting other destructive strength tests on the same cores. The P-wave velocities are typically in the range of 5-6 km/s for low porous, saturated, crystalline rocks, and in the range of 2-3 km/s for porous sandstones. The wave velocity is highly affected by the water saturation. For instance, the velocity almost doubles when samples of marble changes from dry to fully saturated condition (Nilsen and Thidemann, 1993).

3.3 Rock mass deformability

Deformation modulus (E_m) is the relation between applied load and the resulting strain in a rock mass. For rock mass, the deformation modulus includes both the elastic and non-elastic behaviour, in contradict to the deformation for intact rock specimens which is normally calculated from the elastic behaviour. The deformation modulus is one of the most representative parameters for the mechanical behaviour of rock mass (Palmstrøm and Singh, 2001).

Conducting in-situ measurements of the deformation modulus is a comprehensive process that gives results with large variations, even under optimal test conditions. Therefore, empirical solutions may be as good as or better than in-situ tests for estimating deformation modulus (Palmstrøm and Singh, 2001). Suggested empirical equations for predicting the deformation modulus are presented in Table 4. These equations assume isotropic rock mass behaviour (Hoek and Diederichs, 2006).

Table 4. Empirical relations for rock mass deformability (Palmstrøm and Singh, 2001, Panthi, 2006).

Author	Empirical formula	Applicability
Hoek and Diederichs (2006)	$E_{rm} = E_i \left(0.02 + \dfrac{1 - D/2}{1 + e^{((60+15D-GSI)/11)}} \right)$	Isotropic rock mass
Panthi (2006)	$E_m = \dfrac{1}{60} \times E_{ci} \times \sigma_{ci}^{0.5}$	Low UCS

Rock mass properties and considerations

To simplify the estimation of rock mass deformation modulus, Panthi (2006) suggested an equation which links the elastic modulus (E_{ci}) of intact rock samples to the rock mass deformation modulus (E_m). The elastic modulus (E_{ci}) is normally obtained simultaneously as the uniaxial compressive strength (σ_{ci}), and since the empirical formulas for estimating the deformation modulus are often based on surface investigations, which can deviate from the actual underground conditions, a formula of this kind has its advantages. The equation proposed by Panthi (2006) is best suited for weaker anisotropic rocks with low UCS. For massive, sound rocks, Palmstrøm and Singh (2001) suggest a reduction in the elastic modulus (E_{ci}) by 50 percent to obtain an estimate of the rock mass deformation modulus (E_m).

3.4 Discontinuities in rock mass

Discontinuity is the general term for rock mass with low or no tensile strength (Nilsen et al., 2000). The most common discontinuities are joints and weakness zones, both normally caused by tectonic activity. Discontinuities, and weakness zones in particular, may have a severe impact on the safety aspect and the economic aspect of tunnelling. Therefore, weakness zones are necessary to investigate closely (Palmstrøm and Berthelsen, 1988).

Weakness zones can often be seen as lineaments or depressions in the terrain. The type of weakness zones can generally be categorised as either crushed zones caused by faulting or other tectonic activity, or continuous areas of particularly weak rock (Nilsen and Thidemann, 1993). Anderson, referred in Panthi (2006), has suggested three fault regimes based on the principal stresses, namely normal faults, reverse- or thrust faults, and strike-slip faults Figure 8.

(a) Strike-slip Fault   (b) Normal Fault   (c) Reverse or thrust Fault
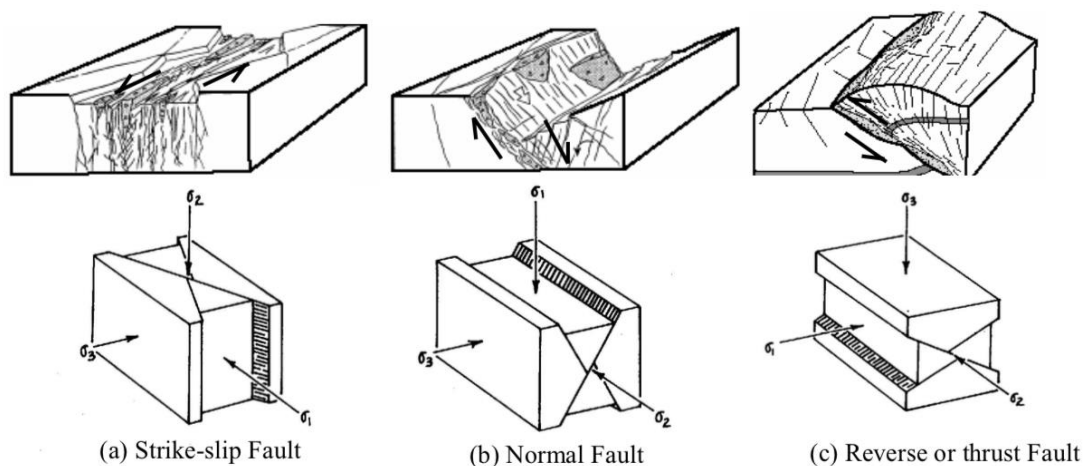
Figure 8. Anderson fault theory on strike-slip fault, normal fault and reverse or thrust fault, from Panthi (2006).

Rock mass properties and considerations

In general, weakness zones due to tectonic activity occur as planar planes into the rock mass, although thrust faults deviate from this behaviour and is difficult to extrapolate into the underground (Nilsen and Broch, 2016). The mechanical properties in weakness zones are significantly reduced and the bedrock and crushed material are therefore easily eroded away, leaving a depression in the ground. In Scandinavia, these lineaments are clearly seen, as a result of glacial erosion. This glacial activity has made it possible to see lineaments on aerial photos and to produce geological maps of possible weakness zones. Weakness zones due to faulting or tectonic activity are by Nilsen et al. (2000) divided into three parts, namely central part, transition zone and surrounding rock mass. The central part is where most of the movement has occurred, and the rocks are highly deformed or crushed. The transition zone is characterised by rock mass disturbed by movement, and the zone is clearly jointed and affected by deformation. The third zone is the almost unaffected surrounding rock mass which may consist of minor faults.

Joints can be defined as "... a discontinuity plane of natural origin along which there has been no visible displacement" (Nilsen et al., 2000). Joints are typically characterised by their orientation, spacing, persistence, aperture and roughness (Nilsen and Thidemann, 1993). In addition, when assessing joints, the weathering and alternation should be considered, for example by using the Q-system. Joints can occur random, but they often form sets where the joints are parallel to each other. Several sets constitute joint patterns, and these patterns may cause instability by forming structures that can affect the stability, such as blocks and wedges.

In Norway, rocks are normally hard and strong, and the stability is often controlled by jointing (Nilsen and Thidemann, 1993). The joint stability is controlled by its shear strength which is difficult and expensive to measure in-situ, however, decent approximation can be obtained by utilizing for instance the Q-system (NGI, 2015). Joints consist of two joints walls. If shear movement occurs, the friction is dependent on whether there is rock contact or not, the waviness of the joint walls and the amount and thickness of joint infill. During shear movement, the shear strength of the joints is also dependent on the intact rock strength, thus, dependent on if the rock breaks during rock contact or if dilation must occur for the shear movement to proceed. The rock wall strength can be considered using methods such as the Schmidt hammer, which however, is not considered in this thesis (Panthi, 2006).

Joints are typically spaced in the order of less than one metre, while faults extend in the order of hundreds of metres to kilometres (Nilsen and Thidemann, 1993).

3.5 Ground water influence and weathering

Scandinavian sound and solid rocks have low or non-permeability, making the water-flow controlled by jointing. The hydraulic conductivity of a single joint can be understood from the Louise-equation referred in (Nilsen and Thidemann, 1993). This equation shows that the flow rate increases eight times if the aperture doubles, thus, the aperture of joints has a significantly impact on the flow rate. However, this equation is only valid for a single planar joint plane where laminar flow occurs. In nature, the flow is dependent on the communication of several interlinked joint planes, and the flow is hindered by joint infill and joint plane surfaces of different characteristics (undulating, rough etc.). This means that estimating the flow rate in-theory is difficult, hence, several methods for measuring the flow has been developed, such as the Lugeon leakage test and water inflow registration. A study on Swedish Precambrian rocks shows that the hydraulic conductivity decreases with depth Figure 9. This is mainly due to increasing confining pressure and less frequent occurring joints (Nilsen and Thidemann, 1993).
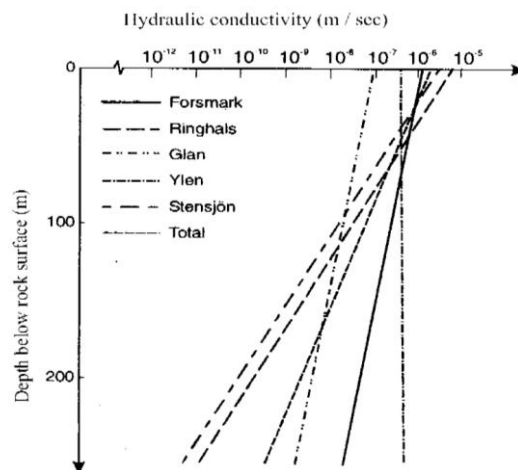
Figure 9. Hydraulic conductivity in Swedish Precambrian rocks (Carlsson & Olsson in Panthi (2006)).

The stability problems caused by water inflow are summarised by Nilsen and Thidemann (1993), and include, among others, the reduction of the stability in weakness zones due to wash-out and dissolution, strength reduction and accelerating weathering of the rocks, stability problems due to freezing water and high water pressure.

Weathering of rocks occurs as mechanical disintegration and chemical decomposition. Mechanical breakdown causes opening of joints, occurrence of new joints and fracturing of individual mineral grains. In cold climates, frost shattering breaks down rocks by expanding water inside cracks, joints and other discontinuities. The chemical decomposition breaks down rock mass by dissolution of minerals, leading to transport of ions and formation of new clay minerals. Weathering is seen as discolouration of the rock and occurs at the surface, as well as at depth in existing joints and discontinuities (Nilsen and Thidemann, 1993). Ultimately, rock disintegrates into soil losing all or almost all its strength (Panthi, 2006) as seen in Figure 10.
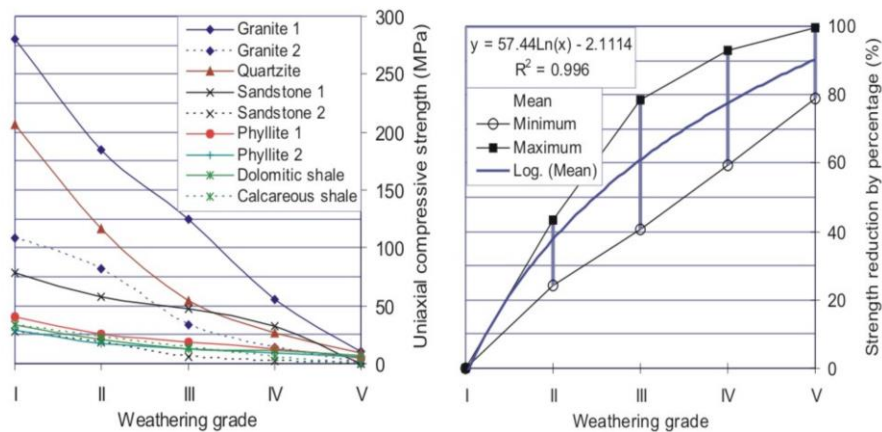
Figure 10. Weakening of rock due to weathering (Panthi, 2006).

3.6 Rock stresses

Rock stresses are one of the factors causing problems in hard rock tunnelling in Scandinavia, in addition to discontinuities and water inflow. Rock stresses are characterised by their direction and magnitude, and occur due to gravitational forces, plate tectonics, topographic variations and magma cooling. There are three principal stresses, acting perpendicular on each other, which usually are denoted as σ_1, σ_2 and σ_3, respectively from largest to smallest magnitude (Nilsen and Thidemann, 1993). The vertical stress from the gravitational force can be calculated at a given depth by the formula below. Until a certain depth, the vertical stress is often equal to the gravitational component.

$$\sigma_z = \rho \times g \times z \qquad \qquad Eq.\ 2$$

where ρ = unit weight (kg/m^3)
$\quad\quad\quad\;\; g$ = gravitational acceleration (m/s^2)
$\quad\quad\quad\;\; z$ = overburden (m)

Rock mass properties and considerations

The horizontal stress is more complicated to estimate since it consists of several components. One of the components in the horizontal stress in elastic rocks is the vertical induced stress. This component can be calculated by the equation below, when the Poisson´s ratio and the vertical stress are known (Nilsen and Thidemann, 1993):

$$\sigma_x = \sigma_y = \frac{\nu}{1-\nu} \times \sigma_z \qquad\qquad Eq.\ 3$$

Figure 11 shows that horizontal stresses at shallow depths are often larger than the vertical stress, and with a wide spread. Therefore, it is necessary with in-situ measurements to obtain an accurate estimate of the in-situ stresses. The high horizontal stresses near the surface are primarily due to plate tectonics and high stresses occurring at plate margins. In Scandinavia, the horizontal to vertical stress is often in the range of 2 to 3 (Nilsen and Thidemann, 1993).
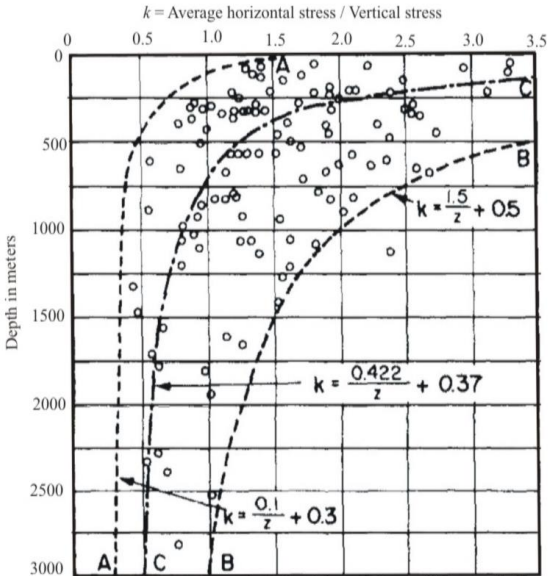
Figure 11. Horizontal to vertical stress with respect to depth below the surface (Panthi, 2006).

In addition to plate tectonics, the horizontal stresses are highly affected by the topographic surface. Nilsen and Thidemann (1993) state that in valleys, the major principal stress is more or less parallel to the topographic surface, and the minor stress is oriented perpendicular to the topographic surface. This tendency is especially important to consider in hydropower building, since most constructions take place near or in steep slopes. Fossen (2016) illustrates the stress state influenced by the topographic variation in Figure 12. Consequently, as the free surface has

Rock mass properties and considerations

zero confining pressure, exfoliation joints may occur near the surface, or any free surface for that matter, such as rock slopes, tunnel walls, weakness zones and topographic surfaces.
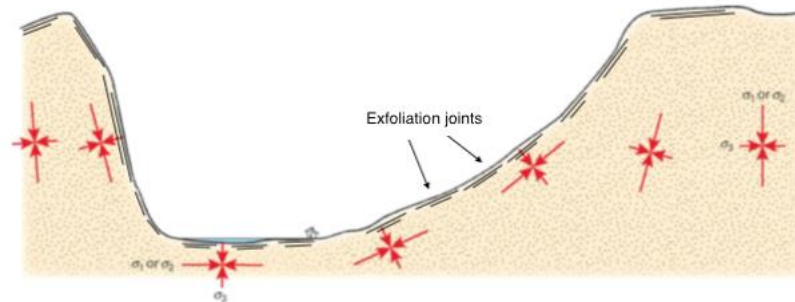
Figure 12. Stress state around steep slopes in the bed rock. The major stresses are oriented parallel to the surface, and the minor stress perpendicular to it. Note the exfoliation joints parallel to the free surface (Fossen, 2016).

When the virgin stresses are known or estimated, the induced stress from excavating in the rock mass may be calculated around a circular opening using the Kirsch equations. The maximum stress around a circular opening is where the σ_1 direction is tangent to the periphery of the excavation, and the minimum tangential stress is where the σ_3 direction is tangent to the periphery of the excavation (Nilsen and Thidemann, 1993). Kirsch equation shown below.

$$\sigma_{t(max)} = 3\sigma_1 - \sigma_3$$
$$\sigma_{t(min)} = 3\sigma_3 - \sigma_1$$

However, circular openings are not considered optimal for every situation, both because the design is unfavourable for the conventional drill and blast method, and because certain situations with anisotropic stress-states may give very high maximum tangential rock stresses or negative minimum tangential rock stresses with circular openings.

To increase or reduce the tangential stresses on the periphery, the geometry of the opening may be optimised. Hoek and Brown, referred in Palmstrøm (1995), have developed two equations for analysing the tangential stresses in the roof ($\sigma_{\theta r}$) and in the walls ($\sigma_{\theta w}$) for different underground openings (Table 5). For Norwegian rocks with typically high horizontal stresses (k of 2-3), tension stresses may occur in the walls ($B < k$) for several underground openings.

$$\sigma_{\theta r} = (A \times k - 1)\sigma_z$$
$$\sigma_{\theta w} = (B - k)\sigma_z$$

Table 5. A and B values for various underground openings. From Palmstrøm (1995).

Tunnel shape and the related A and B values									
	⬭	⌂	⬭	⌂	◯	◯	⬭	☐	⬭
A	5.0	4.0	3.9	3.2	3.1	3.0	2.0	1.9	1.8
B	2.0	1.5	1.8	2.3	2.7	3.0	5.0	1.9	3.9

3.7 Rock mass classification systems

Identification and quantification of rock mass properties is a complex process. To aid in this process a number of classification systems have been developed throughout several decades of rock engineering. Three widely used systems are the Q-classification system (Q-system), the Rock Mass Rating (RMR) system and the Geological Strength Index (GSI) classification system (Palmstrøm and Stille, 2007, Cai et al., 2004). The RMR system is not utilised in this thesis because of its lack of suitable rock support prediction (Panthi, 2006). The Q-system is useful for estimating rock support system design, while the GSI system was developed to estimate input parameters for numerical analysis (Cai et al., 2004).

The Q-system was developed in the 1970s by Barton et al. (1974) based on empirical data. This classification system is based on the rock quality designation (RQD) classification of the rock masses, with further modifications. The Q-system utilises six parameters: *RQD*, joint set number (*Jn*), joint roughness number (*Jr*), joint alternation number (*Ja*), joint water reduction factor (*Jw*) and stress reduction factor (*SRF*) combined in an equation (Barton et al., 1974):

$$Q = \left(\frac{RQD}{Jn}\right) \times \left(\frac{Jr}{Ja}\right) \times \left(\frac{Jw}{SRF}\right)$$

Eq. 4

These six parameters constitute the rock block-size, the inter-block shear strength and the active stress and tables for estimating values are attached in Appendix A. The system was developed as a universal rock mass classification system without considering excavation type and size. However, to account for these two parameters a support chart was developed based on empirical support data to guide in the needed support for the different Q-values. The Q-values have a range of 0.001 to 1000, from exceptionally poor to exceptionally good rock quality, and the Q-system considers all rock types from squeezing-ground to unjointed sound rock masses (Barton

et al., 1974). The support chart has been updated several times, including a thorough review in 2002 of the use of reinforced ribs of sprayed concrete (RRS) as reinforcement. The guidelines for the use of RRS were updated in the NGI (2015) Q-system handbook.

As a consequence of the simplification that the rock mass classification systems use, they should only be used as an empirical rock design tool, and not as a true classification system. Also, the user should hold geological and engineering geological experience and judgement to apply and understand these systems accordingly (Palmstrøm and Stille, 2007).

The GSI system developed by Hoek, Kaiser and Bawden was introduced in 1994 (Hoek, 2000). The system is the only rock mass classification system that is linked to the Mohr-Coulomb and the Hoek-Brown failure criterion, and it was developed with the intention of estimating rock mass parameters for further analysis (Cai et al., 2004). Therefore, the system shall not be used as a stand-alone classification system, since it must be associated with intact rock strength, the constant m_i value in the Hoek-Brown criterion and other rock mass characteristics, for it to be a useful tool for considering the excavation conditions. The system deals with difficulties of interlinking field observations to useful parameters for assessments by using simple charts based on two parameters: the rock mass blockiness and the condition of the discontinuities, obtained by field examinations (Marinos et al., 2007). The applicability of the GSI system is further discussed in connection with the Hoek-Brown failure criterion in section 3.8.2.

3.8 Rock mass failures

3.8.1 Failure types

Excavating in or inflicting load on rock masses changes the stability of the rock masses. In difficult underground conditions, the rock masses may go into failure. Palmstrøm and Stille (2007) have suggested three failure types that may occur when excavating in rock masses: gravity-driven failures, stress-induced failures and water-influenced failures. The first mentioned mainly occurs near surface where discontinuities control the stability (i.e. block falls, cave-in). The second mentioned occurs where the rock stress oversteps the rock mass strength and failures such as buckling, slabbing or rock bursts take place. The last-mentioned type often takes place in heterogeneous rock masses containing swelling materials or dissolvable minerals, or by influencing rock block falls in gravity-driven failures by lowering the shear strength of joint surfaces.

3.8.2 Hoek-Brown failure criterion

Throughout the time of engineering geology, several failure criterions have been developed, among these the widely accepted Hoek-Brown failure criterion. This criterion is based on empirical triaxial failure data. It is modified several times to be adjusted for weaker and jointed rock masses (Nilsen and Broch, 2016). The generalised Hoek-Brown failure criterion is presented below (Hoek et al., 2002).

$$\sigma_1' = \sigma_3' + \sigma_{ci} \left(m_b \frac{\sigma_3'}{\sigma_{ci}} + s \right)^a \qquad\qquad Eq.\ 5$$

where

σ_1' = maximum effective principle stress at failure

σ_3' = minimum effective principle stress at failure

σ_{ci} = uniaxial compressive strength of the intact rock

m_b = reduced value of the material constant m_i

$s\ and\ a$ = dependent on rock mass characteristics

The required properties for utilizing the formula are summarised as intact rock strength (σ_{ci}), the material constant m and the rock mass constants s and a (Hoek et al., 2002). These constants relate to the GSI system followingly: $m_b = m_i * e^{(GSI-100)/(28-14D)}$, $s = e^{(GSI-100)/(9-3D)}$ and $a = \frac{1}{2}+1/6(e^{-GSI/15}-e^{-20/3})$. The m parameter is an adjusting parameter for the failure envelope for various rocks. The parameter has no physical meaning even though different values are connected to different rock types. The m parameter was established by trial and error (Li, 2018). However, when the parameter is increased, the rock mass may withstand higher major principle stress with the same confining stress. The disturbance factor (D) relates to the blast damage and de-stressing in excavations. In excavation with excellent blast control and tunnels excavated by tunnel boring machines (TBM), the recommended value is 0 (Nilsen and Broch, 2016).

The applicability of the Hoek-Brown criterion is discussed in Hoek (2000). The criterion requires isotropic rock and rock mass behaviour. The criterion assumes failure on discontinuities planes, meaning there must be sufficient discontinuity sets, spaced close enough, to expect an isotropic behaviour of the rock mass. This means that the block sizes must be small compared to the excavation size. This principle is illustrated in Figure 13.
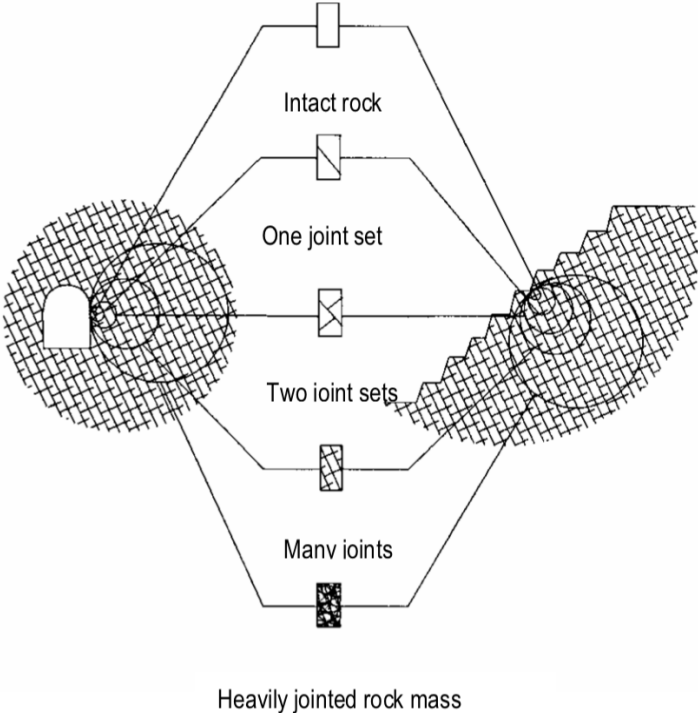
Figure 13. Rock mass transition from isotropic, intact non-jointed, to anisotropic jointed and finally to isotropic, densely jointed as the scale increases (Hoek and Brown, 1997). The Hoek-Brown criterion is not applicable in the case of one and two joint sets.

The rock mass at small scale may be considered as a non-jointed isotropic rock mass, and, as the scale increases, it may be considered as an anisotropic rock mass controlled by one or two joint sets. At a large enough scale, the rock mass becomes isotropic again through dense jointing. For cases where the rock mass is anisotropic, where block sizes are in the same order as the excavation or where a discontinuity plane controls the stability, the Hoek-Brown criterion should not be used.

3.8.3 Post-failure behaviour

Post-failure behaviour is important in rock engineering since the rock material can carry load after the peak-strength is reached. From an engineering perspective this is unlike tradition construction philosophy, where the stress in materials is kept within the elastic region (Hudson and Harrison, 2000).

Rock mass properties and considerations
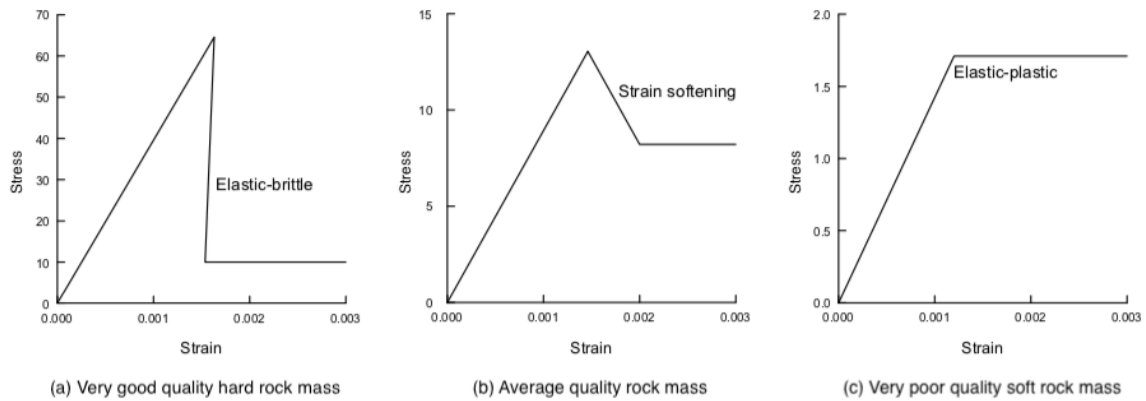
Figure 14. Post-failure behaviour of rock masses suggested by Hoek and Brown (1997).

In rock mass, when the peak strength is reached, the rock mass may be considered as failed. In simplified terms the failure point can be defined as the transition from elastic (reversible deformation) to plastic (permanent deformation) behaviour. Hoek and Brown (1997) define the post-peak behaviour dependent on how the failure develops. In hard, good-quality rock mass, the failure is brittle, meaning, it occurs sudden and with a significant reduction in the strength. In average-quality rock mass, the strength descends until a point where the rock mass behaves plastically. For very low-quality rock masses, the post-failure behaviour is plastic, meaning that it shows no reduction in strength but accumulates strain at a constant stress rate with no change in strength or volume. This behaviour is defined as respectively elastic-brittle, strain softening and elastic-plastic, shown in Figure 14.

3.8.4 Time-dependent effect

In zones of weak material, the material deforms as a result of the induced tangential stresses from the excavation. This results in a visco-plastic zone of fractured (yielded) rock mass which propagates inwards in the tunnel walls as the maximum stresses gradually move deeper into the intact rock mass, beyond the plastic zone (Panthi, 2006). This is illustrated in Figure 15.
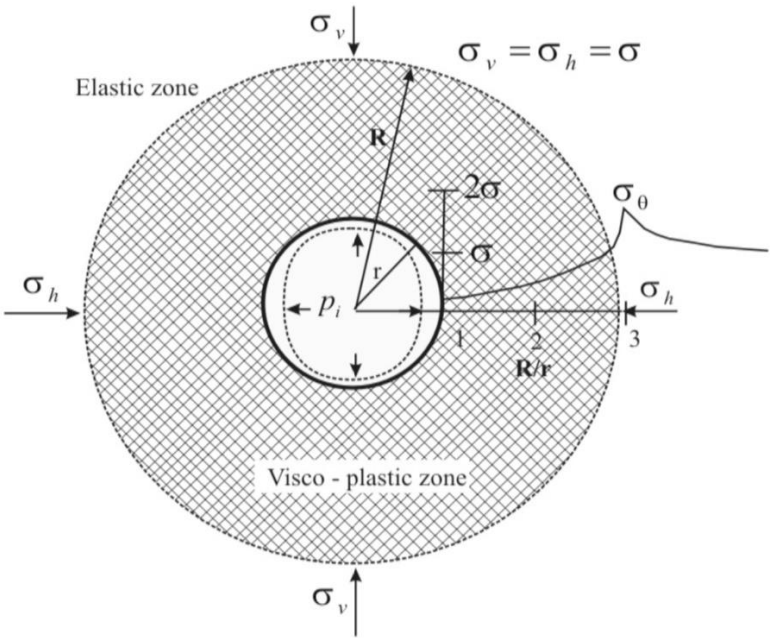
Figure 15. Squeezing in a circular tunnel, where R indicates the radius of the visco-plastic zone and p_i the support pressure. Found in and described by Panthi (2006).

4 The case of Stutakvelven inclined shaft

4.1 Svandalsflona hydropower scheme

Svandalsflona hydropower project is a part of the Røldal-Suldal hydropower scheme and is located in Odda commune in Hordaland County in southern Norway. Svandalsflona hydropower project has been operative since 1977 and has averagely produced 42 GWh annually in the period 1981-2010, with a capacity of 20 MW (NVE, Undated). Svandalsflona powerhouse utilises three reservoir lakes, western and eastern Middyrvatnet and Stutakvelven, with a gross head of approximately 220 m. The water level in Middyrvatnet is regulated between approximately 1190 and 1230 metres above sea level (m.a.s.l). The Stutakvelven lake, connected to the main waterway system through a 170 m long inclined shaft, functions as both a surge shaft and an inlet tunnel (Panthi, 2014), and the setup is illustrated with the original drawings in Figure 16. It was in this tunnel that the sudden burst flood killing two people, took place in 2009 after the initial collapse in 2008.
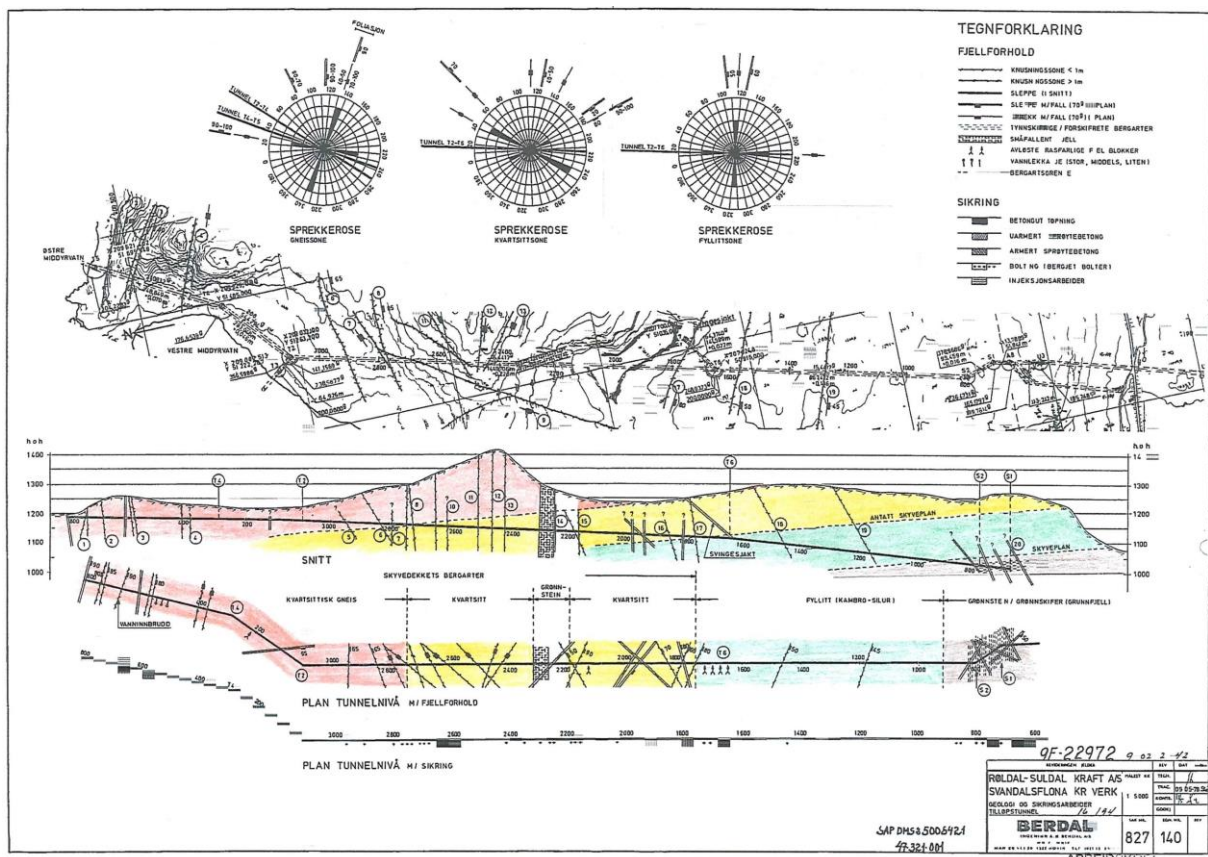
Figure 16. Original construction drawing modified with colours of Svandalsflona waterway system and geological setup by Berdal AS (1978c).

4.2 Stutakvelven inclined shaft

Stutakvelven shaft is orientated approximately S64ºW-N64ºE with an inclination of approximately 45º towards west-southwest. The inclined shaft has a theoretical cross-section of 13 m² in the upper part, and 4 m² in the lower part. The construction drawing shows how the cross-section of the upper shaft was intended by design (Figure 17). It was in this section that the failure occurred. The shaft was supposed to be excavated from bottom-to-top using Alimak raise climber and drill and blast method. However, because of the weakness zone encountered at approximately 1215 m elevation, the Alimak-excavation was stopped, and it was decided to use traditional shaft sinking method from the top.
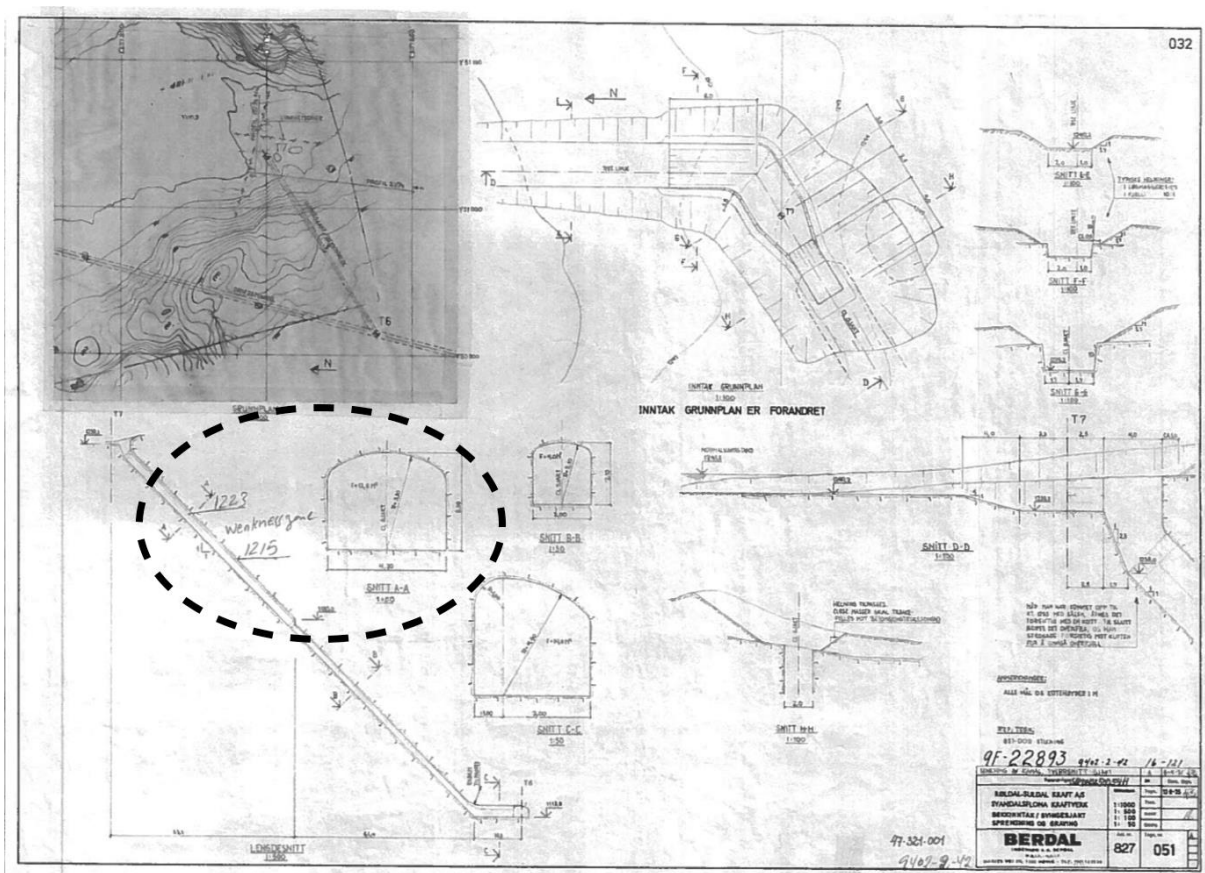
Figure 17. Construction drawing of the Stutakvelven inclined shaft by Berdal AS (1978a).

The weakness zone led to significant overbreak during excavation causing increase in the cross-section area (Figure 18). At the intersection point of the weakness zone and the shaft, several clay zones were identified. The weakness zone was secured with a rectangular cast concrete construction, leaving an empty space in the crown. The invert was secured using brace beams with shotcrete in between. The walls were secured using thick casted concrete and they were

The case of Stutakvelven inclined shaft

secured with brace beams in the invert and a planar casted plane in the roof. In addition, a hatch was constructed in the upper part of the concrete plane in the roof. The weakness zone resulted in a much larger cross-section as illustrated in Figure 19.
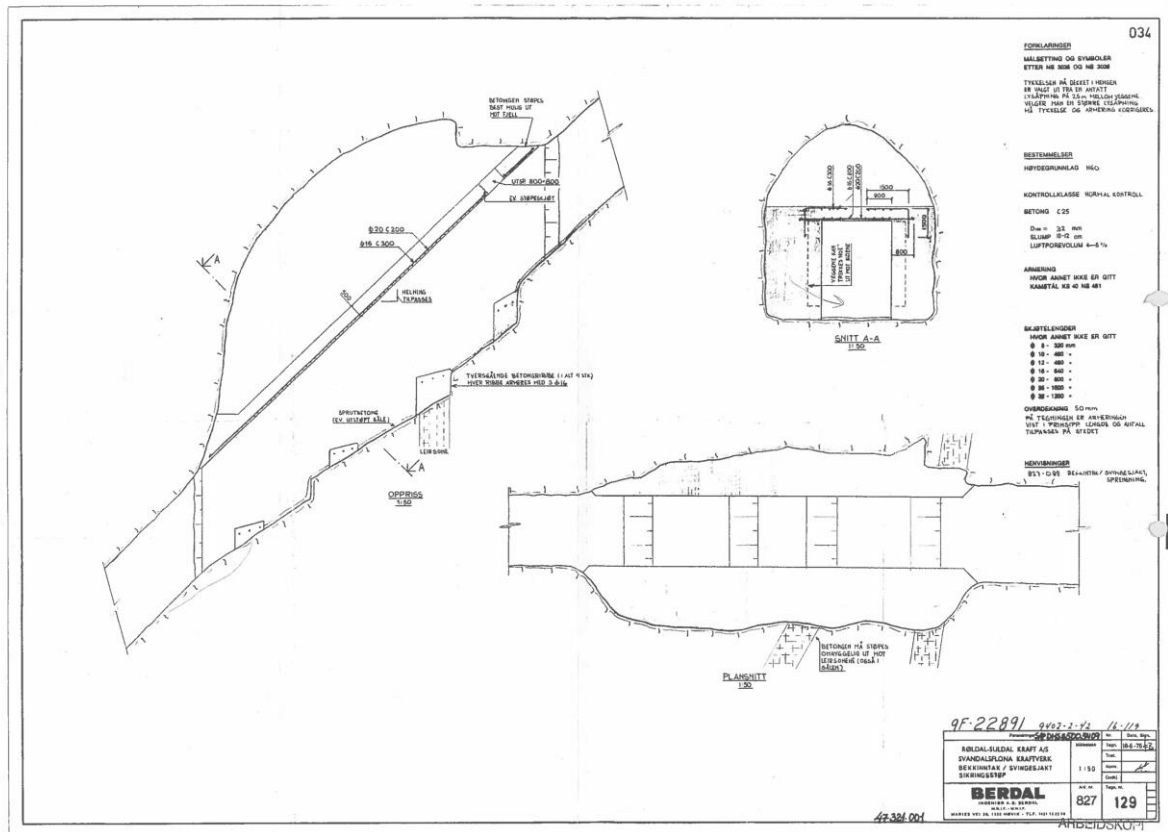
Figure 18. Construction drawings of the concrete lining in the shaft where the weakness zone intersects (Berdal AS, 1978b).
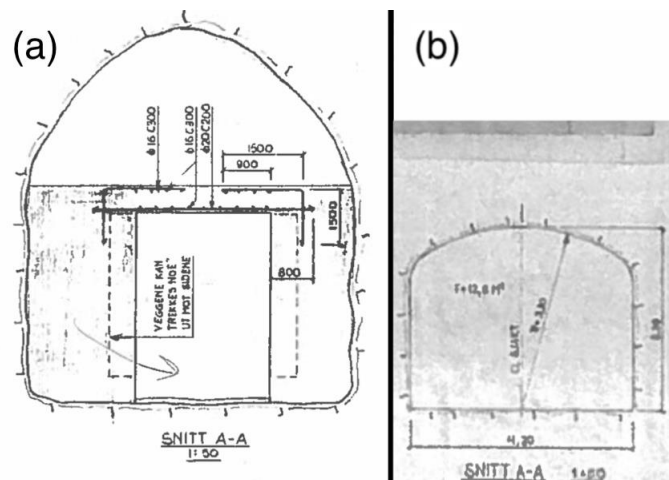
Figure 19. Drawings of the actual (a) and intended (b) cross-section of the shaft based on figure 17 and 18. The rectangular opening in the cast concrete in (a) is 2,5 m. The scales of the two cross-sections are adjusted relatively and show significant difference in the intended and actual size.

4.3 The collapse and the burst flood

Panthi (2014) has elaborated on a series of events that according to him led to the sudden burst flood in 9 May 2009. In May 2008 it was discovered that the water level in Stutakvelven lake was abnormal high and at a stagnant position. This was the first indication of a blockage in the shaft. A sinkhole with a diameter of 8 m in the topography was found, and the diameter was approximately 5 m in the rock mass deeper down (Figure 20). The diameter at surface was wider due to lose crushed material, in all fractions, which most likely had slide into the sink hole. This was a clear indication of a collapse in the shaft. The sinkhole was located in the crushed zone near the gatehouse (Panthi, 2014).
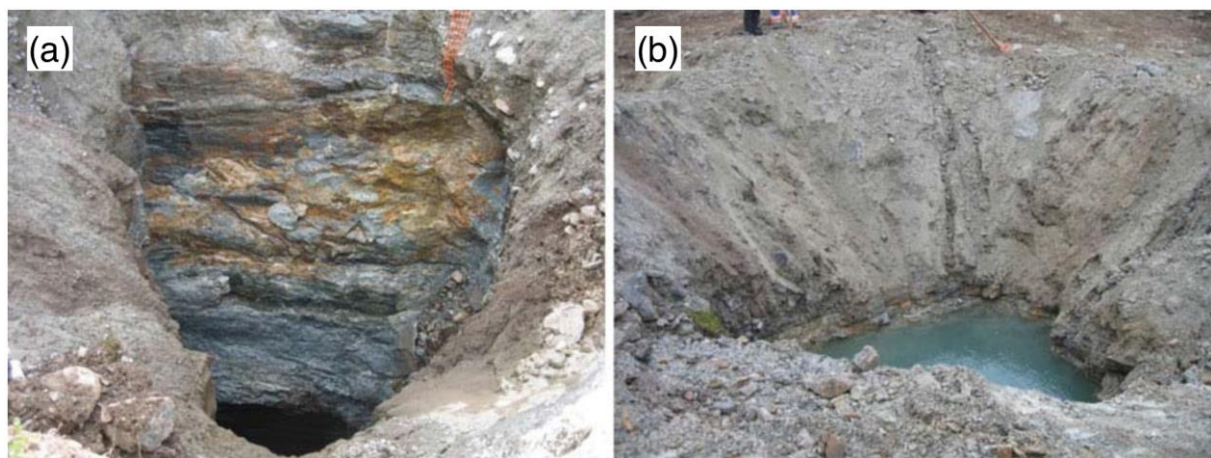
Figure 20. (a) Rock mass in sink hole (July 2008). (b) Water-filled sink hole in September 2008 (Photos by Norsk Hydro referred in Panthi (2014)).

Further investigations showed that some water flowed through the slide deposits in the shaft (Figure 21). This was confirmed by shutting down the powerhouse, closing the stoplogs and draining the headrace tunnel. It was then observed that the water in the sinkhole drained, thus, the drainage capacity of the slide deposits in the inclined shaft was larger than the leakage through the stoplogs. After inspection in June 2008 it was decided to run operation as normal until April 2009, because of the leakage water flowing freely through the deposits.

The case of Stutakvelven inclined shaft
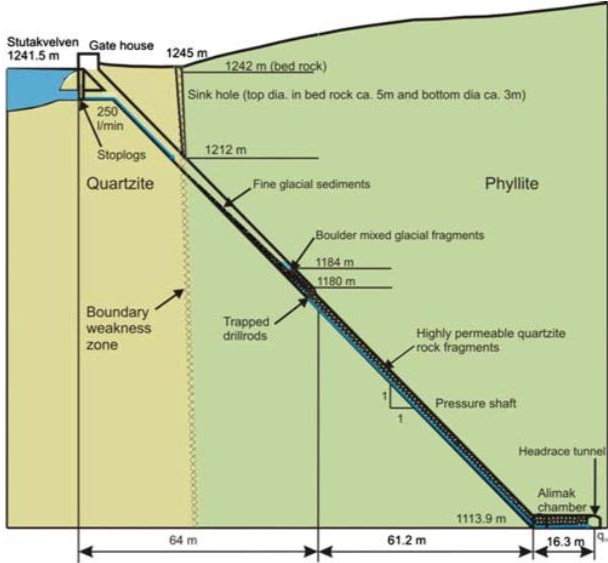
Figure 21. Illustration of the situation in Stutakvelven shaft after the initial collapse from Panthi (2014). Note the transition in the shaft cross-section at elevation 1180, and that the slide deposits have clogged where the shaft narrows in. It is illustrated that the slide deposits have some permeability. Sink hole has a diameter of approximately 3 m at tunnel depth.

In the days before the burst flood it was considerable snowmelt and rainfall in the catchment of the sinkhole (Panthi, 2014). This rainfall and snowmelt are estimated to be more than two times the inflow from the stoplog-leakage. This large amount of water could according to Panthi (2014) have scoured/eroded the clay zones, now exposed due to fractured cast concrete, and these particles may have settled within the slide deposits further down the shaft reducing the permeability of the slide deposits. In addition, this water may have transported glacial sediments from the surface through the sink hole and/or through the joints. All this together caused the build-up in the water pressure resulting in the burst flood killing two people 9 May 2009.

The photos in Figure 22 indicates a washed-out hole below the upper braced beam. This might have been the cause of the initial failure of the lining, which led to slide deposits clogging the shaft. The clay zones were now exposed. The slide deposits had some permeability which led to the decision of running the operation as normal until spring. However, because of the large amount of rainfall and snowmelt it is suspected that the clay zones were eroded, and that the material was deposited within the slide material reducing the little permeability causing a build-up in the water pressure. This resulted in the burst flood that took place during the attempt to clear all the slide masses.

The case of Stutakvelven inclined shaft
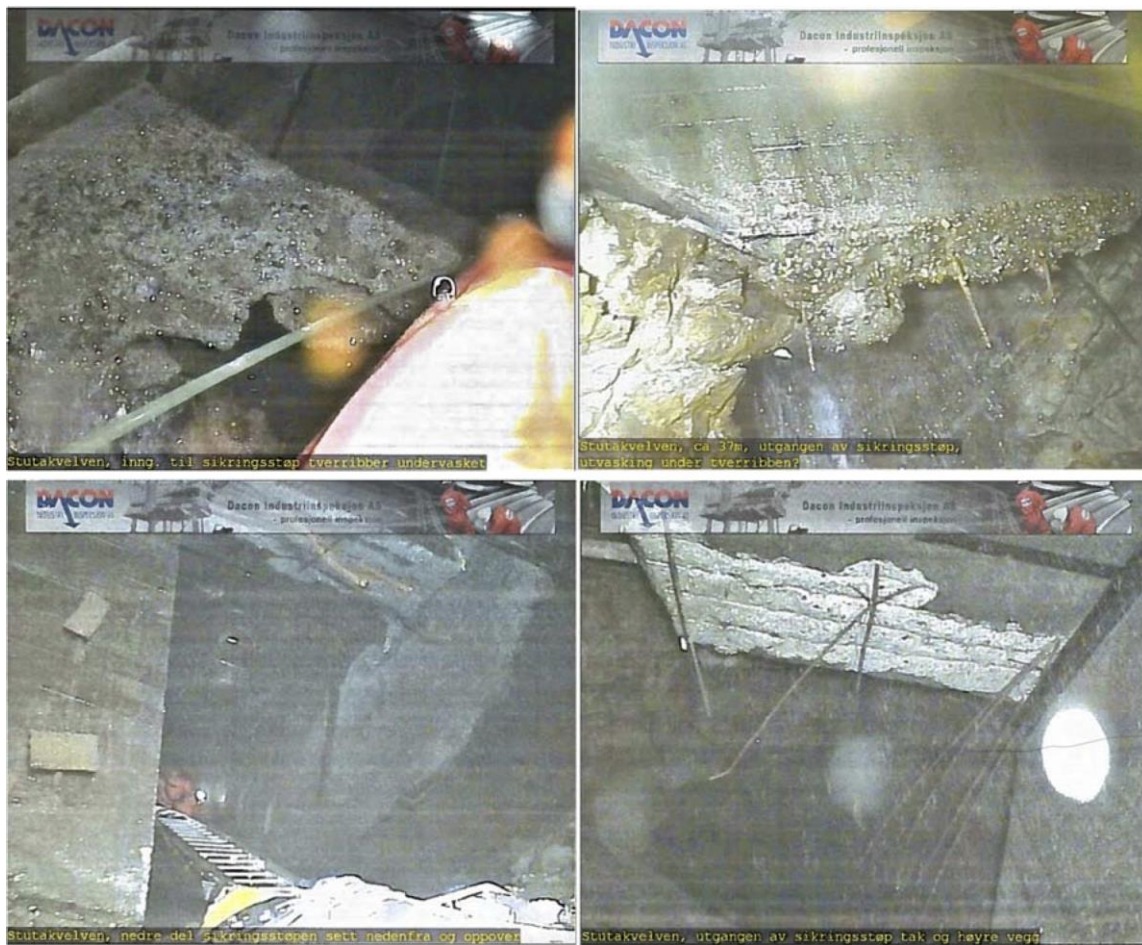
Figure 22. Indicates outwash under the brace beams in the invert where the clay zones exist. The cast concrete is damaged in walls and in the crown in the lower end. Photo taken post both the collapse and the sudden burst flood, and originates from Neupane and Panthi (2018).

To be able to assess the stability the regional and local structural geological conditions are highlighted.

4.4 Regional structural geology

4.4.1 Overview of project area

Svandalsflona hydropower project is sited within rocks from the Caledonian orogeny in southern Norway. The closing of the Iapetus ocean and the collision between Baltica and Laurentia formed the Caledonian mountain range through compression. The assumed direction of the compression during collision is illustrated in Figure 23b. This has led to a numerous thrust nappes (allochthones) separated by thrust faults and with rocks of different age, metamorphosis grade, deformation and formation environment, characteristic for the Caledonian mountain range (Bergh, 2003). After the collision the continents drifted apart, causing the compressional forces to decrease and the collapse of the Caledonian mountain range

begun. In the collapse, the over-thrusted nappe complexes were thinned out by extension and shear faults, and it is assumed that the direction of the extension of the continents were in opposite direction as the collision (Fossen et al., 2013).
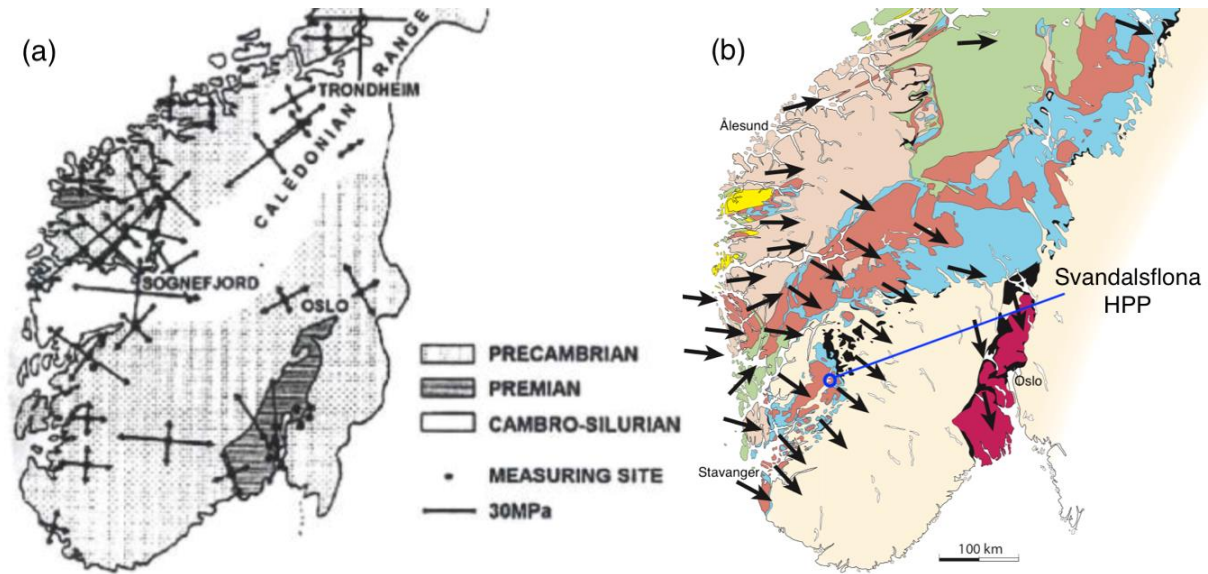
Figure 23. (a) Horizontal stresses in southern Norway, by Myrvang referred in Li (2018). (b) Caledonian lineation directions as a result of the Caledonian orogeny (Fossen et al., 2013).

The Caledonian nappes are thrusted in from the west and northwest, and what is now left from the mountain range covers the land in a front oriented southwest to northeast, extending northwards. The Precambrian basement rocks in the south (Figure 23a) are slightly, if at all, affected by the over-thrusted nappes which now are eroded away. The Precambrian basement on the west-coast surrounding Ålesund are partly affected by thrust nappes and might have been transported on a kilometre scale. The unaffected basement is referred to as autochthonous, and the partly affected and short transported basement is referred to as parautochthonous. The nappes, however, are transported tens to hundreds of kilometres and are referred to as allochthons. These allochthones are divided into uppermost, upper, middle and lower allochthones, where the uppermost are most affected and have been transported the furthest, in general. The rocks surrounding Svandalsflona project area are mainly from the middle and the lower allochthones and represented respectively as brown-reddish and blue colours in Figure 23b. The area around Svandalsflona HPP also consists of deposited sediments on the Precambrian basement rocks, which are shortly transported, that is, parautochthonous, and may be seen as phyllites and other low-grade rocks (Fossen et al., 2013, Fossen, 2016).

The case of Stutakvelven inclined shaft

The horizontal rock stresses in Norway are approximately oriented parallel or perpendicular to the Caledonian contractional regime. In southern Norway, the major horizontal stress is oriented northwest-southeast and the minor stress is oriented northeast-southwest, as illustrated in Figure 23a by Myrvang referred in Li (2018). This is consistent with other findings that together prove that rock stresses in the earth coincide with tectonic movements, in general (Li, 2018).

4.4.2 Geological setup by Panthi 2014

The project area is according to Berdal referred in Panthi (2014) divided into three main geological formations consisting of over-thrusted nappes from the Caledonian orogeny, Cambro-Silurian basement and Precambrian basement. The inclined shaft area is located within quartzite and phyllite separated by a weakness zone intersecting the shaft. The weakness zone strikes roughly east-southeast to west-northwest with the phyllite on the south side and the quartzite on the north side as illustrated in Panthi (2014) shown in Figure 24.
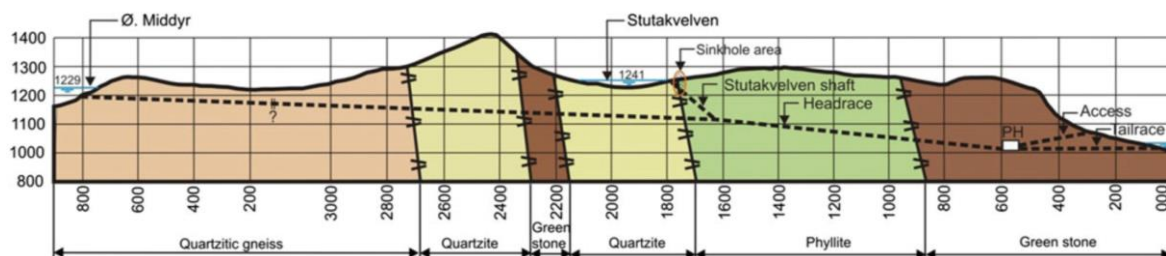
Figure 24. Longitudinal profile of waterway system and geological conditions of the Svandalsflona hydropower project (Panthi, 2014).

As a consequence of the Caledonian orogeny and the over-thrusted nappes the area is deformed. Panthi (2014) has defined based on Berdal two main joint systems with a strike and dip respectively N15ªE to N45ªE steeply dipping eastwards and N80ªE to N130ªE dipping southwards. The weakness zone at Stutakvelven shaft area is described as highly fractured with cubical-like rock material mixed with clay, silt and sand (Panthi, 2014).

4.4.3 Review of NGU bedrock maps

The Røldal-Suldal area consists of a great variety of geological units as shown in the Røldal 1314 I (Figure 25) and Haukelisæter 1414 IV (Figure 26) bedrock maps mapped by respectively Jorde (1977) and Naterstad (1988). In the surrounding area of Svandalsflona the autochthonous Precambrian basement consist of large-scale folds and faults. This indicates both ductile and

The case of Stutakvelven inclined shaft

brittle deformation, as expected for orogenic areas. On the east side of Valldalsvatnet and Røldalsvatnet, the over-thrusted nappes are oriented sub-horizontal to gently dipping.
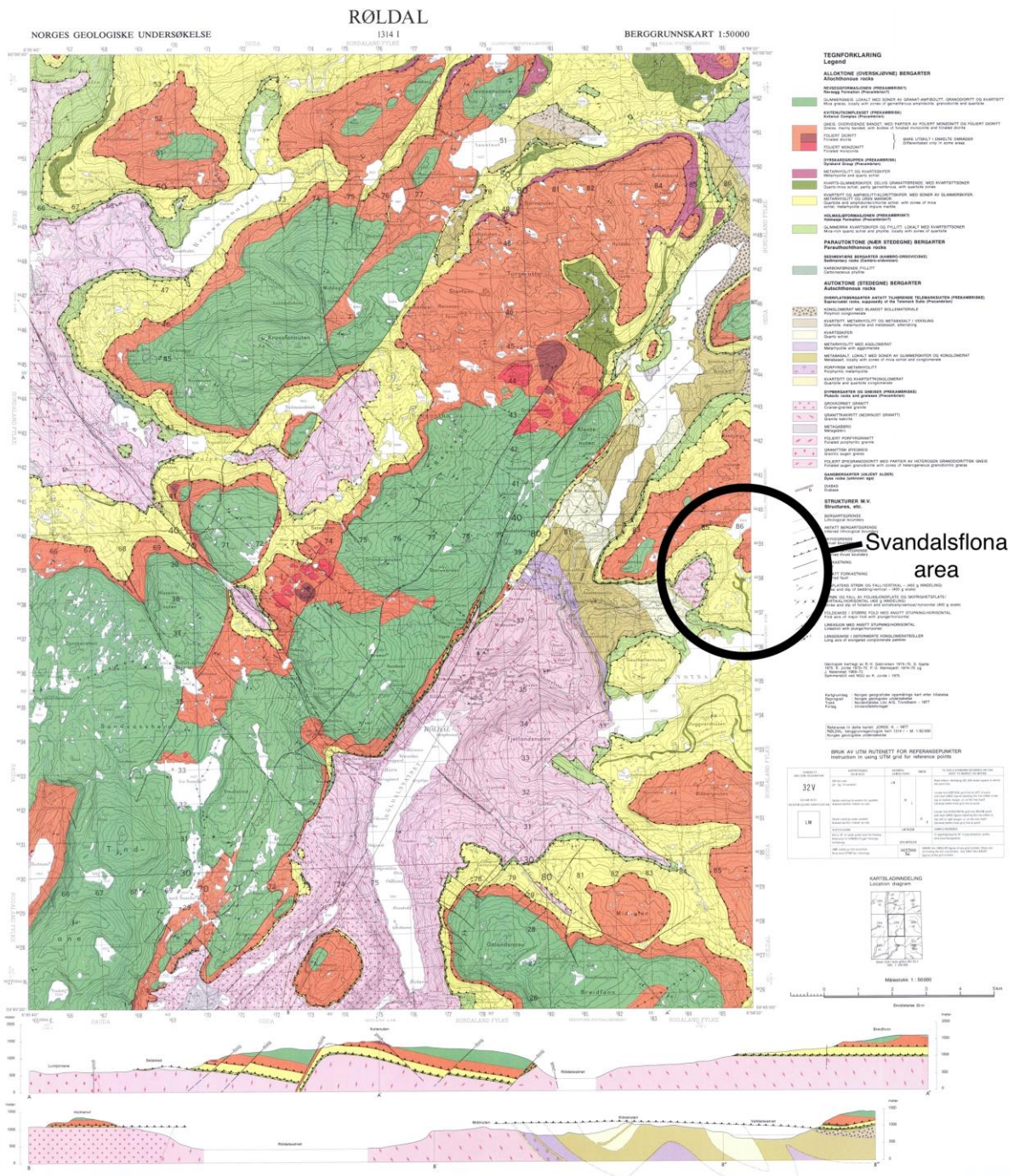
Figure 25. Bedrock map of the surrounding area of Svandalsflona HPP by Jorde (1977). Svandalsflona HPP marked with a black circle. The cross-sections are oriented NE-SW and NW-SE.

The Svandalsflona area consists of allochthonous over-thrusted nappes with Precambrian origin in the stratigraphic order Kvitenut complex, Dyrskard group and Holmasjøformasjonen (Figure

25). The Kvitenut complex consists of gneiss, mainly banded, with bodies of foliated monzonite and foliated diorite. The Dyrskard group is divided into three units which consists of metarhyolite and quartz schist, the other of quartz-mica schist, partly garnetiferous with quartzite cones, and the third of quartzite and amphibolite/chlorite schist, with zones of mica schist, metarhyolite and impure marble. The underlaying Holmasjøformasjonen consists of mica-rich quartz and phyllite, locally with zones of quartzite. All nappes are overlaying the Precambrian basement consisting of mica-rich quartz schist and phyllites.

Figure 26. Bedrock map of the surrounding area of Svandalsflona by Naterstad (1988). The area of Svandalsflona is marked with a black circle.

5 Field mapping at Stutakvelven

5.1 Introduction

The field mapping at Stutakvelven gate house area was conducted at 18-19 September 2018. The aim was to assess the structural geology by surface investigations and collect rock samples representative for the inclined shaft area for the laboratory investigations. The mapping was conducted with a geological hammer, geological compass, field sketch book, GPS and camera. In addition to this, a field map based on the construction drawing was used as well as images from norgeibilder.no. The stereographic projections in this chapter are made in the Stereonet 9 freeware by Allmendinger et al. (2011) and Cardozo et al. (2013).

The weakness zone intersecting Stutakvelven shaft is marked as weakness zone 17 by Berdal AS (1978c). The weakness zone is located close to the intake gate house and can be observed as a terrain depression. No rock walls can neither be seen nor measured in this area because of the area being covered in rock fragments (Figure 27). Therefore, mapping around the area was an alternative way to estimate the rock mass in the inclined shaft area. The position of the sink hole could not be located either.

Figure 27. Gate house and the area covering the sink hole on the left backside of the gate house, seen as a terrain scar. Photo taken towards WSW, looking downstream the shaft, oblique to the weakness zone 17.

5.2 Simplified field map

A brief desk study on the geological structures in the field area was conducted pre the field investigations. Figure 28 shows a simplified field map prepared based on the construction drawings (Figure 16). The map shows the area around Stutakvelven shaft, where the weakness zone 17 is intersecting the inclined shaft. Upstream the shaft the two reservoirs are located, and downstream the shaft the Svandalsflona powerhouse is located. All weakness zones marked by Berdal are indicated with red lines. The waterway system is indicated with stippled lines.
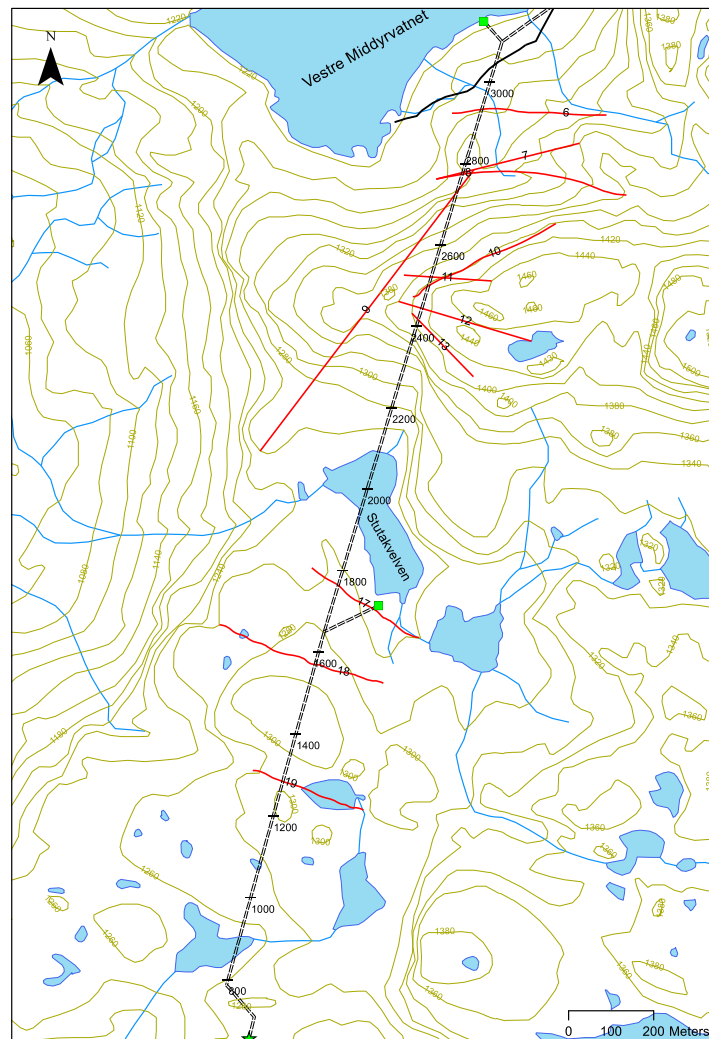
Figure 28. Simplified field map based on the construction drawings (Figure 16).

5.3 Overview of the mapped area

Figure 29 shows compilation of the field investigations at Stutakvelven area.
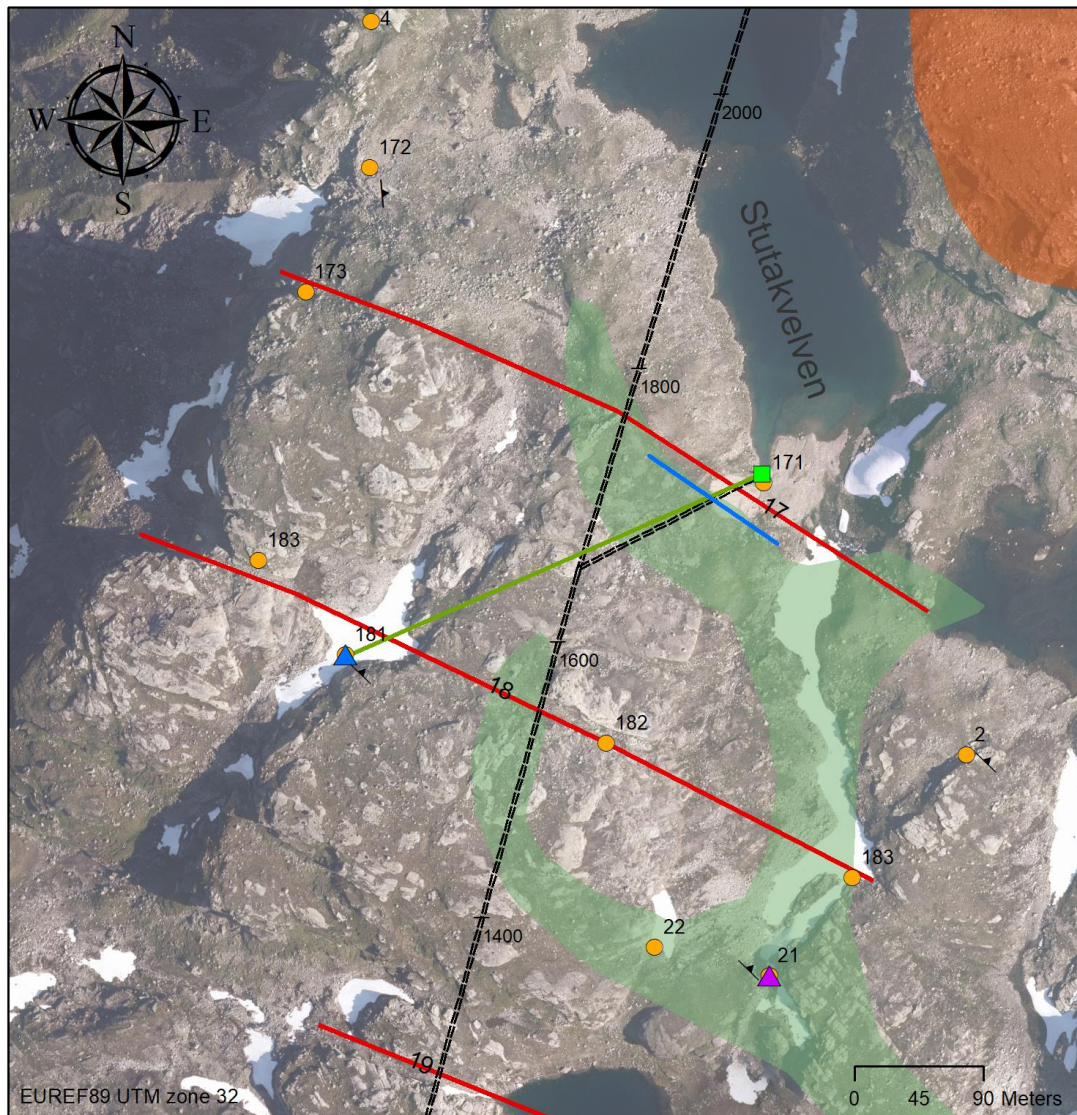
Legend

⬊	Strike and dip	====	Headrace tunnel and shaft
★	Power house	▬▬▬	Weakness zones
🟩	Gatehouse		**Bedrock map N50**
🔺	Location 2.1 (sample)		**Rock type (NGU N50)**
🔺	Location 1.5 (sample)		Gneiss, mainly banded, with bodies of foliated monzonite and foliated diorite
🟠	GPS points		Quartz-mica schist, partly garnetiferous, with quartzite zones
—	Chainage		Quartzite and amphibolite/chlorite schist, with zones of mica schist,
▬▬	Cross-section numerical model		metarhyolite and impure marble
▬▬	Adjacent cathetus		

Figure 29. ArcMap compilation of the field work. Note that the quartzite layer constitutes most of the area and are therefore left colourless.

5.4 Locations surrounding weakness zone 17

5.4.1 Location 1.5

Location 1.5 is located 350 m south-west of the gate house in the weakness zone 18 (blue triangle in Figure 29). The weakness zone can be seen as a terrain depression, 20-30 m wide, with a well exposed rock wall. This location is considered relevant based on the observation of the similarities between the dark, fine to medium grained, quite homogenous rock mass layer (Figure 30) and the rock mass in the sinkhole shown in Panthi (2014)(Figure 20). In addition, the rock mass in location 1.5 consist of distinct joint sets making the rock mass cubical as also described for the rock mass in Panthi (2014). The weakness zone 18 has similar orientation and dimension as weakness zone 17. Therefore, it could be likely that deformation and jointing at this location reflects the situation in and around weakness zone 17. This statement is supported by the considerations of Nilsen and Thidemann (1993) where parallel faults often has the same characteristic features.

According to the NGU N50 bedrock map (Figure 25) this area is located within quartzite and amphibolite/chlorite schist, with zones of mica schist, metarhyolite and impure. The impression of the area is that the geology is complex with deformation and different lithologies.

The weakness zone 18 has a strike of approximately N120ºE dipping steeply towards south (Figure 30). Three distinct joint sets are recorded in this location, whereas one set is perpendicular to the weakness zone (J1), one is parallel to the weakness zone (J2) and lastly joints parallel to the foliation. J1 is dipping steeply towards northwest, J2 is dipping steeply towards south and the foliation joints is dipping gently towards northeast. The mean values of the measured joint sets are presented as stereographic projection in Figure 30.

J1 and J2 both have large persistence, well above 3 m. J1 has a spacing of approximately 20-40 cm and J2 has a spacing of 5-10 cm in the most fractured areas closest to the weakness zone (transition zone). Approximately ten meters away from the zone the spacing significantly increases which gives the rock mass a higher quality, for example, the RQD is mapped from 50 to 80. The mapped Q-parameters are mainly based on observation in the layer labelled as "series 1", and the mapped values are presented in Table 6.
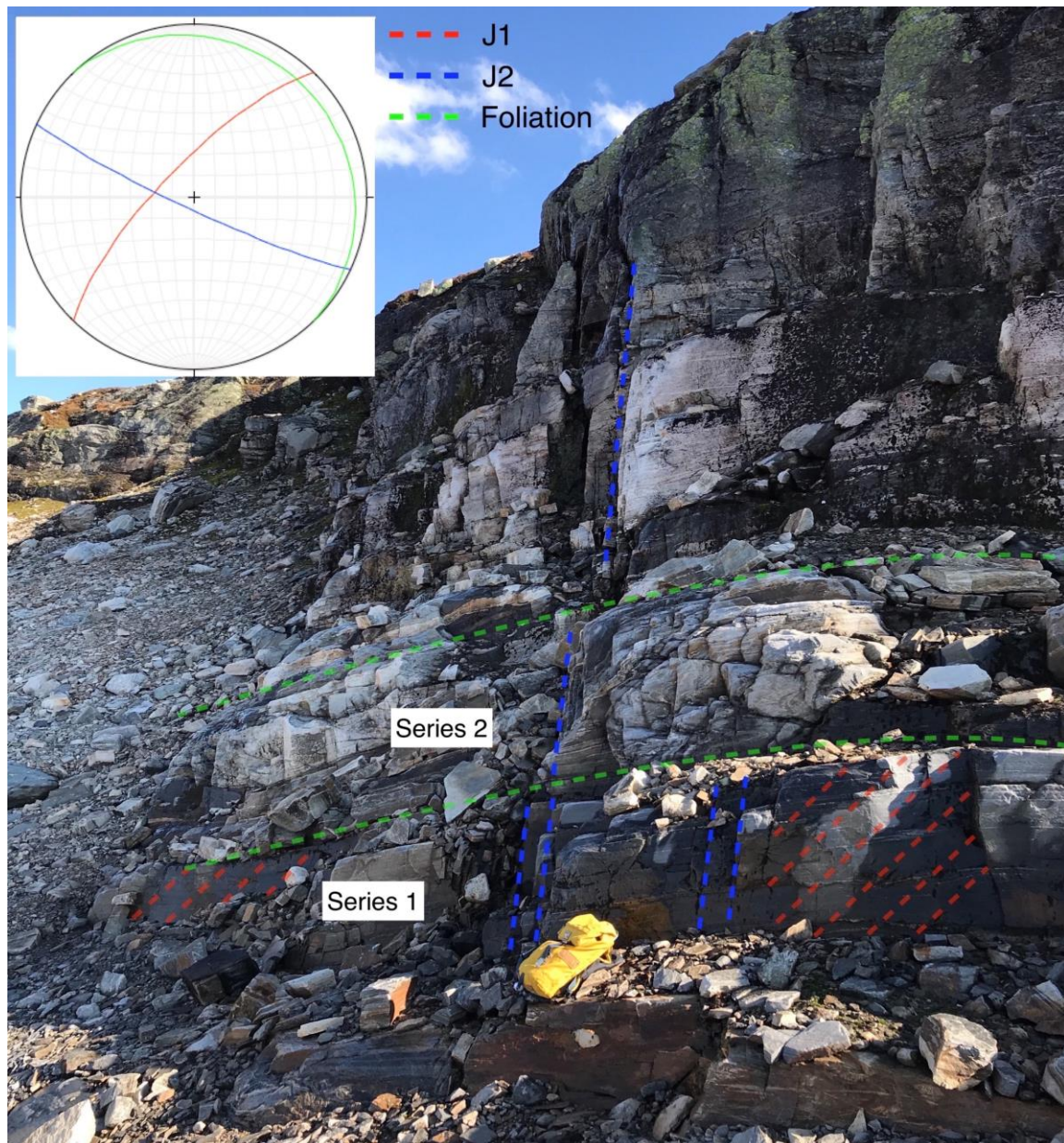
Figure 30. Location 1.5 found at the weakness zone 18, where samples of series 1 and 2 were collected. The length of the rucksack is approximately 45 cm, and the photo is taken towards direction ESE (106º). The stereographic projection shows the mean values of the measured joint sets.

The rock mass shows local variation, and this location is in or close to the by Berdal AS (1978c) assumed thrust plane between the quartzite and gneiss (Figure 16). Figure 31 illustrates some of the geological variations found at this location and this deformation zone is believed to consist of, as discussed in section 6.4.3, banded gneiss on top of mylonite. Another important observation, is the dark-brownish, silty or sandy clay coating found behind a jacked-out block seen in Figure 32, which influences the Ja value for this area.

Figure 31. Deformation zone in location 1.5. Picture taken towards east-southeast (114º).

Figure 32. Joint infill location 1.5 in the layer "series 1". Silty or sandy clay coating. Alternating darker and lighter foliation. The photo is taken towards direction SE (132°).

The strike and dip measurements at this location indicates the possibility for this rock mass to be representative for the rock mass in the shaft area where the failure occurred, based on the assumption of a planar plane. This is illustrated by a simple model in Figure 33 made from a profile graph plot from ArcMap. The foliation plane is considered as the hypotenuse in a right-angled triangle, and the aerial distance between point 1.5 and the gate house as the adjacent cathetus. The elevation difference in these two locations equals the opposite cathetus. By trigonometry the opposite cathetus was found and subtracted from the elevation at location 1.5. The calculation gave the intersection point of the foliation layer (green stippled line) and the y-axis (elevation axis). Thus, for 8 degrees dip, the calculation gives 1280 m – (320 m * tan 8) and for 14 degrees dip the calculation gives 1280 m – (320 m * tan 14), resulting in an elevation interval of 1200 – 1235 m for the darker rock mass layer at the y-axis (below the gate house). This shows that the lower interval of the darker rock mass layer intersects the shaft and the weakness zone between 1209 m and 1236 m, which coincides well with the findings of the lower interval of the weakness zone at 1212 m elevation (Panthi, 2014). This illustrates how the rock mass at location 1.5 may be representative for the rock mass in the inclined shaft failure area.

Field mapping at Stutakvelven
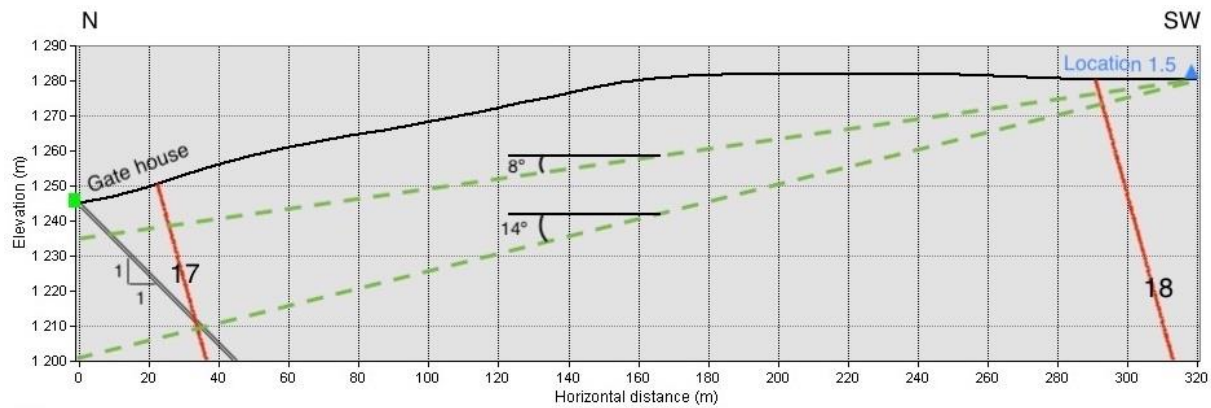
Figure 33. Illustration of how the rock mass at location 1.5 could be representative for the rock mass in the shaft. Vertical-horizontal axis not to scale. The cross-section N-SW is shown and marked as adjacent cathetus in the overview map in Figure 29.

However, the presented model is based on a few measurements in an area of complex geology. The model is also a simplification and does not account for complex structures such as faults and folds. The validity of the model depends on planar planes which might be the case when considering the rock mass on a regional scale, illustrated by the geological boundaries in the geological maps by NGU (Figure 25, Figure 26). In addition, this model is based on true dip for the calculation, which should be used for the perpendicular distance between the strike of the rock mass layer and the gate house, but the distance which is used in the calculation deviates from this perpendicular distance by 22 degrees. That means, the length of the adjacent cathetus would be 295 m instead of 320 m, followingly changing the intersection point from 1200 m to 1206 m in the lower interval, making it less likely that the rock mass is found where the shaft and the weakness zone intersects. Still, the darker rock mass layer would be very close to the intersection point of the shaft and the weakness zone. However, this change is considered minor, especially when taking into account that the layer-thickness is unknown, and that the foliation dips steeper than the used dip, for instance at location 2.1 located south-eastwards, which would lower the intersection point in the lower interval shown by green stippled line. Based on this reasoning, samples for series 1 and 2 are collected at location 1.5.

This model represents a solution-oriented thinking in a difficult mapping situation with limited time and without access to the shaft, and the simplification of the model must be highlighted.

5.4.2 Location 2.1

Location 2.1 is located 350 m south of the gate house. At this location a layer of dark-greyish colour, fine to medium grained with millimetre thin foliation alternating lighter and darker

bands with thicker bands of quartzite/feldspar is observed. This reminds of the rock mass in location 1.5, hence, also to the one in Panthi (2014). However, in this location the folding occurs more frequently with vergence indicating top to east-southeast (Figure 34). According to NGU N50 bedrock map (Figure 25) this area is located within quartz-mica schist, partly garnetiferous, with quartzite zones.
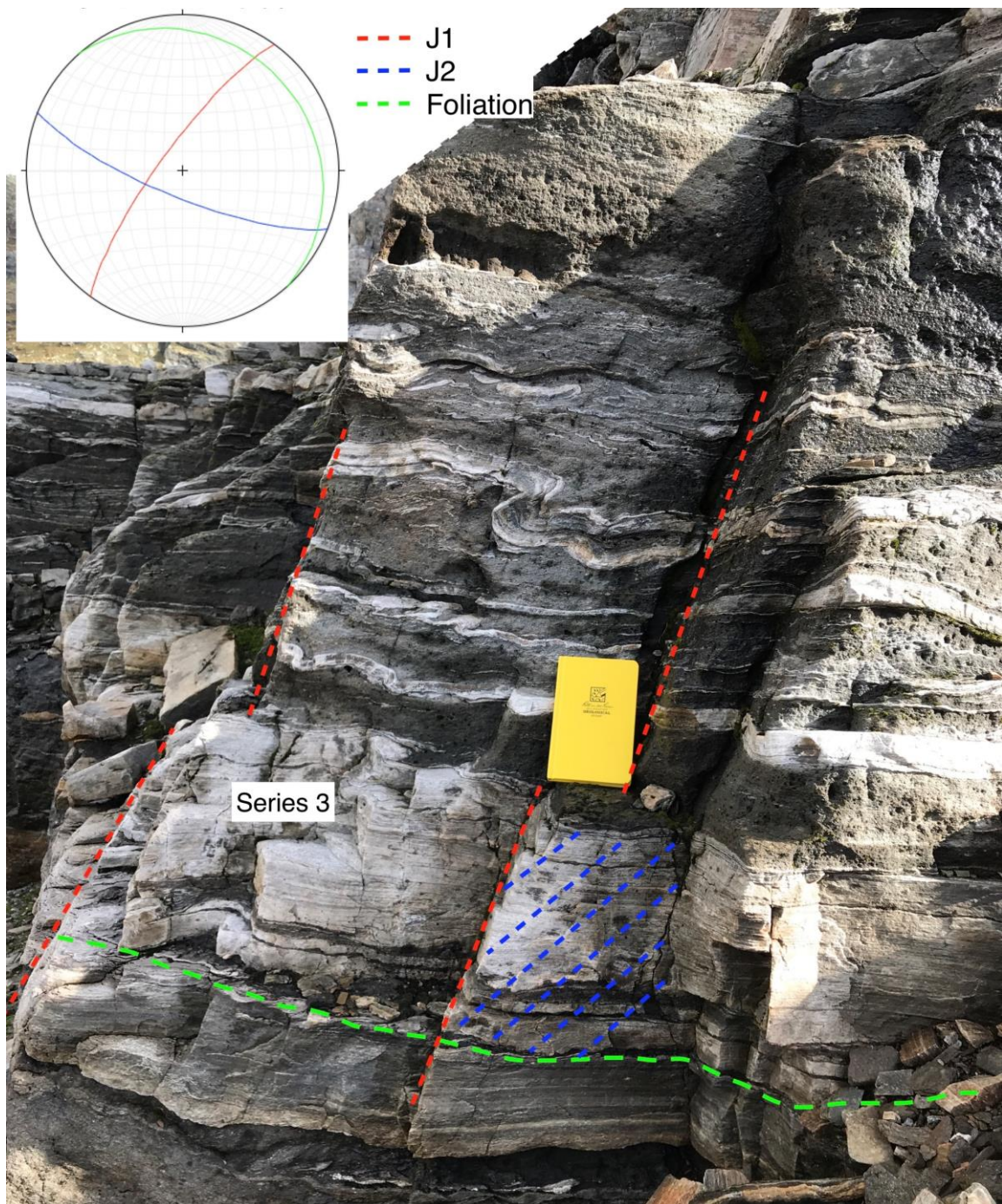
Figure 34. Location 2.1 where series 3 was sampled. Joint set 1 is indicated with red stippled lines, joint set 2 with blue stippled lines and the foliation joint set is indicated with a green stippled line. The geological sketch book for scale is 20 cm, and the photo is taken towards direction northeast (038º). The presentation of the stereographic plot is the mean values of the measurements.

Field mapping at Stutakvelven

The measurements of the foliation and the joint sets are similar to the measurements recorded at location 1.5, and with the same reasoning as for location 1.5 it was also chosen to sample here. However, it was chosen to sample from the light mica-rich layer ("series 3" in Figure 34) in order to extend the input parameters for, inter alia, numerical modelling.

Figure 35. Overview of the location 2.1, where the sample which constitutes series 3 was collected. Picture takes towards northeast (049º).

Two distinct joint sets and foliation joints are observed at this location. The orientation of these three joint sets (Figure 34) are similar as the ones measured at location 1.5. J1 is oriented at high angle to the J2 joints. The J2 joints are oriented parallel to weakness zones 17 and 18. The less distinct foliation joints dips gently towards northeast. However, the foliation joints are seen clearly in layers 5-10 m above this location (Figure 35). All three discontinuities have a persistence more than 3 m. J1 has a spacing of 5-40 cm, J2 has a spacing of 20-60 cm and the foliation joints have a spacing of 5-20 cm. The mapped Q-parameters are presented in Table 6.

5.4.3 Location 4

This area is marked as quartzite by both Berdal AS (1978c) and Jorde (1977) and is located on the north side of weakness zone 17. The rock mass is apparently more solid with a higher Q-value, but also here three distinct joint sets can be seen (Figure 36). All three joint sets have a persistence more than 3 m. The J1 joints are dipping steeply towards northwest, with a spacing of 40-60 cm. The J3 joints are dipping steeply towards west-southwest, with a spacing of 100 cm. The foliation joints are dipping gently towards east, with a spacing of 10-20 cm. The J2 joints are not observed at this location, however, the J3 joints are approximately rotated 30 degrees (N→E) relatively to the J2 joints and could originally be oriented as J2 joints. This could mean that deformation has reoriented J2 joints to J3 joints in this location, and it is therefore not certain that these J3 joints exists in the shaft area.

Figure 36. Rock mass at location 4. Bibek for scale.

For the stability assessments it is assumed that this rock mass has an equal quality, or most likely better quality, than the one mapped in relation to weakness zone 17 and 18 (location 1.5, 2.1 and 22). Therefore, no particular emphasis is laid on this location, but it is used to estimate which joint sets are recurring and are likely to occur in the shaft area.

5.4.4 Location 1.7.2

At this location four joint sets are mapped (Figure 37). The persistence of J1, J2 and the foliation joints are more than 3 m, and for the J3 joint set the persistence is between 1-3 m. The strike and dip of these joint sets coincide well with the other measurements (Figure 40). The foliation dips in the opposite direction as most of the other recordings (180º added to the strike), which indicates undulation (or folding) of the layers. The recorded spacing is for J1 40 cm, for J2 from 20 to 100 cm, for J3 100 cm and for the foliation joints from 10 to 40 cm. J3, found at both location 4 and 1.7.2, is not weighted to same extent as the other joint sets based on that J3 is only found at these two northernmost locations in the quartzite zone.
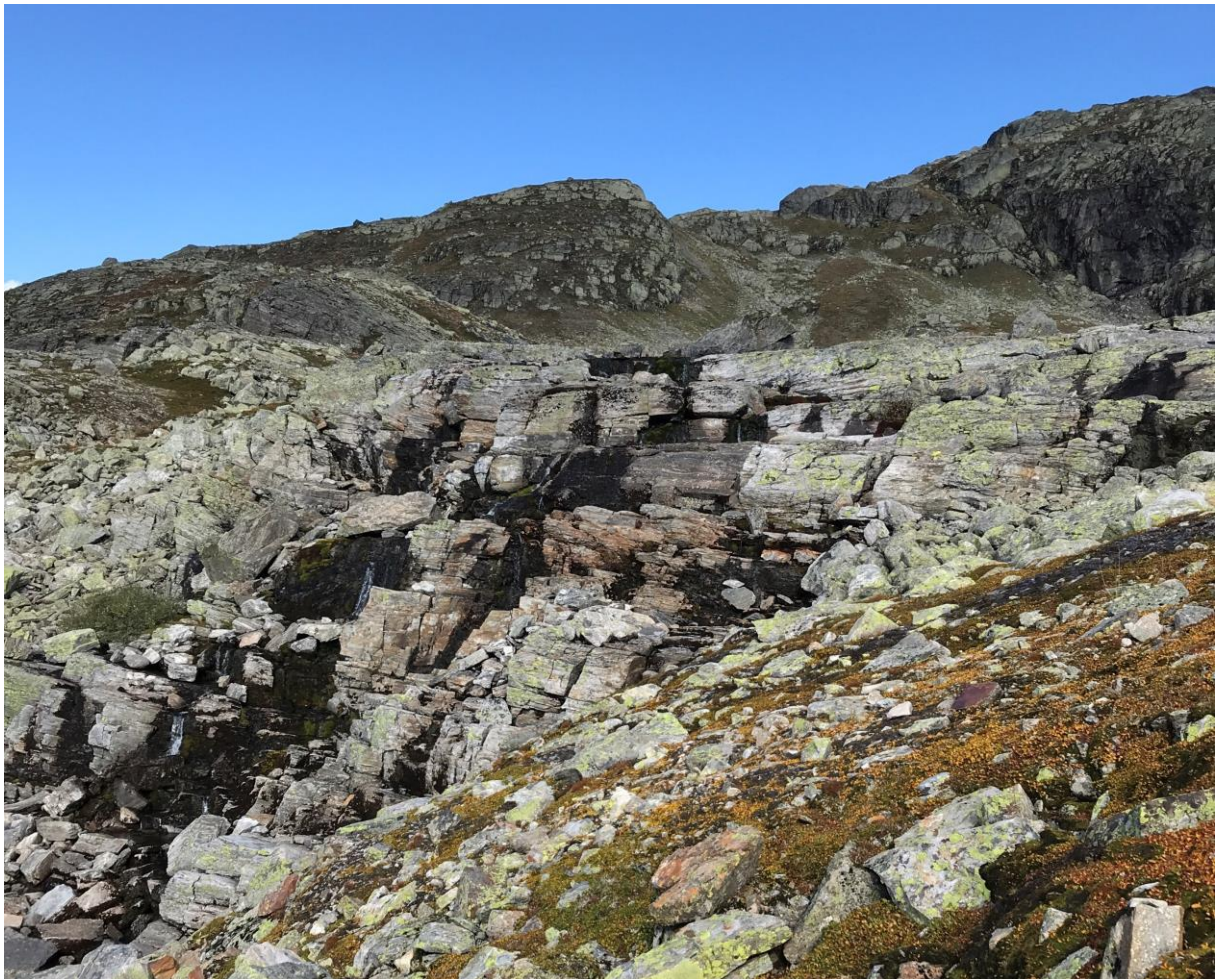
Figure 37. Overview of location 1.7.2. Picture taken towards north-northeast (014º).

5.5 Shaft area and weakness zone 17

The weakness zone 17 was observed close to the gate house as terrain depression. The strike was estimated roughly from two points in the zone. No dip measurements were possible to map close to the gate house because of the lack of measurable rock exposures. However, at GPS location 1.7.3 (Figure 29) the assumed fault plane was measured in the range N110-120ºE dipping 75-85ºS in a valley approximately 20 m wide (Figure 38). At GPS location 1.7.2, 100 m north-northeast of 1.7.3, joints parallel to the weakness zone were measured in the range from N100ºE to N125ºE dipping steeply towards south.

Figure 38. Location 1.7.3 where the fault plane of weakness zone 17 is found. Picture taken towards N284ºE.

Field mapping at Stutakvelven

In Figure 39, all the joint sets mapped are summarised as a pole plot and the relevant joint sets, as discussed earlier, are presented in a rose diagram. All three diagrams are based on the mean values of the measured strike and dip of each set in each location. The details linking the measurements to the associated localities can be seen as great circles in a stereographic projection in Figure 40.
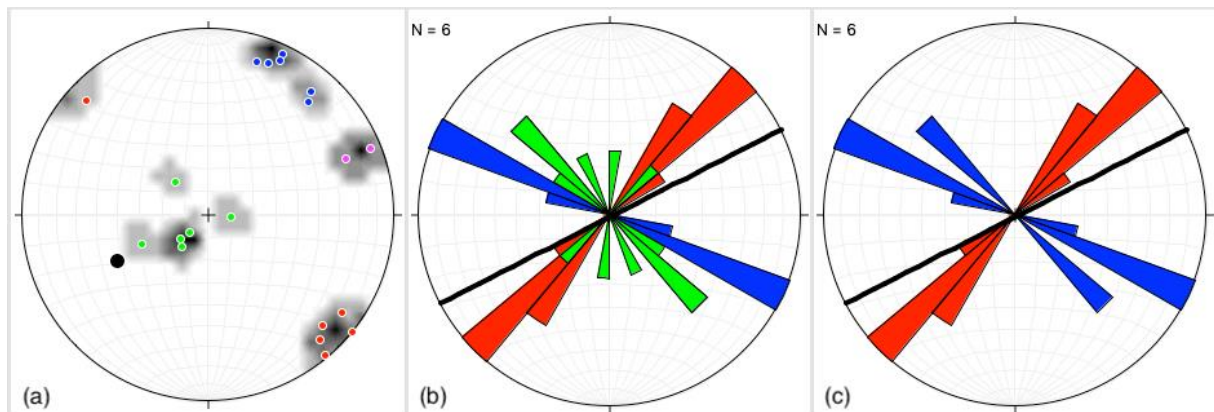
Figure 39. The mapped joint sets at Stutakvelven shaft area, whereas J1 is shown as red markings, J2 as blue, foliation joints as green and J3 as pink (only in (a)). Each pole plot represents the mean value of each set at each location. (a) Pole plot of all measurements mapped, and the shaft presented as a line (black dot). (b)(c) Joint sets considered most relevant for Stutakvelven inclined shaft area. Stutakvelven shaft is presented as a black line. Figure (c) is shown without the foliation joints to present the full extent of J2. The stereographic projection of these joint sets with their associated localities are found in Figure 40.
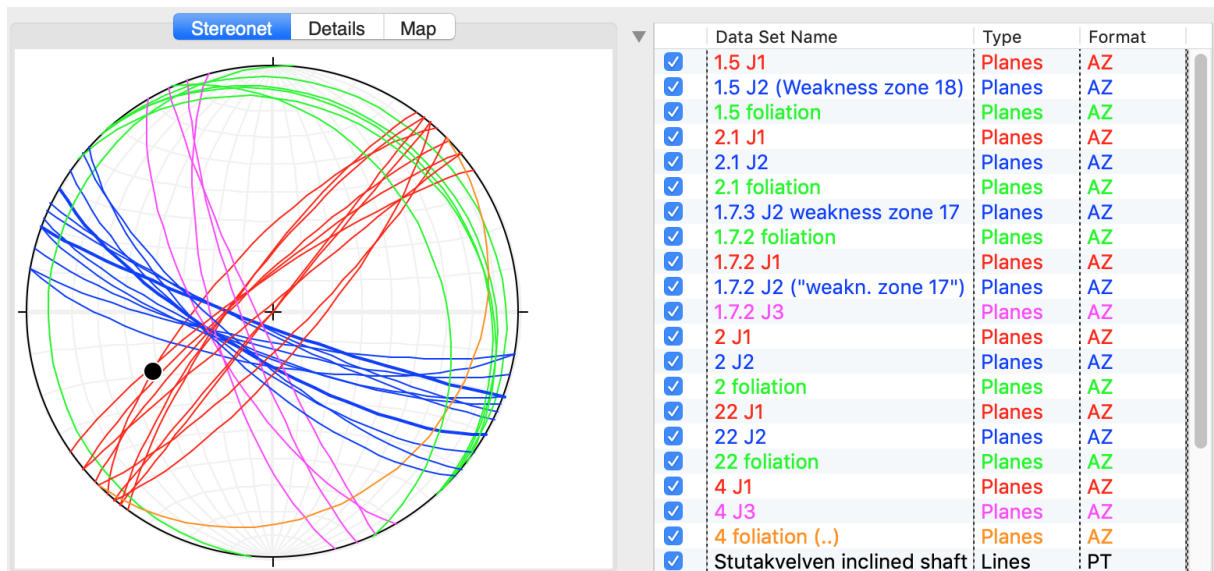
Figure 40. Stereographic presentation of measured discontinuities at Stutakvelven inclined shaft area. The orientation of the shaft is illustrated as a line (black dot). Joint set is 1 shown with red great circles, joint set 2 (J2) is shown with blue great circles (weakness 17 zone with thick blue great circles) and the foliation/foliation joints are shown with green (and orange) great circles.

Field mapping at Stutakvelven

Nilsen and Thidemann (1993) state that in shallow or intermediated tunnels, the axis of the tunnel should be along the bisection line of two predominant joint sets, also avoiding parallelism to other joint sets. This means, optimally for the Stutakvelven shaft, would have been to rotate the axis approximately 20 degrees towards west, to increase the angle between the shaft axis and the predominant joint set, J1 (Figure 39 and Figure 40), giving the axis almost a westward orientation. Nilsen and Thidemann also state that dependant on the nature of the joint surface, it is recommended to choose an intersecting angle between the underground opening axis and the joint direction of at least 25º. Considering the dip of J3, similarly oriented as the plunge of the shaft axis, these angles are around 25-30º potentially causing instability problems along the shaft. However, as discussed, it is possible that the J3 is not present in the shaft area thereby not influencing the stability. In theory, there is also a bisecting line north-northwest to south-southeast of the two predominant joint set, J1 and J2, which means in theory that the shaft could have been considered constructed in this orientation. Too acute angles between the joint sets and the tunnel axis may give stability problems over longer distances in the tunnel, causing the possibility of de-stressed areas leading to slides of blocks and wedges. Therefore, the intersecting angle should be as large as possible.

The field mapping at Stutakvelven area show that three distinct joint sets exists i.e. foliation joints, cross-joints to the weakness zone (J1) and joints parallel (J2) to the weakness zone 17 (Figure 40). The tendency of the strike of the foliation joints ranges from N120ºE to N140ºE and with a gentle dip towards north-northeast. For J1 the strike ranges from N35ºE to N50ºE dipping steeply southeast and northwest. For J2 the strike ranges from N100ºE to N135ºE dipping steeply southwards.

At location 1.7.2, a joint set (J3) dipping steeply southwest was recorded. It corresponds to one of the joint sets mapped by Berdal AS (1978c) in the quarzitic zone, but it is not considered representative for the inclined shaft area based on that the findings are only mapped at this location and location 4 close by (marked as pink joints in Figure 40). The difference in orientation in J3 and J2 may also be due to a slight rotation of joints originally oriented as J2. No further emphasises is laid on this joint set.

5.6 Q-parameters, Q-values and rock support chart

5.6.1 Discussion on the Q-parameters

The Q-parameters and Q-values from the most relevant locations for the inclined shaft area are summarised in Table 6. The estimated values for the weakness zone are presented in Table 7. The RQD value is estimated using a method of measuring intact core bits longer than 10 cm over 1 m length along an axis, performed in three perpendicular directions to capture geological variations. The method is still highly dependent on local variations. In or in relation to weakness zones the RQD may be reduced to no intact core bits (RQD 10), thus, giving a drastically lower Q-value. In communication with Panthi 26 April 2019 the suggested RQD value for weakness zone 17 is 25 based on the sugar-cubical formed rock mass in the zone.

The Jn values in the transition zone and surrounding rocks are estimated by surface investigation and may be regarded as too high compared to the underground situation especially where sub-horizontal joints exist. As mentioned in the Q-system handbook (NGI, 2015), jointing often occur more frequently at the surface, both due to crumbling in schistose rocks and high horizontal stresses (exfoliation joints). Myrvang (1999) mentions that ex-foliation joints seldom occur deeper than 50 m below surface. For instance, at location 1.5, the Jn is given a value of 9, but the foliation joints (counted as joint set number 3), which are surface-parallel, could be considered as a random set or as non-existing (in-depth), giving a Jn value of 6 or 4. On the other hand, this indicates that exfoliation joints do exist in the depth of the failure at Stutakvelven, making the consideration of the Jn value difficult. It is possible that the correct estimation at this location is 3 joint sets plus one random joint set giving the Jn a value of 12, as might be indicated in Figure 30 at the layer marked as "series 2", where cubical rock mass exists. This consideration requires engineering geological experience and is normally verified by observations during excavation.

For the weakness zone itself the rock mass at surface only consists of lose rock fragments, and the Jn could therefore be considered to 20, as suggested in the Jn table (Appendix A) for crushed and earth like material. This value is used in the numerical assessments for the weakness zone in the Hanekleiv road tunnel by Mao et al. (2012). However, for the Stutakvelven weakness zone it is suggested by Panthi in personal communication 26 April that a Jn of 15 is appropriate. This is in accordance with the Jn table for four or more joint set, random heavily jointed "sugar cube" rock masses.

Field mapping at Stutakvelven

The Jr value is mapped to 1 in the transition zone, and this value is also used for the weakness zone. The value fit the Jr table (Appendix A) for smooth, planar surfaces as well as thicker clay zones hindering rock-wall contact during shearing. This description fits both the transition zone and the weakness zone.

The mapped Ja value is most likely not entirely correct for the weakness zone, as the underground condition may be very different in crushed rock regarding the infill material. As mentioned in Panthi (2014) there are thick layers of clay within the weakness zone. This may give a Ja value as high as 10 (Appendix A)

The Jw value in the transition zone and surrounding rock is guessed at based on the presence of several joint sets which may give the rock mass some hydraulic conductivity by joint communication, and that some occasional outwash may occur due to inflow through these joint sets. This assumption puts the Jw in class "B" with a value of 0.66 (Appendix A). For the weakness zone itself it is suggested by Panthi in personal communication 26 April 2019 to use 0.33 for the weakness zone.

The SRF values are based on the parameter table attached in Appendix A. For the surrounding rocks in shallow low stress condition a value of 2.5 is suggested, and for the shallow (< 50 m) weakness zone a value of 5 is suggested. These values are therefore used.

5.6.2 Q-values of adjacent and surrounding rocks

Table 6 summarises the mapped and discussed Q-parameters and values for the locations surrounding weakness zone 17. The rocks in the transition zone are of very poor quality, and the rocks in the surrounding area are estimated to poor to fair quality.

Table 6. Mapped Q-parameters and calculated Q-values Eq. 4 at the Stutakvelven shaft area. The overview of mapped location is found in Figure 29.

Location	RQD	Jn	Jr	Ja	Jw	SRF	Q
1.5 (1.5.1)	50 (80)	9 (4-6)	1	3	0.66	5	0.2 (0.9)
2.1	40	6	2.5-3	1	0.66	2.5	4.4-5.2
22	45	9	2	1	0.66	2.5	2.6
4	70	9	3	1	0.66	2.5	6.1
2	85	6	2-3	1.5	0.66	2.5	5.0-7.4

5.6.3 Q-values of weakness zone 17

For the weakness zone itself, the Q-values are estimated in Table 7 based on the discussion in section 5.6.1. The quality of the rock mass in the weakness zone is extremely poor.

Table 7. Q-parameters and Q-value for weakness zone 17. Q calculated from Eq. 4.

Location	RQD	Jn	Jr	Ja	Jw	SRF	Q
Weakness zone	25	15	1	10+	0.33	5	0.011

5.6.4 NGI support chart

To indicate the rock support needed for the rock mass in the shaft area and in the weakness zone, the empirical Q-chart system is utilised (NGI, 2015). This chart (Appendix B) is based on the rock mass quality and the equivalent dimension of the underground. The equivalent dimension is found from the span or height of the excavation divided by the excavation support ratio (ESR).

$$Equivalent\ dimension = \frac{Span\ or\ height}{ESR}$$

The ESR is found in the ESR table in Appendix A. For hydropower tunnels the ESR is recommended to 1.6, however, with a Q-value equal to or lower than 0.1, the ESR is recommended to 1.0 because of the risk of severe instability problems such as cave-ins.

The mapped Q-values in the surrounding area of the weakness zone and the estimated values for the weakness zone is the basis for the following assessments.

For the weakness zone with extremely poor rock mass quality (Q = 0.011), ESR of 1.0 is used, which gives an equivalent dimension of 6. This indicates support category 7. This category suggests fibre-reinforced sprayed concrete > 15 cm and reinforced ribs of sprayed concrete (RRS II) and systematic bolting with a spacing of 1.0-1.2 m.

For the transition zone with a Q-value of 0.2 - 0.9, an ESR of 1.6 is suggested. This gives an approximately equivalent dimension below 3 (4.2/1.6 = 2.6) where no empirical data exists. Support category 4 and 3 is suggested for the transition zone, whereas support class 4 fits the main part of the transition zone. This category suggests fibre-reinforced shotcrete with a

thickness of 6-9 cm and systematic bolting with spacing approximately of 1.5 m. However, it should be considered if using an ESR 1.0 is appropriate in the part of the transition zone with the lowest quality (Q = 0.2), dependant on the geological conditions in the underground excavation. This would indicate support category class 5.

For the surrounding rock mass, the Q-values are in the range of 2.6-7.4, and with an ESR of 1.6 the support category 1 is suggested, that is, unsupported or spot bolting. The rock mass quality and rock support chart are attached in Appendix B and the indicated support class are marked in green.

5.7 Final remark

The mapped geological structures at Stutakvelven shaft area are fairly consistent with the findings of Berdal (Figure 16). Panthi (2014) presents based on Berdal two main joint sets steeply dipping towards south and east. The absence of the gently dipping foliation joints in the construction drawings of Berdal may be explained by different purposes of the mapping, whereas Berdal focusing on the entire Svandalsflona waterway system while the purpose of this mapping mainly is the Stutakvelven shaft area. This is supported by the absence of the orientation of Stutakvelven inclined shaft in the construction drawings, ergo, not considered decisive for the overall stability. Furthermore, as discussed in section 5.6.1, the sub-horizontal (ex-foliation) joints might be considered non-existing or of less importance for the deeper seated headrace tunnel, although relevant for the shallow area of Stutakvelven inclined shaft. It could also be that mapping in deeper and more inaccessible valleys would have given other measurements.

Lastly, a brief desk-study was conducted post field-investigation, normally conducted pre field-investigations. The study shows that several other possible weakness zones intersects the weakness zone 17 (location 1.7.2 and 1.7.3 in Figure 29), as illustrated in Figure 41. These weakness zones should have been identified before conducting the field investigations in order to evaluate the nature of the zones and their orientations. These zones which are not identified by Berdal might play a role in the stability of the pressure shaft, and possibly a role in the overall stability of the waterway system.
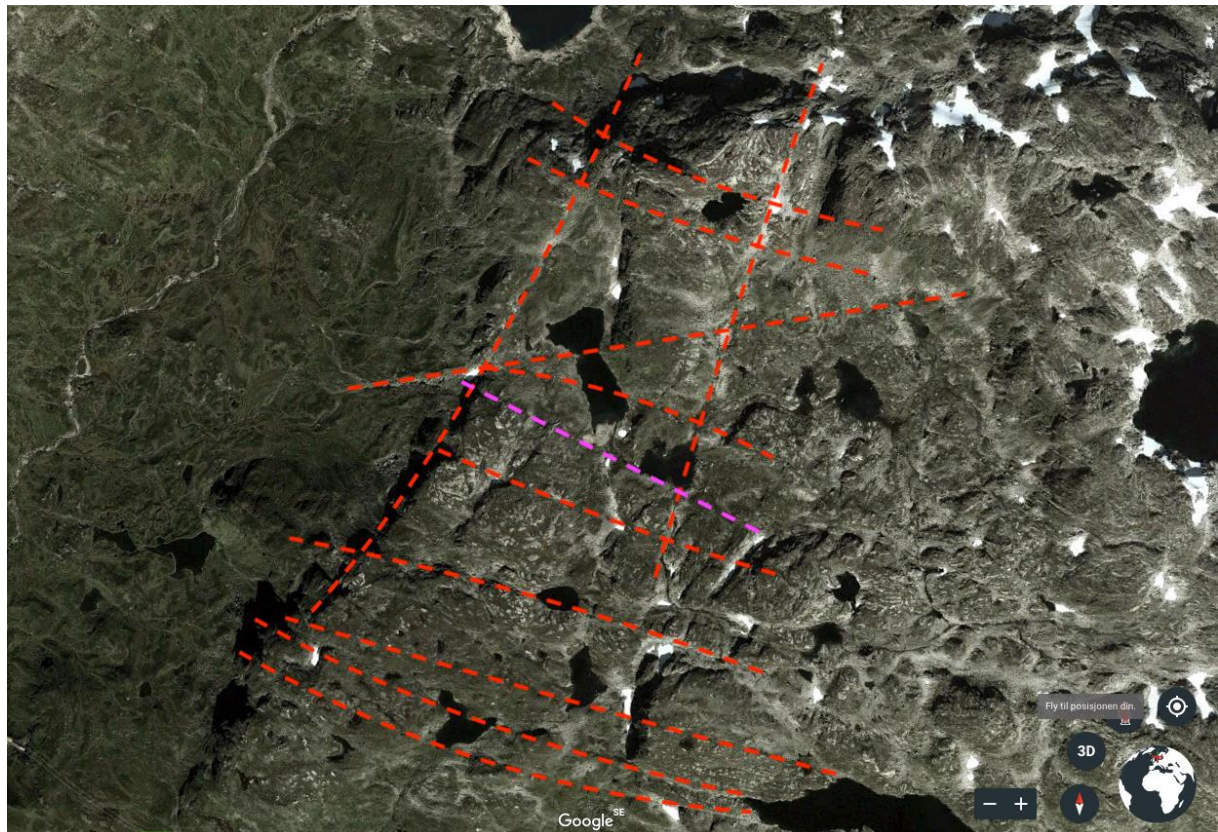
Figure 41. Study of aerial images of the area around Stutakvelven shaft. Several possible weakness zones are identified as terrain depressions, marked with red stippled lines. The weakness zone 17 is marked with a pink stippled line. Modified screen dump from Google earth.

6 Rock mechanical laboratory testing

6.1 Introduction

Several rock laboratory tests have been carried out on the rock samples from Stutakvelven shaft area. The tests were carried out to establish rock mass properties and to use the results as input for further analysis. The results are also intended to be used in the ongoing research on long-term stability in a PhD project. The tests were conducted at the NTNU/SINTEF rock mechanical laboratory in the period from 15 October 2018 to 19 November 2018. The author has been involved in all processes in the preparation of the samples as well as the rock mechanical testing. The Brazil test, point-load test, free swelling test, tilt test, sound velocity test and establishment of the density have been conducted by the author. The coring, the uniaxial strength testing and interpretation of the stress-strain curves have been conducted by Senior engineer Gunnar Vistnes, which also supervised in all of the laboratory testing. In addition, the mineralogical analysis was carried out by Laurentius Tijhuis at the NTNU mineralogical laboratories.

The rock samples that constitute series 1 and 2 were sampled at location 1.5 and the rock sample that constitutes series 3 was sampled at location 2.1. Because of existing joints in the samples, the drill core was reduced from 50 mm to 34 mm for the cylindrical UCS specimen. This also left space for the 50 mm cores intended for the Brazil test which was drilled in a perpendicular direction to the cylindrical UCS specimen.

The UCS cores, Brazil cores and point-load specimens were saturated for approximately 2 weeks and stored for approximately 30 days or more.

6.2 Test standards and procedures

6.2.1 Uniaxial compressive strength test

The UCS test can be conducted to establish the UCS, the Youngs modulus and the Poisson´s ratio. At NTNU, this test is carried out in a RTR-4000 apparatus capable of 4000 kN axial load and 140 MPa confining pressure, in accordance with the International Society of Rock Mechanics test standard (Bieniawski and Bernede, 1979). The apparatus measures the axial deformation by two extensometers and the radial deformation by one extensometer. All data is

continuously logged into datasheets which can be used to generate stress-strain curves for interpreting the rock properties.

A total of 10 UCS cores were extracted from the four field samples. Four cores were extracted from series 1, three cores from series 2 and three cores from series 3. The 34 mm cores were drilled perpendicular to the foliation (strongest direction) and sawed into a length of approximately 2.5 times the diameter. The core ends were grinded to ensure that the contact planes are perpendicular to the length axis, which ensures that the applied load is distributed evenly on the core ends. The core length, diameter and mass were measured with an electronic Vernier calliper weighted with a digital weight with an accuracy of 0.01 g. The diameters were measured at right angles both two times in the upper-height, two times in the mid-height and two times in the lower-height, as specified in the test standard. The average value of these measurements was used for calculating the cross-section as well as for calculating the density of each core. The density was calculated by the weighted mass divided by the calculated volume. The cores that did not meet the requirements of the test standard were used for the point-load testing.

Finally, all cores were encased by a plastic stocking (membrane) prior to the testing, to protect the extensometers from bursts and the specimen from disintegration. During the testing, the load was applied at a constant rate of approximately 0.5 and 1.0 MPa per second, dependent on the specimen peculiarities (controlled by Gunnar Vistnes). For sample 1.1, the axial extensometers were mounted directly onto the specimen, while for the other samples the axial deformation were measured between the metal-pistons in the apparatus.

6.2.2 Brazil test

The Brazil test may be conducted to measure the uniaxial tensile strength. The method measures the strength indirectly, and is based on the empirical conclusion that most rocks fail tensional when put under biaxial stress, whereas one of the principal stresses is tensile and the finite is compressive (ISRM, 1978a). At NTNU, the test is conducted with a hydraulic GCTS Testing System jack capable of 100 kN, and is carried out in accordance with the test standard suggested by the ISRM (1978a). The tensile strength σ_t is calculated by the equation below:

$$\sigma_t = 0.636 \times \frac{P}{Dt} \qquad\qquad \textit{Eq. 6}$$

$$\text{where} \quad P \quad = \text{load at failure (N)}$$
$$D \quad = \text{diameter (mm)}$$
$$t \quad = \text{thickness (mm)}$$

In order to conduct the test, 50 mm cores were drilled parallel to the foliation for the samples constituting series 1 and 2. For series 3, no cores were possible to extract. The cores were sawed in discs approximately 0.5 times the diameter. The intended contact points were marked to ensure that loading occurred perpendicular to the foliation, and the diameter was measured at these contact points. The thickness of the discs was measured in the centre. For series 1, a number of 14 discs were tested and from series 2, a number of 6. The discs were wrapped with masking tape before mounting and inflicting load onto them. The applied load rate was aimed at 0.2 kN per second, and the load at failure was recorded.

6.2.3 Point-load test for anisotropic strength properties

The point-load test can be used to classify the direction-dependent strength properties, as discussed in section 3.2.3. At NTNU, the testing is carried out in a 100 kN GCTS hydraulic jack. The ISRM (1985) suggests classification by the Point Load Strength Anisotropy Index $I_{a(50)}$, which is the ratio between the lowest and highest direction strength values. The strength values are found by the Point Load Strength Index I_s (Eq. 7), which is suitable for 50 mm cores. For other diameters the correction equation should be used (Eq. 8).

$$I_s = \frac{P}{D_e^2} \qquad \qquad Eq.\ 7$$

$$\text{where} \quad P \quad = \text{recorded load at failure (N)}$$
$$D_e^2 \quad = D^2 \text{ for diametral tests}$$
$$= 4A/\pi \text{ for axial tests}$$
$$A \quad = WD = \text{min. cross-section of a plane}$$
$$\text{through the platen contact points}$$

$$I_{s(50)} = F \times I_s \qquad \qquad Eq.\ 8$$
$$where \quad F = (D_e/50)^{0.45}$$

The cylindrical cores which did not qualify for the UCS test, were tested diametric and subsequent axial, to use all the material in the point-load test. The diameter of the cores is denoted D in the diametrical test, and denoted W in the axial test (Figure 42). The length of the

specimen is for the diametrical testing denoted *L* and specified to be more than 0.5 times time diameter, and for the axial testing the length is denoted *D* and specified to be between 0.3 and 1.0 times the diameter (*W*). Therefore, the contact platen points, were placed to give cut-off in lengths between 0.5 – 1.0 times the diameter, to meet the requirements of both tests (ISRM, 1985). The load was applied at a rate of approximately 0.2 kN/s until failure. The length *D* was noted post-failure.
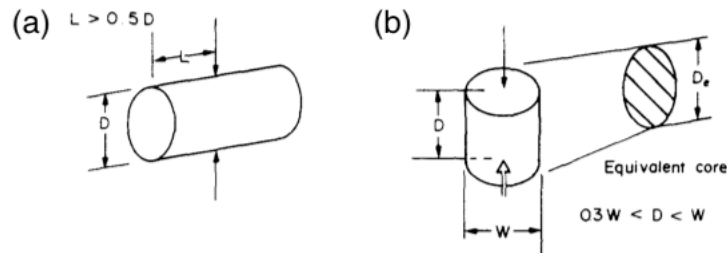
Figure 42. (a) Diametrical test. (b) Axial test. Figures from ISRM (1985).

6.2.4 Tilt test

The basic friction angle can be decided from a 3-core test method, suggested by Li et al. (2017). At the NTNU laboratories, an air-driven tilt machine with a mounted inclinometer inclines the cores, which are placed as pyramids with the two bottom cores locked and the top core free to slide as the machine inclines. The measured friction angle (φ_{3C}) is used to calculate the basic friction angle (φ_b) by the equation below.

$$\varphi_b = \varphi_{3C} - 2°$$ *Eq. 9*

The tests were conducted with the prepared UCS cores, both with dry and wet cores, 10 times for each series, 5 times in opposite length directions. For each round the specimens were slightly rotated to avoid damage to the sliding area. The areas for wet testing and dry testing were separated by pen-markings.

6.2.5 P-wave velocity test

The primary wave velocity can be established by a low frequency ultrasonic pulse technique, as suggested by Rummel and Vanheerden (1978). This method is a non-destructive method, measuring the travel time of electric signal between a transmitter and a receiver, through the specimen. To improve the energy transmission between the specimen, the receiver and the

transmitter, ultrasound gel should be applied to both ends of the specimen. The p-wave velocity (v) is calculated by the equation below.

$$v = \frac{d}{t_p} \; [m/s]$$

<div align="right">*Eq. 10*</div>

where d = distance between transmitter and receiver (mm)

           t_p = travel time (µs)

Before conducting the test, the apparatus was calibrated by measuring the travel time on a uniform test core, with known velocity and length. The tests were conducted on the saturated UCS cores, hence, the tests were conducted normal to the foliation.

6.2.6 Free swelling test

The swelling properties of rock powder may be investigated by a free swelling test. The test quantifies the material volume change, from dry to sedimented state, by the factor *FS* and classifies the activity into four classes, namely non-active, low active, medium active and high active. The test is based on Statens vegvesen (2016) handbook in laboratory methods. Materials with a *FS* below 80 percent are classified as non-active.

The powder for the free swelling test was made from the already tested UCS cores, by crushing and grinding. Firstly, the cores were crushed in a jaw crusher with 5 mm spacing, and then a second time with 2.5 mm spacing in separately rounds for each series. Secondly, 40 g of the crushed material was selected and grinded in a vibratory disc mill for 4 minutes. It was attempted to extract the 40 g material for the grinding in a way so that the selected mass was representative for the jaw crushed material, with both powder and rock fraction of different sizes. Lastly, the powder was dried at 105 degrees for 20 hours.

The test was carried out by measuring 10 mL powder (V_t) in test cylinders which were used to sprinkle the powder into 45 mL distilled water in measuring cylinders. The sedimented volume (V_l) was read off after 1 and 3 days, and the *FS* was calculated by the equation below.

$$FS = \frac{V_1}{V_t} \times 100$$

<div align="right">*Eq. 11*</div>

6.3 Results

6.3.1 Uniaxial compressive strength test

Rock properties obtained from the uniaxial compressive strength test are presented in Table 8 as average values ± the standard deviation. The average values are based on 4 cores for series 1, 3 cores for series 2 and 3 cores for series 3. Core 3.3 was excluded because of odd deformation behaviour and because of the small length to diameter ratio. The specific core information and stress-strain curves are attached in Appendix C.1and Appendix C.2.

Table 8. Results from uniaxial compressive testing.

Series	UCS (MPa)	E-module (GPa)	Poisson's ratio
1	66 ± 17	47,4 ± 12,6	0,42 ± 0,17
2	222 ± 25	49,3 ± 0,9	0,41 ± 0,04
3	197 ± 2	41,2 ± 2,2	0,29 ± 0,02

The failures in series 1 occur along existing joints, which are closely spaced in the sample 1.1.2 and 1.1.1 (Figure 43). The observed failure planes of sample 1.1.1, 2.3 and 3.2 were measured roughly with a protractor with angles, respectively to 19, 21 and 31 degrees to the loading direction. In series 2 and 3, both axial splitting and shearing as well as a combination of these two, apparently occurred.

Figure 43. Cores after the uniaxial compressive test.

6.3.2 Brazil test

In total, 20 discs were tested, all normal to the foliation, of which 14 consisted of series 1 and 6 of series 2 (Figure 44). Two discs from series 1 (sample 1.1.6 and 1.2.8) were excluded from

the results because of failure planes next to the platens contact points. The tensile strength of each disc was calculated by Eq. 6 (Appendix D) and are presented in Table 9 as an average value ± the standard deviation for both series 1 and 2. Note the weathered fracture planes perpendicular to the drilling direction in for sample 1.1.3 and 2.3.

Table 9. Average tensile strength found from Brazil test.

Series	Tensile strength σ_t (MPa)
1	19,0 ± 4,3
2	17,3 ± 2,5
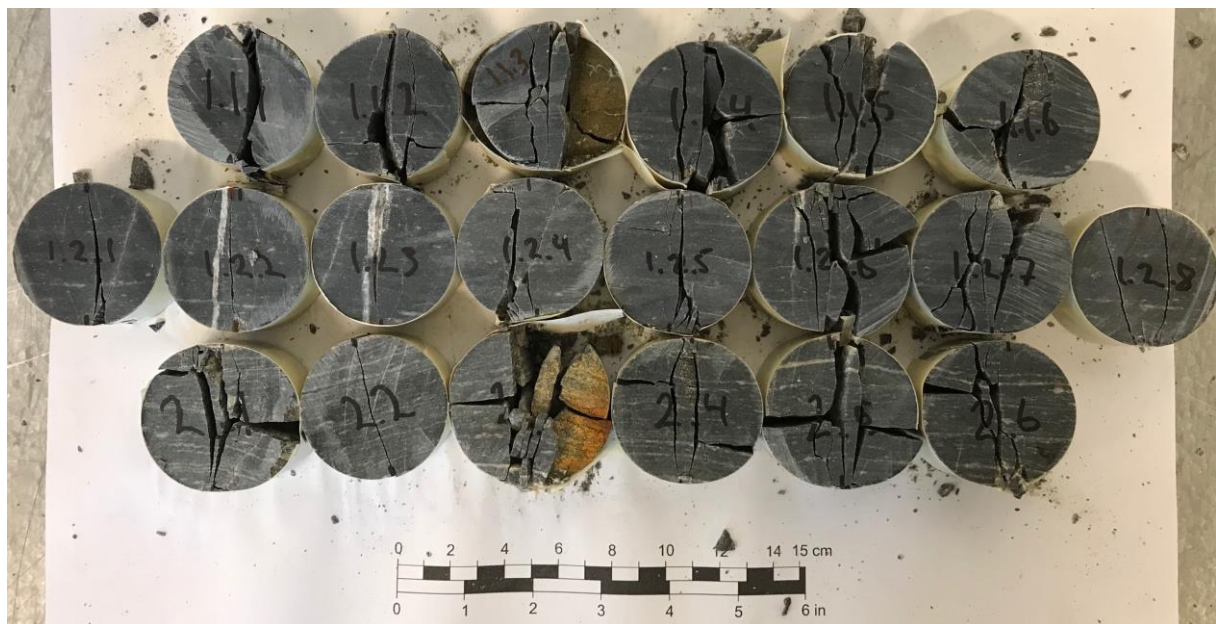
Figure 44. Discs after the Brazil tests. Note the weathered planes normal to the viewing direction.

6.3.3 Point-load test

For the point-load test, 71 tests were conducted, of which 66 were found to be valid from the test standard. From series 1, a number of 6 diametral (d) tests, parallel to the foliation, and a number of 8 axial (a) tests, normal to the foliation, were valid. In series 2, 16 diametral and 14 axial tests were considered valid, and for series 3, 11 diametral and 11 axial tests were found to be valid. The Point Load Strength Index (I_s), calculated by Eq. 7 and Eq. 8, and the Point Load Strength Anisotropy are presented in Table 10 as mean values ± the standard deviation.

Before calculating the mean values, the highest and lowest values in each test were excluded in series 1, and the two highest and lowest in both series 2 and 3 were excluded, in accordance

Rock mechanical laboratory testing

with the ISRM (1985) test standard. Note the similar results in series 1 and 2. All measurements and calculations are attached in Appendix E.

Table 10. Average results of point-load strength.

Series	Mean $I_{s(50)\_d}$	Mean $I_{s(50)\_a}$	$I_{a(50)}$
1	9,3 ± 1,9	15,0 ± 2,0	1,6
2	8,3 ± 0,6	14,5 ± 1,7	1,7
3	3,0 ± 0,5	10,6 ± 0,8	3,5

6.3.4 Tilt test

The tilt test was conducted with 9 cores, 3 from each series. For series 1, core 1.1.2 was excluded from the testing because of the surface depression due to jointing. In series 3, the top-core, which is the one to slide, was significantly shorter than the other two cores (Figure 43). The mean values of the basic friction angles were calculated by Eq. 9 and are presented in Table 11 as mean values ± the standard deviation. Full information on the results is attached in Appendix F.

Table 11. Average mean values of basic friction angles.

Series	Mean φ_b (dry)	Mean φ_b (wet)
1	29,8 ± 1,4	31,6 ± 1,1
2	33,9 ± 1,4	33,7 ± 0,9
3	33,2 ± 2,1	33,4 ± 1,1

6.3.5 P-wave velocity test

The velocity test was conducted on all the cylindrical UCS cores. The p-wave velocities were calculated by Eq. 10, based on the measured travel time and the core length (Appendix C.1). The mean velocity for each series is presented in Table 12.

Table 12. The mean calculated p-wave velocity for the UCS cores.

Series	P-wave velocity (m/s)
1	5562
2	5502
3	3061

6.3.6 Free swelling test

The free swelling test results are presented in Table 13. According to the used test standard (Statens vegvesen, 2016), rocks from all three series are classified as non-active (FS < 80%).

Table 13. Results from free swelling test where the FS is calculated from Eq. 11.

Series	FS (%)
1	75 - 80
2	75
3	75 - 80

6.3.7 X-ray diffraction analysis

The X-ray diffraction analysis is attached in Appendix G, and the mineral composition suggested by Laurentius Tijhuis are presented in Table 14. In the table, plagioclase substitutes albite, mica substitutes muscovite or phlogopite and alkali feldspar substitutes microcline.

Table 14. Interpretation of mineral composition from the XRD analysis.

Mineral (-group)	Series 1 (%)	Series 2 (%)	Series 3 (%)
Quartz	42	35	62
Alkali feldspar	31	28	15
Plagioclase	21	30	6
Mica	5	6	15
Chlorite	1	1	2
Sum	100	100	100

6.4 Discussion on the results

6.4.1 Introduction

The results indicate the compressive strength and tensile strength of the samples, their strength anisotropy, p-wave velocity, density, mineral composition and friction angle. These properties are discussed in the following. Based on the findings, series 1 and 2 are considered as one lithology in the further assessments, and series 3 as another. Because of this, series 3 is discussed separately.

When carrying out laboratory testing there are several factors to consider. For example, for both the UCS and the Brazil test, too few specimens were tested according to the test standard. This may affect the mean value. The diameter of the Brazil cores was only measured once, and not twice at right angles as suggested by the test standard. During loading, the load rate was at times considerably higher than the recommended 0.2 kN/s for both the Brazil and the point-load test. The swelling test in particular is difficult to carry out correctly, for instance, the measured volume can be affected by air pockets as well as the degree of compaction before sprinkling the rock powder into a measuring cylinder. More importantly, the field samples are selected and does not necessary represent a random or a representative selection of the in-situ conditions.

6.4.2 Rock strength

Based on the UCS test, the specimens of series 1 and 2 can be classified by the ISRM (1978b) in the strongest direction as respectively strong and very strong. The point-load strength further indicates a very high strength perpendicular to the foliation, and high to very high strength parallel to the foliation (Nilsen et al., 2000). As discussed in section 3.2.1, the results of the UCS should be adjusted using *Eq. 1*, to compensate for the impact the size has on the strength.

The UCS found for series 1 is approximately one third of the strength found for series 2. The point-load strength on the other hand, indicates that these two series have similar strength. The conflicting strength indications in these two test methods can be explained by the unfavourable joint set in the UCS cores in series 1, seen in Figure 45, which is absent in the smaller specimens. This coincides with the Hoek-Brown illustration (Figure 13), where a specimen goes from intact rock to intact rock with a discontinuity as the sample size increases. This explanation is substantiated by the visual observation that the fracture in sample 1.1.2 has gone through an older, dark-greenish coated surface with fine grains, which easily peeled off. Similar discoloured weathered discontinuity planes were observed in both series 1 and 2 in the Brazil test discs. The tensile strength for these rocks is high.
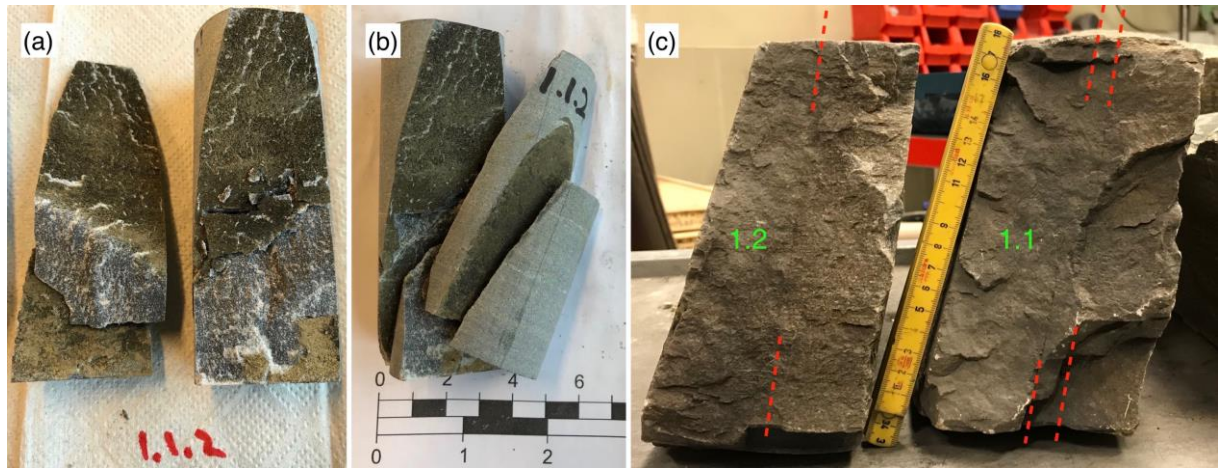
Figure 45. (a) and (b) show the unfavourable joint sets and spacing in rock sample 1.1 and 1.2. Some degree of weathering along these joint planes may be seen as discolouration of the surface. (c) shows the discontinuities pre-drilling. The shape of the field samples indicates the joint sets measured at location 1.5.

During the testing it was observed that the saturation occurred in the outermost parts of the specimens, as well as where the joints existed. After two weeks of saturation, the mass increase of the specimens in series 1 and 2 were only between 0,09 and 0,17 percent (Appendix C.1). The rocks can therefore be considered as highly impermeable and/or non-porous.

Figure 46. Rock sample which constitutes series 3.

Series 3 may also be classified as very strong in the strongest direction, that is, normal to the foliation. However, the strength parallel to the foliation is only medium, which makes the tested rock samples highly anisotropic, according to the point-load classification. The series 3 has twice the mica content as series 1 and 2, approximately 15 percent, and twice the chlorite (Table 14). The specimen in this series is not as stiff as in the two other series, with almost 10 GPa lower E-module and 0.1 lower Poisson´s ratio. This specimen is also more affected by saturation. This series has a density of approximately 2.65 g/cm^3 and the sample brought from the field is shown in Figure 46.

6.4.3 Lithology

The XRD analysis indicates a similar mineral composition for both series 1 and 2. According to the XRD analysis and the swelling test, no swelling minerals are present. The content of quartz and feldspar constitutes more than 90 percent of the mineral content in both series (Table 14).

The grain size is fine to medium for series 1 and medium for series 2 (Nilsen et al., 2000), measured around 0.2 mm, and series 2 consists of more frequently occurring bands of quartz/feldspar (Figure 43 and Figure 44). These two series have moderately strength anisotropy (Table 3), and this anisotropy may be explained by the preferred mineral orientation and the presence of flaky minerals (Panthi, 2006). The mean values of the measured density are found to be approximately 2.65 g/cm^3 (Appendix C.1). The asperities and properties of the specimen surface gives series 1 a friction angle of approximately 30 degrees and series 2 a friction angle of 34 degrees.

As for classifying the specific rock type, series 3 is considered as a quartz-mica schist, based on the schistose fabric, the content of quartz and mica as well as the high anisotropy (Nilsen et al., 2000), in addition to that the local area is marked as quartz-mica schist, according to NGU (Figure 29).

Series 1 and 2 are more challenging to characterise. The rocks are sampled within an area marked as quartzite by NGU (Figure 29). The area is also marked by Berdal (Figure 16) as a thrust plane which most likely has influenced the rock mass in the area. Furthermore, the area consists of igneous rocks such as rhyolite and diorite which corresponds well with the XRD analysis if classified in accordance with Streckeisen (1980). At first, it was expected to observe

phyllite in the area, which led to the search of a fine-grained, darkish rock. This was found at location 1.5. However, closer investigations of the samples led to the findings of lack of luster, very high strength and stiffness, only moderately anisotropic strength properties and a fabric partially more on the macroscopic scale than the microscopical and the appearance of deformation bands. This witnessed of a higher degree of metamorphism in the rocks, and that the strength corresponded better with the Norwegian gneisses found in Høien et al. (2019). The assumed phyllite is marked as an underlaying sub-horizontal layer which may be found westwards and southwards of the sampling location.
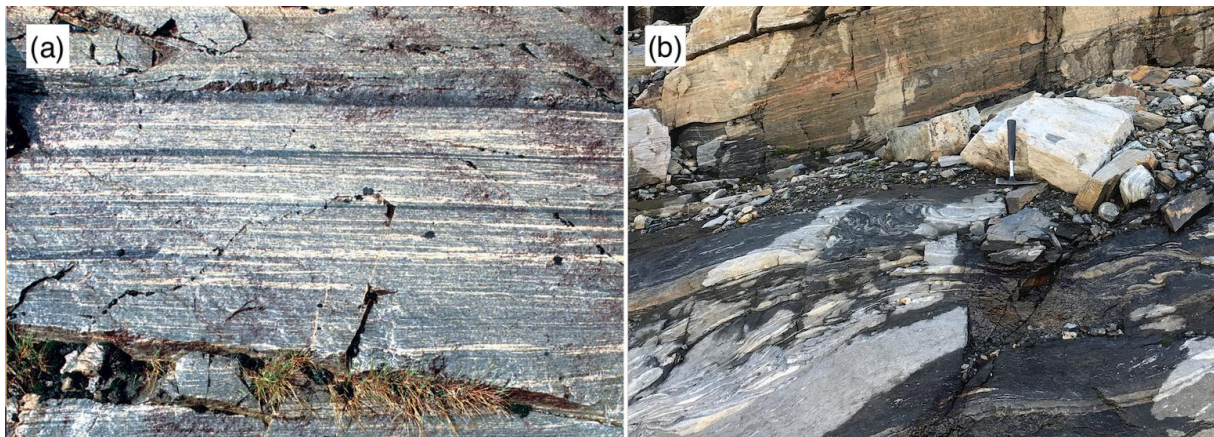
Figure 47. (a) Migmatite gneiss found in Fossen et al. (2013). (b) Location 1.5 where sampling of series 1 and 2 was collected.

Series 1 and 2 show some variations, whereas series 2 is coarser grained and consists of more distinct light-pink bands of feldspar/quartz, as indicated in Figure 47b (in the top) and Figure 43. The fabric resembles the fabric seen in the Norwegian migmatite gneiss (Figure 47a) found in Fossen et al. (2013), indicating high metamorphosis. This fabric also reminds of the banded gneiss seen in the report from NGU (2015), which in fact is recorded in the area by NGU (Figure 29). However, the grain sizes are very roughly found to be around the border of fine to medium grained, varying around 0.2 mm, and therefore it should be considered if the sampled rock should be considered as a kind of schist, as also mapped by NGU at several places.

Because of the local variations in the rock mass, it is hard to classify an area as one specific rock type. However, it is believed that the collected samples should be classified as banded gneiss for the series 2, substantiated by the tectonic stratigraphy with the overlaying gneisses (Figure 16), and as mylonite for the series 1 as a result of the deformation in the area which may be seen as faults and folds of small and large scale.

6.4.4 Final remark

To summarise, it is found for series 1 that the discontinuities have a very small spacing and that they control the strength. The RQD mapped in field could, based on this, be significantly lower than first estimated. For series 2 and 3, the discontinuities have larger spacing and the intact rock specimens have a very high UCS. For the further stability assessments, the discontinuities are of most interest. The conducted investigations reflect some of the geological varieties in the Stutakvelven shaft area. The series 1 may reflect the situation in or close to the weakness zone intersecting the Stutakvelven shaft area, that is, the transition zone. Series 2 and 3 may reflect the situation in the surrounding rock of the weakness zone.

7 Stability assessment of Stutakvelven

7.1 Introduction

The stability assessment is carried out as a numerical analysis using the program RocScience RS2 in order to understand more on how the failure at Stutakvelven could occur. The presented models are cross-sections of the tunnel within the weakness zone, the adjacent rock mass and the surrounding rock mass. For the analysis the generalised Hoek-Brown criterion is used under the assumption that the rock masses in the failure zone are heavily fractured to the extent that the behaviour is considered isotropic. The post-failure behaviour is considered elastic-plastic or soft-straining (Trinh and Jonsson, 2013).

The input data are mainly obtained from the GSI parameter calculator based on the field investigations and the laboratory testing. The input parameters are to some extent adjusted based on theory, guidance and by trial and error. How the parameters are adjusted is discussed continuously.

The approach of the numerical modelling for rock masses with one well-defined discontinuity is discussed in Marinos et al. (2007). The Hoek-Brown criterion may be applied to the rock mass as a whole and the weakness zone superimposed as a significantly weaker element. The weaker element can be modelled by selecting a GSI value in the lower part of the GSI chart to reflect the bad rock mass quality in a weakness zone. This approach is considered as a continuum model. Other approaches mentioned is shear testing of soft clay fillings which is not executed in this thesis. The chosen approach simplifies the model since no joint sets and other discontinuities are used directly and the method is considered as a pragmatic approach in this case.

7.2 The setup for the weakness zone

7.2.1 Excavation boundary

The intended excavation is constructed after the drawings of Berdal, with a width of 4.2 m, and with a height of 3.3 m giving a cross-section of approximately 12.8 m^2 (Figure 17). The actual excavation is approximately 6 m high and 6 m wide and is shaped after the support construction drawings by Berdal (Figure 18). The cross-sections are located from 1215 m.a.s.l after Panthi (2014) giving an overburden of approximately 38 m for the intended excavation and 35 m for

the actual excavation (Figure 48 and Figure 49). The excavations are executed in one stage and all cross-sections are looking upstream.
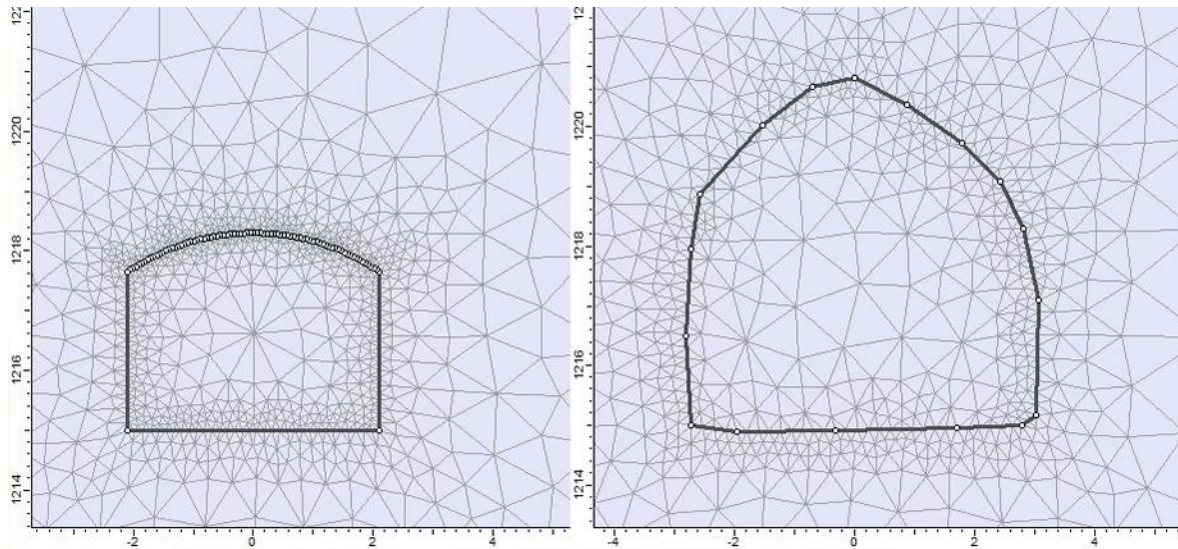
Figure 48. Intended cross-section compared to the actual cross-section in the weakness zone. Excavation boundaries based on the construction drawings in Figure 19.

7.2.2 External boundary

The external boundary is fixed in accordance with the RocScience RS2 tutorial for an open surface model, that is, the surface restraint is free, the side edges are fixed in x-direction and the lower edge of the boundary is fixed in y-direction. In addition, the two lower corners are fixed in both directions (Figure 49). For the mesh, a graded type with 3-noded triangles is used, with 110 nodes and with a gradation factor of 0.1. The external boundary is set to be more than 5 times the excavation width, adapted from Trinh and Jonsson (2013). The topographic surface is constructed from a profile graph plot in ArcMap, marked as a blue line in Figure 29, looking upstream the shaft.
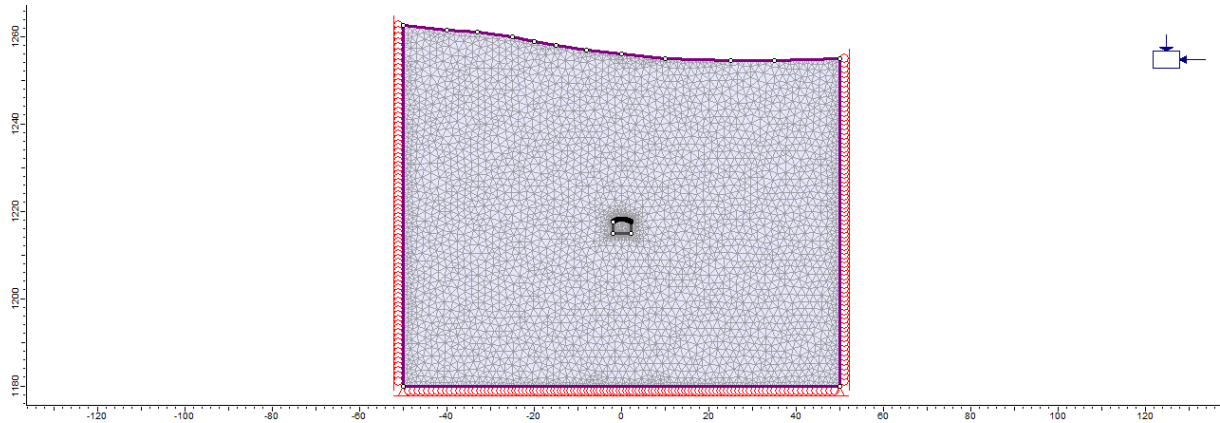
Figure 49. External boundaries of the set-up. Topographic surface constructed from profile graph plot (location of cross-section in Figure 29).

7.2.3 Rock mass parameters

The Hoek-Brown constants are estimated using the parameter calculator in RS2. The input values for the calculation are based on the original GSI chart found in Li (2018). As a first indication of the parameters for the weakness zone the lower values representative for a crushed and poorly interlocked heavily broken rock mass with very poor surface quality are chosen. This give m_b/m_i, s and a values of 0.040, 0 and 0.60 and deformation modulus, Poisson's ratio and GSI values of 1000, 0.3 and 10 (Appendix H). The s value used during modelling was approximately $5 * 10^{-5}$.

The GSI value for the weakness zone is set to 16, based on the Q-assessments during the field investigations. Using the relation suggested in Barton 1995 referred in Barton (2002) a Q-value of 0.011 gives RMR of 21, and the relation GSI = RMR – 5 (Barton and Grimstad, 2014) gives GSI = 21 – 5 = 16.

$$RMR \approx 15 \times \log(0.011) + 50 = 20.62$$

Regarding the rock strength Hoek and Brown (1997) suggest as a general guidance for tectonically disturbed rocks that the lowest obtained strength values should be used. In Figure 10, Panthi (2006) illustrates how the intact rock strength may be reduced significantly from weathering, down to almost zero strength. As stated in Panthi (2014) the rock mass in the weakness zone at Stutakvelven was intensively fractured and had extremely weak quality. It is assumed that this highly fractured rock mass is significantly weathered, and that substantial amount of clay occurs. The intact rock strength is therefore reduced with 80-90% percent of the

measured strength, giving a first input value of approximately 25 MPa (σ_{ci}), however this was later adjusted to 27 MPa as discussed in section 7.4.1. The reduction of intact rock strength is verified during personal communication with Panthi 26 April 2019.

The global rock strength found by RocLab in RS2 using input parameters from Table 15, is approximately 1.9 MPa. This equals the rock mass strength (σ_{cm}) calculated by the equation of Barton (2002) and is somewhat lower than the strength calculated by the equation suggested by Panthi (2006). These equations are found in Table 2 and the calculations are shown below.

$$\sigma_{cm} = 5\gamma \times \left(\frac{\sigma_{ci}}{100} \times Q\right)^{\frac{1}{3}} = 5 \ x \ 2.65 \ x \left(\frac{27}{100} \times 0.011\right)^{\frac{1}{3}} = 1.9 \ MPa$$

$$\sigma_{cm} = \frac{\sigma_{ci}^{1.50}}{60} = \frac{27^{1.50}}{60} = 2.3 \ MPa$$

The intact rock constant m_i is set to 10 in the GSI parameter calculator. This gives a m_b of 0.42 which corresponds well with the m_b/m_i of 0.04, and it also corresponds well to weakness zone material. Each of the rock types have a large interval resulting in large variations in possible values. Since the confining pressure increases downwards, the relative strength also increases downwards, and the relatively increase in strength can be controlled with the m_i value. A higher m value gives a higher failure envelope in the Hoek-Brown criterion. A lower m value leads to further failure deeper in the rock mass below the tunnel, which is also a possible scenario, although not assumed and therefore not modelled in the following.

The modulus ratio (MR) found by laboratory testing is approximately 200 for the intact cores in series 2 and 3 (Marinos, 2019).

$$\frac{E_i}{\sigma_{ci}} = MR$$

This gives E_i of 5400 MPa for the estimated strength (σ_{ci}) of 27 MPa which corresponds to the material in the weakness zone. The intact rock modulus is the basis for the calculation of the rock mass deformation modulus (E_m). Utilizing the correlation equations by Hoek and Diederichs (2006) and by Panthi (2006), the rock mass modulus is approximately estimated to

respectively 200 MPa and 470 MPa. In discussions with supervisor the first mentioned is found to be too low and therefore 470 MPa is used. The deformation modulus impacts the displacement drastically. The equations are found in Table 4 and the calculations are shown below.

$$E_{rm} = 5400 \, MPa \left(0.02 + \frac{1 - 0/2}{1 + e^{((60 + 15*(0) - 16)/11)}} \right) = 205 \, MPa$$

$$E_m = \frac{1}{60} \times 5400 \times 27^{0.5} = 468 \, MPa$$

The density of the rock mass is set to 2.65 g/cm3, which may be too high since fractures and weathering reduces density. However, the sensitivity analysis of the parameter shows that it does not change the occurrence of failures significantly. The density was tried down to 2.22 g/cm^3. The default Poisson's ratio in RS2 is 0.25, the ratio is however lowered to 0.15 to coincide better with the value used in Basnet and Panthi (2018).

The disturbance factor (D), if used, is recommended to be limited to an area of maximum 2-3 m around the excavation periphery (Hoek et al., 2002). In this model, the D factor is not applied because of the surrounding rock of the excavation has already completely failed, and because of uncertainty connected to establishing the boundary of the damaged zone. It is however noted from the sensitivity analysis that the D factor reduces mb, s and the calculated E_m. In addition, for the sink hole to occur the rock mass between the tunnel and surface, and not only the area surrounding the excavation, must be of bad quality. This consideration makes the D factor of less importance in this 2D analysis.

The assumed behaviour of the rock mass is a hybrid between the elastic-plastic behaviour and soft-straining (section 3.8.3). Therefore, some residual values are used. The reduction in the values are significantly lower than for instance in Trinh and Jonsson (2013) because of the low quality rock mass in the weakness zone.

Hoek and Brown (1997) suggest using a dilation angle of 0 in weak rock mass quality. The use of dilation reduces the yield zone surrounding the tunnel significantly and it less likely with a failure between the tunnel and surface. It is therefore kept at recommended 0.

7.2.4 Rock stresses

The in-situ stresses are influenced by several factors as highlighted in section 3.6. For the numerical modelling the gravitational stresses and to some extent the tectonic stresses are considered. In lack of in-situ measurements, the magnitude and orientation of the stresses may be guessed based on relevant theory. The in-situ stresses related to a weakness zone are illustrated in Figure 50 by Li (2018). This indicates no or little rock stresses in the crushed zone, and a peak in the stresses surrounding the zone. This is caused by the difference in the material stiffness, whereas the material in the weakness zone is soft and compressible making the rock stresses deflect into the stiffer adjacent rock mass (Li, 2018). A weakness zone functions as a free surface and the stresses in the surrounding rock will be re-oriented parallel to the weakness zone surface, that means, the minor principle stress acts normal on the plane and the major principles stresses parallel to it. In a shallow weakness zone, the stresses are influenced by both the topographic free surface and the weakness zone surface.
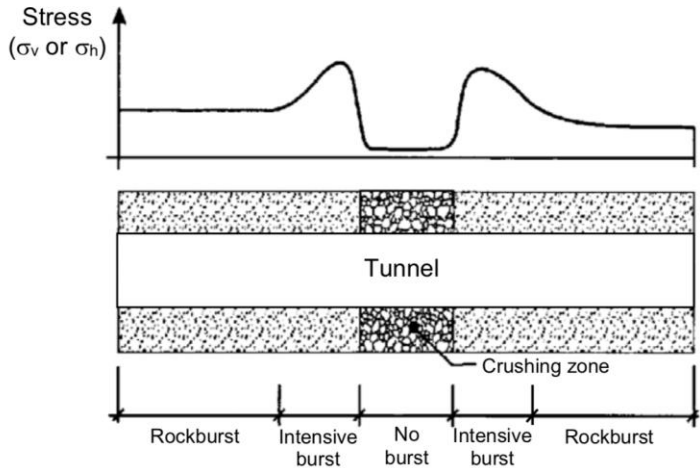
Figure 50. Distribution of in-situ rock stresses by Li (2018).

The model is simulated with gravitational stress (actual ground surface conditions) and with a horizontal-vertical factor, *k,* of 1.5, and no other horizontal component. The values are discussed with and approved by Panthi 26 April 2019. The major principle stress in this case is oriented horizontally and parallel to the weakness zone surface, that is, oriented approximately west-northwest to east-southeast acting normal to the tunnel walls. The vertical stress component is calculated from *Eq. 2* giving approximately stress condition of 1 MPa, which coincides well with the model pre-excavation.

Stability assessment of Stutakvelven

$$\sigma_z = 2.65 * 9.81 * (35 \text{ to } 38) = 0.9 \text{ to } 1.0 \, MPa$$

7.2.5 Summary of the input parameters for the weakness zone

Input parameters for the rock mass within the weakness zone are presented in Table 15.

Table 15. Input parameters for the numerical modelling of the weakness zone at Stutakvelven Shaft.

Parameter calculator		Field and body stress model	
σ_{ci} (MPa)	27	Poisson's ratio	0.15
GSI (residual)	16 (11)	Unit weight (MN/m³)	0.0265
m_i (residual)	10 (8)	Field stress type	Gravity
MR	200	Eff. stress (horiz/vert in plane)	1.5
Disturbance factor	0	Eff. stress (horiz/vert out-of-plane)	1.5
Dilation	0	Horiz. stress (in plane) (MPa)	0
		Horiz. stress (out-of-plane) (MPa)	0
Hoek-Brown constants			
m_b	0.498 (0.333)		
s	$8.84*10^{-5}$ ($5.07*10^{-5}$)		
a	0.5571 (0.5798)		
Generalised Hoek-Diederichs			
E_i (MPa)	5400		
E_{rm} (residual)(MPa)	470		

The input parameters for the concrete lining are presented in Table 16. The lining is based on the construction drawing (Figure 18) where the C25 quality concrete with a thickness of 0.5 m is suggested.

Table 16. Lining properties of cast concrete.

Thickness (m)	0.5
Youngs modulus (MPa)	30000
Poisson's ratio	0.15
Compressive strength (MPa)	30
Tensile strength (MPa)	3
Material type	elastic

7.2.6 Summary of the input parameters for the adjacent and surrounding rock mass

Weakness zones are areas of weaker rock mass quality relatively to the adjacent and surrounding rock mass. The relatively high-quality rocks mapped in the field are used as input parameters and summarised in Table 17. A brief model is carried out. For the adjacent and surrounding rock mass it is laid no emphasise on possible changes in the stress regime. The values found for the adjacent rock mass are based on mapping at location 1.5 and for the surrounding rock mass the approximate mean value from Table 6 is used. The procedure for calculating values is similar to the ones used for the weakness zone.

Table 17. Input parameters used for the GSI calculator for the adjacent rock and the surrounding rock mass of the weakness zone.

Parameter calculator (adjacent / surrou.)		Field and body stress model	
σ_{ci} (MPa)	66 / 190	Poisson's ratio	0.25
GSI (residual)	35 (20) / 55 (35)	Unit weight (MN/m^3)	0.0265
m_i (residual)	10 (8)	Field stress type	Gravity
MR	200	Eff. stress (horiz/vert in plane)	1.5
Disturbance factor	0	Eff. stress (horiz/vert out-of-plane)	1.5
Dilation	0	Horiz. Stress (in plane) (Mpa)	0
		Horiz. Stress (out-of-plane) (Mpa)	0

This model is carried out with the purpose of underlining that the weakness zone actually is a weakness zone, and to briefly assess the stability conditions in the adjacent and surrounding rock mass. This has led to the values being roughly estimated, for instance, the anisotropy and scale factor are not considered. Although, a brief sensitivity analysis for the UCS of the surrounding rock was carried out (down to 53 MPa) without yielding.

7.3 Simulation of the cave-in at Stutakvelven

7.3.1 Excavation method and lining method

After completing the setup, the excavation for the intended cross-section was used to estimate the yielded zone, indicating the cross-section of the actual tunnel condition during construction. At this second stage, two models followed: One without any lining to simulate how the failure may have developed and one to simulate the lining which kept the tunnel stable for 30 years. The yielded zone around the excavation without lining was used for another excavation

boundary representing step 3 and 4. This third and last excavation boundary was only modelled without any support, because it was not considered likely that the rock mass could fail to this extent without the lining already being failed. By adding one extra stage to the third excavation the failure developed all the way to the topographic surface.

Two models of the applied lining were simulated: One with the concrete lining suggested by Berdal similar to the rectangular cast concrete, and one with full concrete lining around the whole periphery (Figure 51). For the rectangular lining a structural beam element with two joints is used to simulate the horizontal top plane. The plane is given the same properties as the lining itself, that is, 0.5-m-thick C25 grade concrete.
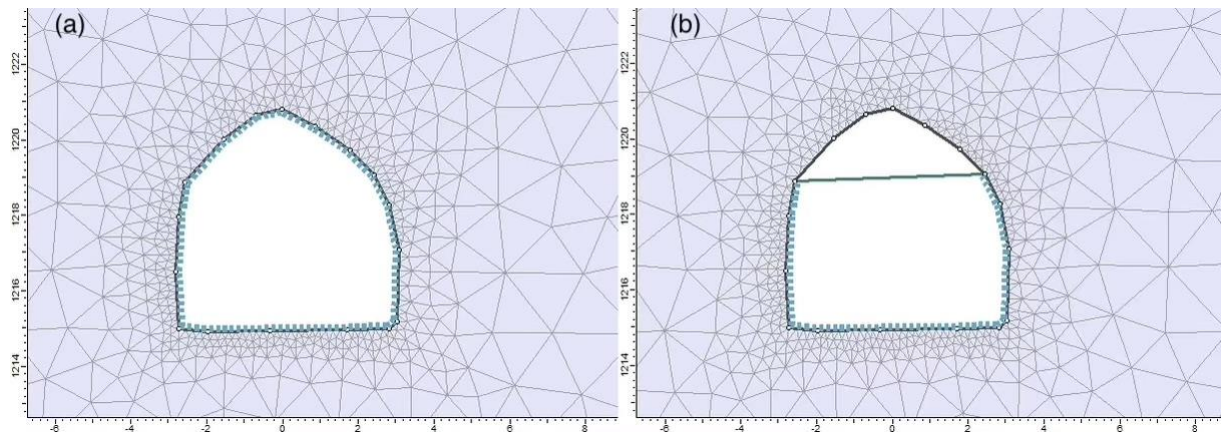
Figure 51. (a) Full concrete lining. (b) Imitated lining from the construction drawing by Berdal (Figure 18).

7.3.2 Development of the failure in the weakness zone

The development of the failure is illustrated in a four-step-model (Figure 52). The first step (a) is the intended cross-section. The second step (b) indicates the situation after excavation through the weakness zone, that is the actual cross-section. Step 3 (c) indicates the situation as the rock mass around progressively yields, simulated by another excavation equal to the yielded zone in step 2. The last step (d) indicates total failure of the rock mass, using the same excavation with one additional stage.
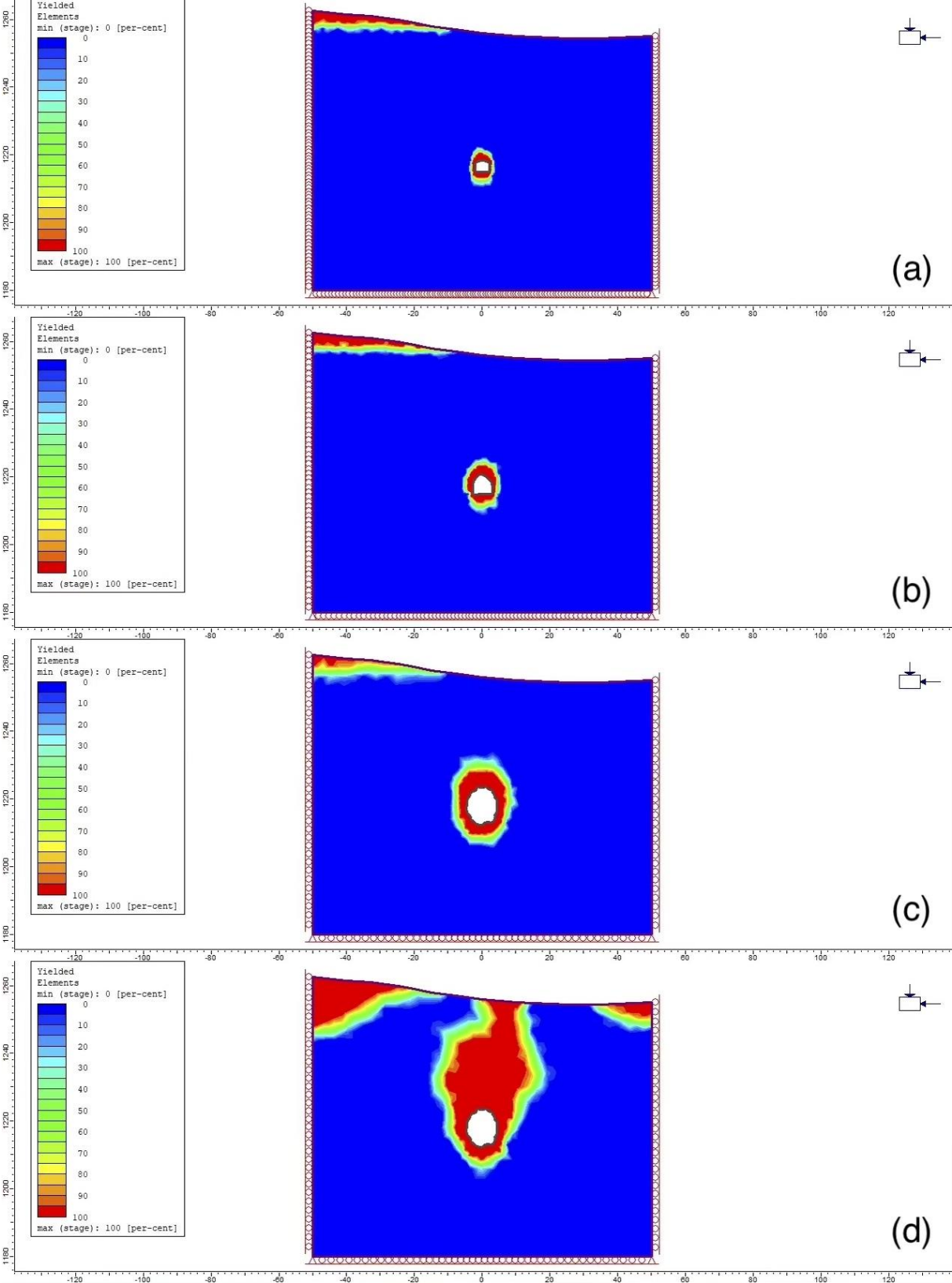
Figure 52. The four-step-model showing the development of yielded elements in the weakness zone at Stutakvelven shaft, looking upstream.

In Figure 53, the in-situ conditions are examined further with regard to the step 2 (Figure 52b). With this in-situ condition, two rock support models are simulated. Figure 53a illustrates the excavation with a full concrete lining. This situation shows no yielding in the lining nor in the rock mass, and the situation is considered stable. In Figure 53b, it is attempted to illustrate how the actual rock support may have interacted with the rock mass. From this model it can be observed serious stability issues in the crown. The plastic zone extends more than 2.2 m vertically above the arc. The rock support gives enough pressure to stabilise the walls and the invert.
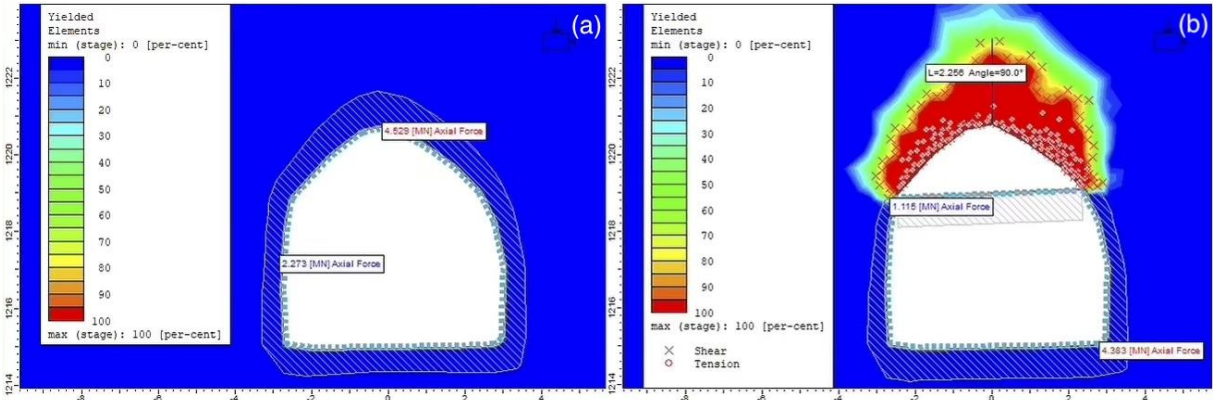
Figure 53. (a) No yielded elements with full concrete lining in excavation stage 2. (b) Yielded elements with imitated lining used during construction. Note that the cross-section is modelled where brace beams in the invert are used. In the actual excavation these beams only occur at intervals.

The situation in step 2 was further analysed. Figure 54a shows the deformation and deformation vectors scaled by 10. The most displacement occurs in the left side of the roof (looking upstream). The total displacement is 2.7 cm. From Figure 54b the major principle stress can be observed with scaled stress trajectories. Stability problems might occur in the roof due de-stressing, giving low tangential stresses and no to little confining pressure. The model indicates no yielding in the rock support, and that the lining keeps the confining pressure high enough to prevent the rock mass behind the lining from yielding.
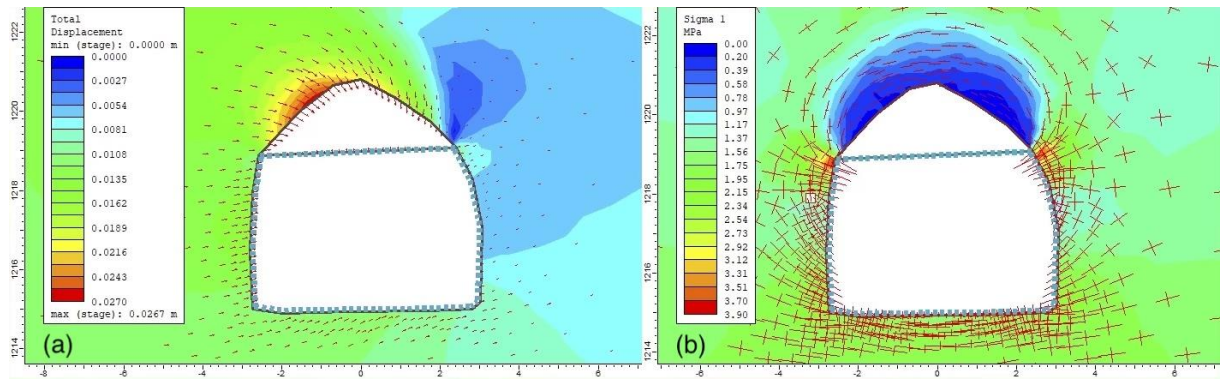
Figure 54. Indication of the rock mass condition after installation of cast concrete looking upstream (a) Total displacement with deformation vectors scaled 10 times. (b) Major principle stress with scaled stress trajectories, also showing stress concentration in the upper corner. The model shows a clear de-stressing in the rock mass potentially cause rock fall.

The situation at step 3 (Figure 52c, d) was further analysed. Figure 55 indicates the excavation at step 3 with two stages after the excavation. In stage 1 (a) the major principle stress deflects and increases above and below the tunnel. In stage 2 (b) the rock fails, and the overburden does not carry any stress, which also leads to further concentration below the tunnel. The displacement pre-failure (c) occurs mainly on the left side of the tunnel (looking upstream) in the order of 8 cm, and post-failure (d) the rock mass shows displacement above the roof in the order of 80 cm.
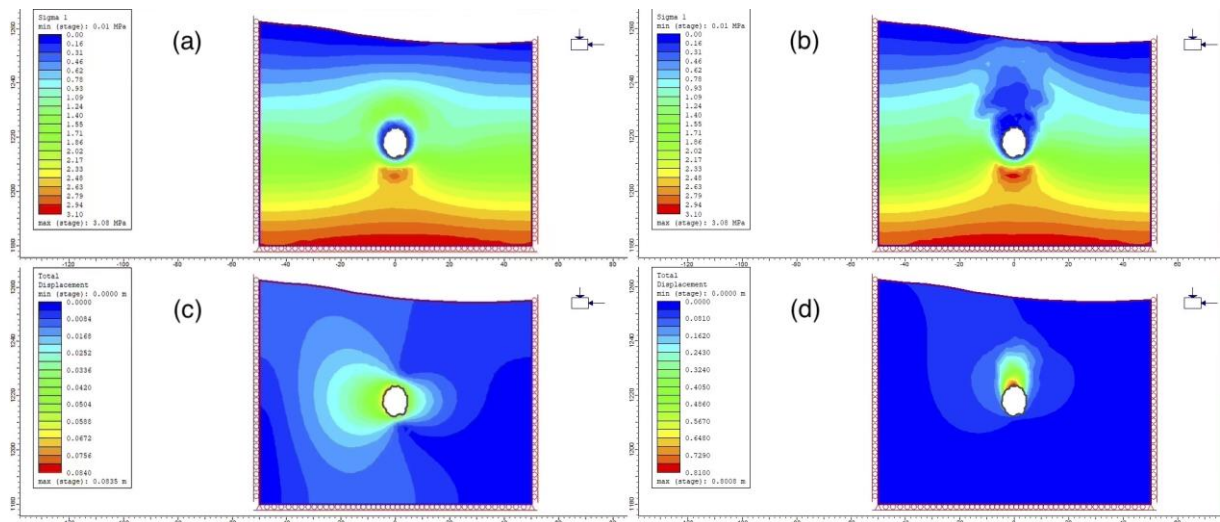
Figure 55. All figures looking upstream the shaft (a) Indicates the major principle stress pre-failure (b) Indicates the major principle stress post-failure (c) Displacement in the rock mass pre-failure (d) Displacement in the rock mass post-failure.

7.3.3 Adjacent and surrounding rock mass

The modelling of the adjacent rock mass is presented in Figure 56. The modelling of the surrounding rock mass is presented in Figure 57.
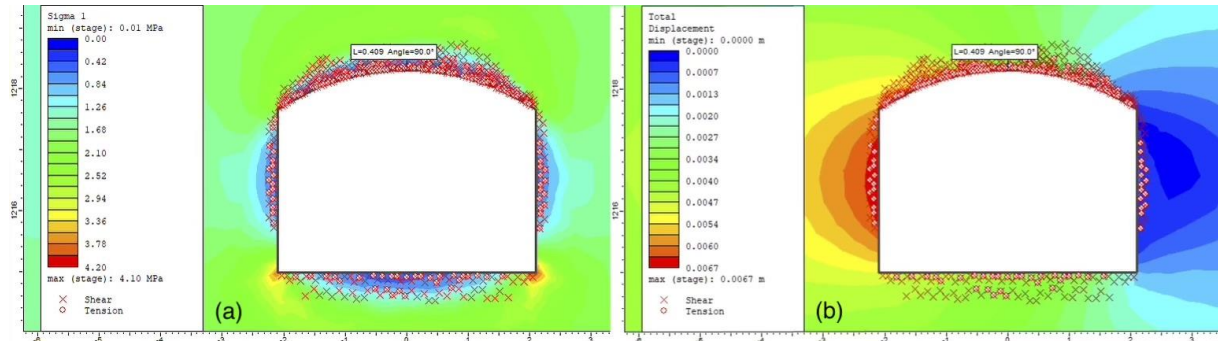
Figure 56. Adjacent rock mass of the weakness zone at Stutakvelven. (a) Major principle stress with yielded elements. (b) Displacement and yielded elements. Maximum displacement in left wall looking upstream ($6,7*10^{-3}$ m).
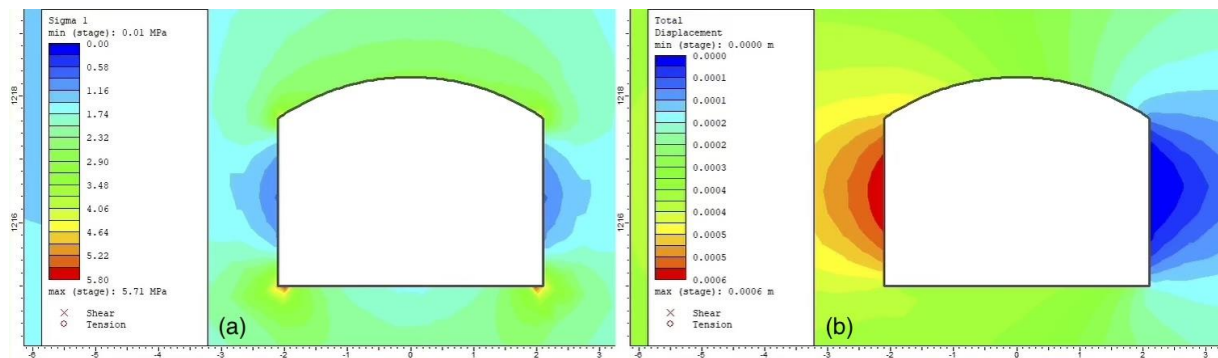
Figure 57. Surrounding rock mass of the weakness zone at Stutakvelven. (a) Major principle stress with zero yielded elements. (b) Maximum displacement of $6*10^{-4}$ m).

7.4 Discussion

7.4.1 Development of the cave-in

Several methods for excavation and simulation of the failure was attempted. The-four-step-model shows failure towards the topographic surface and that the rock mass in general still carries stress. The failure does not occur exactly where the sink hole was found in the topography, and during this modelling it was tried to simulate a failure with the same placement. This was tried in several ways. By running the model with a horizontal component of 0.5 MPa and simulating the development of the failure by lowering the intact rock strength, a yielded zone towards the actual location of the sinkhole (20-30 m eastwards) was observed, illustrated

in Figure 58. This scenario, however, was discussed with the supervisor and it was considered not likely that this weakness zone could carry this much horizontal stress.
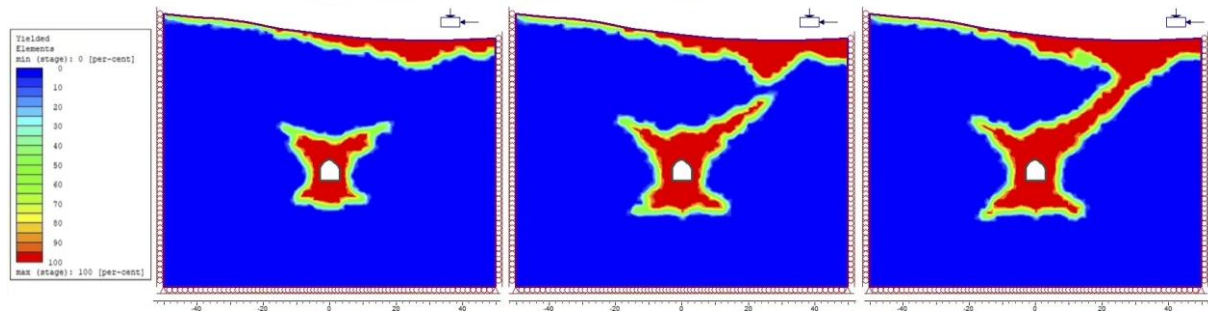
Figure 58. One of the attempts to simulate the failure at Stutakvelven shaft with a sink hole in the topography.

It was further attempted to simulate a weaker zone within the weakness zone, based on the discussion in Panthi (2014) whereas the sink hole had a large catchment area. This could possible drain towards the tunnel after excavation, hence, lowering the strength of the rock mass in the drainage zone. This was without success in the model. During the discussion with supervisor it was found that a suitable methodology for simulating the failure was a step-wise excavation of an expanding yielded zone, as illustrated in the four-step-model in Figure 52.

To increase the likeliness of the input parameters being close to the in-situ conditions, it was attempted to simulate the difference in the original cross-section and the actual cross-section which was the result of outfall and overbreak in the rock mass in the weakness zone area. In order to achieve this, the intended cross-section by Berdal AS (1978a) was modelled and excavated. Around this opening a yielded zone occurred. This yielded zone was compared to the actual cross section and the parameters were adjusted in order to increase the similarity of the yielded zone and the actual cross-section, as illustrated in Figure 59. At first, the yielded zone was considered too large around the whole periphery, and this was circumvented by increasing the intact rock strength. This is in fact in accordance with Marinos et al. (2007) whom states that a common mistake is to underestimate the rock mass strength using both a low UCS and a low GSI, giving the rock mass a double penalty. When the fully yielded rock mass could be excavated to the desired periphery it was considered as a useful guidance for the in-situ rock mass conditions.
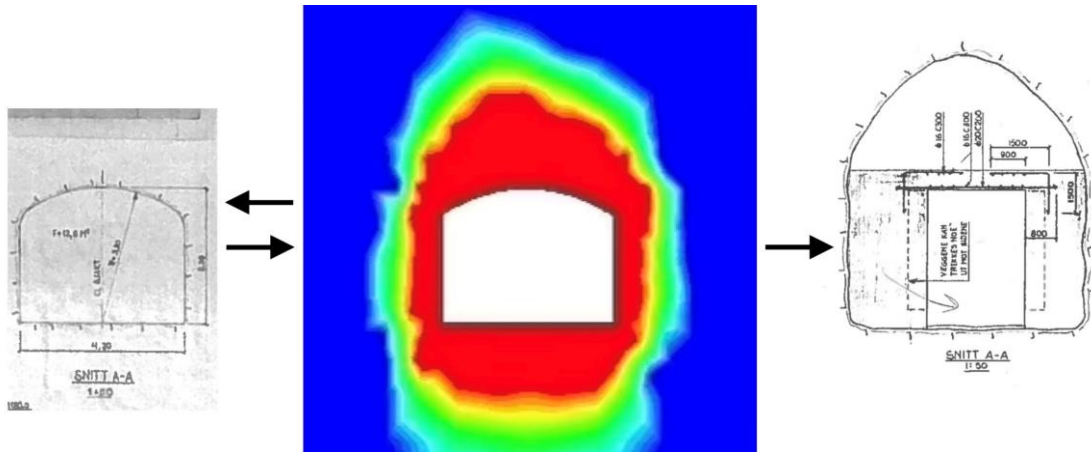
Figure 59. The intended cross-section used as an estimate of the rock mass parameter to develop a yield zone similar to the actual cross-section in the weakness zone.

The development of the four-step-model (Figure 52) shows that the failure reaches the topographic surface. This means that the rock mass is of poor enough quality for this to happen. This may also reflect the situation where outwash behind the lining occurs, leading to failure in the rock mass and loss of contact between the cast concrete and the rock mass. This model does most likely not reflect the realistic situation because it was simulated without any rock support, however, simulation with the rectangular concrete construction clearly shows the same tendency of failure above the roof and towards to surface (Figure 53b), when the empty space in the roof is left unsupported. This may indicate that the failure may occur in several different ways. This development occurs in smaller steps, and several steps is needed, however, the fact that this development occurs indicates that the simulation without support may be used to emphasise the validity of the model. In addition, taken in consideration the uncertainty with the rock support quality, as discussed in Panthi (2014), as well as the fact that the lining failed, means that the model without rock support can be used for illustrative purposes in relation to the area where the lining failed.

The four-step-model clearly shows development of the yielded zone towards the surface over time. As for triggering factors in yielding the rock mass, several causes may be of significance. It is likely that the failure developed from the bad rock mass in the invert by erosion, which removed stabilising material and allowed for propagation of the yielded zone.

Exactly where the failure occurs might be caused by many varying factors and is not possible to simulate with this 2D model. However, it can be seen from the topographic profile that the location of the sink hole is the lowest point in the terrain, hence, surface water drains towards

this point (in 2D). This drainage, or seepage in the ground, may have destabilised the rock mass by influencing the stress conditions as well as friction conditions by outwash of infill material, resulting in the cave-in, in accordance with the findings in Panthi (2014).

The modelling of the adjacent rock mass shows that some yielding occurs, and that it probably would be advised to use some shotcrete, in accordance with the Q-assessment for rock support. The modelling of the surrounding rock mass indicates very little displacement and no yielding and is therefore in accordance with the unlined support philosophy as well as the Q-assessment indicating no support or spot bolting. The difference in the model results clearly show that zone 17 (and 18) is of significantly lower rock mass quality.

7.4.2 Rock support

The model at excavation step 2 is carried out both with the cast concrete lining suggested by Berdal leaving the empty room in the crown, as well as a fully casted concrete model (Figure 53). The cross-section is considered through the middle of the construction through one of the brace beams. Figure 53b and Figure 54 indicate the situation with an unsupported crown. This shows a yielded zone of more than two metres and stress concentrations in the top corners of the support.

By studying the casted concrete support design, it is noted that the ends of the cast concrete construction apply support pressure to the whole periphery, which is likely to improve the overall stability of the weakness zone. This, however, is not considered in this 2D model and it may be that the model shows too negative estimation. Another important point when simulating the support in 2D, is that the brace beams only occur sporadically in the invert, and therefore it may be that the model shows too optimistic results.

Figure 53a shows the situation in the weakness zone with a full concrete lining. This would be an optimal situation, where the fully cast concrete hinders the development of the yielded zone by applying confining pressure and keeping blocks stable. However, during excavation of the shaft this was not achieved most likely due to the inclination and difficult work conditions.

Kjølberg referred in Palmstrøm (2003) states and illustrates (Figure 60) that several cast concrete structures has failed due to working face challenges such as outfall of rock fragments

in the concrete casting. Such weakening of the concrete may have been a contributing cause for the initial collapse.
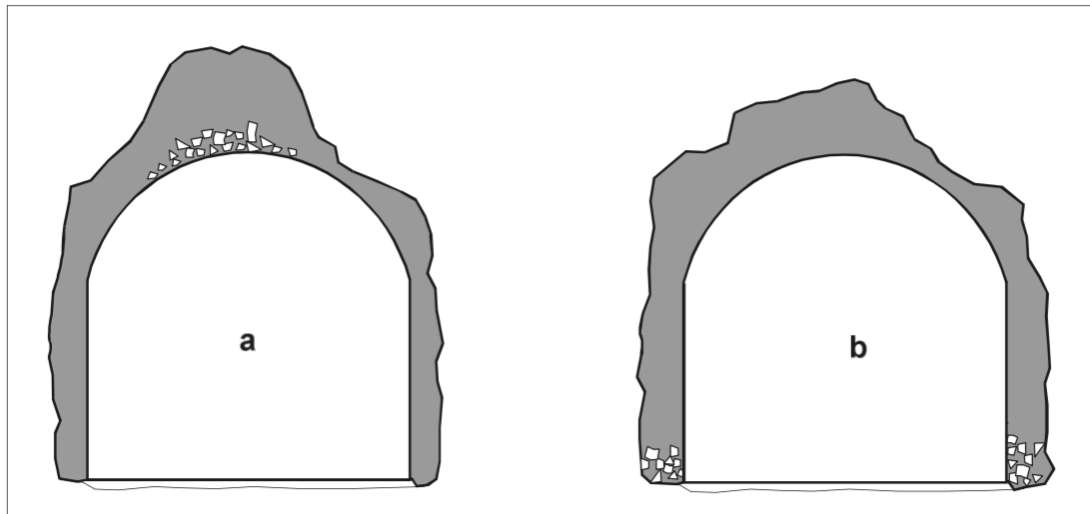
Figure 60. Illustration by Kjølberg referred in Palmstrøm (2003) of bad quality cast concrete. (a) Outfall during casting. (b) Outfall pre-casting post-formwork.

Today it would be likely to use reinforced ribs of sprayed concrete simplifying the installation and achieving stable conditions. However, serious instability may also occur despite the use of reinforced ribs of sprayed concrete, as evidently shown by the case of Matre Haugstad collapse (Brende et al., 2018).

Because of the unstable situation in the crown, two alternatives are considered in addition to the fully casted model, namely rock bolts and shotcrete. These alternatives are chosen because it was likely that these were considered as alternatives for stabilizing the crown. These alternatives are illustrated in Figure 61 (rock bolts) and Figure 62 (shotcrete). How the situation in the crown was actually left, is uncertain. In general, it is observed that the empty space, lined or unlined, has impact on the yielding, redistribution of the stresses and displacement allowed.

Figure 61 illustrates the use of M22 3-m-long rock bolts in the empty space in the crown. Rock bolts were used in the main waterway system. This shows a significant reduction in the yielded zone, of almost 1.5 m. The bolts are anchored well within the intact rock mass zone (elastic zone) and are far from reaching their capacity, meaning the rock bolts function well in this regard. However, with a significantly fractured rock mass the rock bolt plates without shotcrete may not have been sufficient to stabilise the cubical rock mass, making the bolting ineffective.
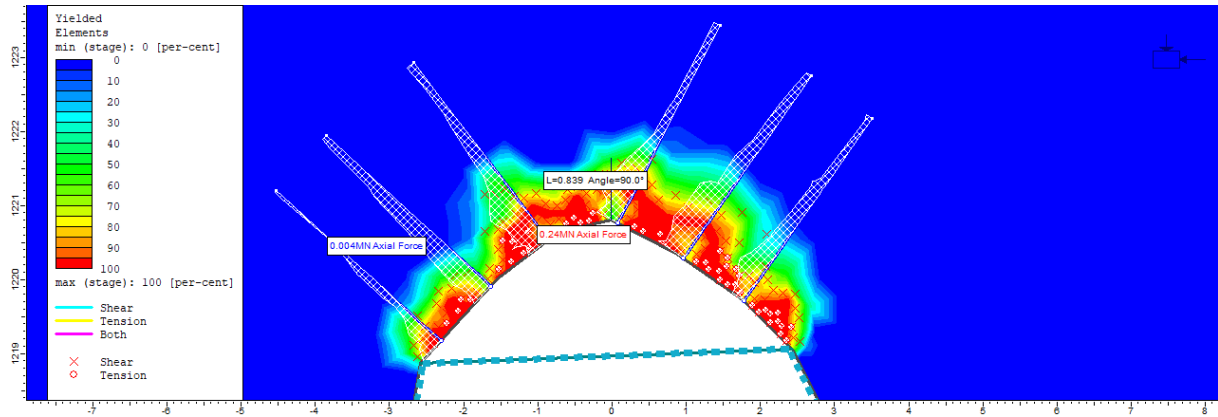
Figure 61. M22 3-m-long rock bolts (Vik Ørsta, Undated) in addition to the used rectangular cast concrete.

Figure 62 illustrates the use of shotcrete (7 cm thickness 35 MPa compressive strength) in the empty space above the fully casted lining. Compared to the unlined situation the yielded zone is reduced significantly, the confining pressure is improved and the stress concentration in the upper corners are also reduced. However, it is still seen yielded zones in the crown.
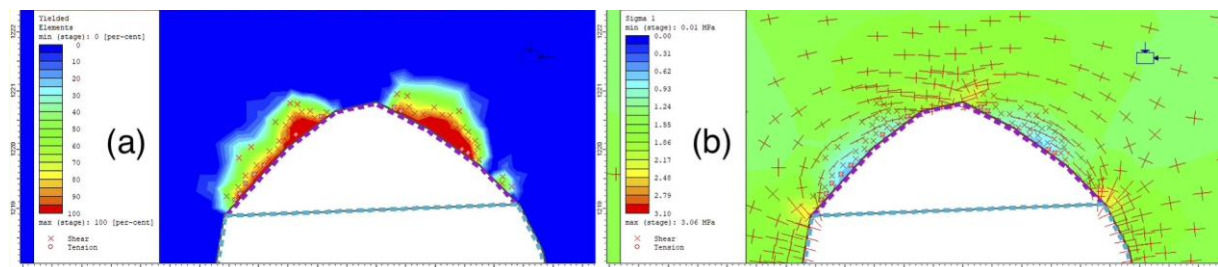
Figure 62. Shotcrete lining (in purple) in the empty room above the cast concrete (a) yielded zone (b) sigma 1 with stress trajectories.

To summarise, despite the solid cast concrete, the development of the yielded zone could eventually have led to an increase in the support pressure (p_i) of the lining (Figure 54b) as a result of time dependent effects or erosion. Ultimately, this may have led to pressure exceeding the strength of the support which further led to the cave-in, as illustrated in step 4 in Figure 52d.

7.4.3 Model quality

The intersecting angle between the cross-section of the tunnel and the weakness zone is not perpendicular. This will affect the model in several ways, and particularly how the rock stresses are oriented with respect to the cross-section. This implies that it would be more optimal to simulate the conditions of the shaft with a full 3D model. If the angle is too acute with a limited width of the weakness zone, the cross-section would end up showing parts of intact rock mass.

Stability assessment of Stutakvelven

This 2D model is therefore based on the assumption that the width of the weakness zone is sufficient enough to present a 2D cross-section within the weakness zone. Panthi (2014) estimated the sinkhole diameter at tunnel level to approximately 3 m (Figure 21), which indicates a certain width of the weakness zone.

Yielding in the topographic surface pre-excavation might be explained by the rollers in the external boundary. The rollers hinder the horizontal displacement induced by the rock mass itself, and therefore only vertical displacement is possible without fracturing the rock mass (Figure 63). This leads to occurring tension failures in the rock mass, which is most likely a model-related problem and not an actual situation in the weakness zone. The effect of this is unknown. This yielding is not dependent on excavation as it occurs pre excavation in all scenarios.
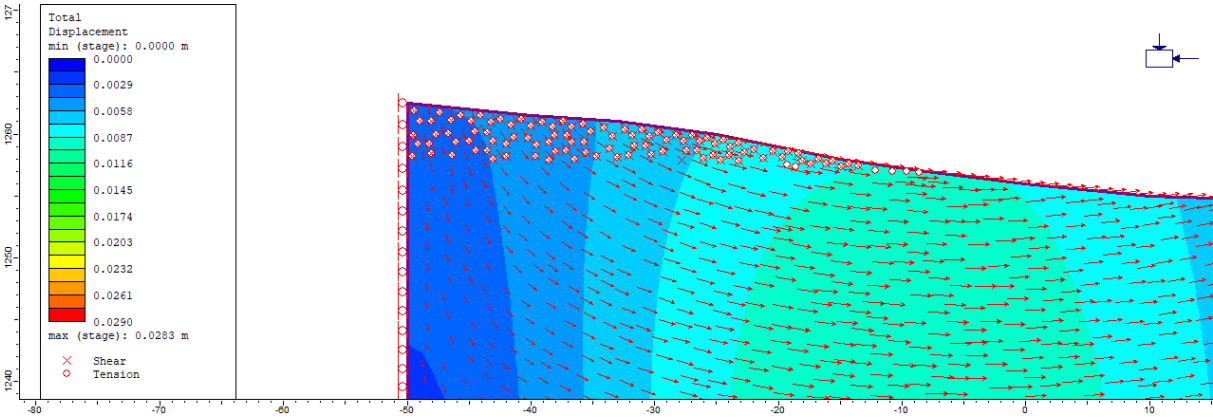
Figure 63. Total displacement model, showing yielded elements (tension) and deformation vectors in the upper left corner, pre-excavation.

The method used for estimating rock mass parameters between step 1 and step 2 does not fully coincide with the practical aspect of tunnelling using drill and blast method. It is likely that a more precise estimate would be obtained using a disturbance zone (D factor) surrounding the tunnels periphery, lowering the strength in this area, to reflect the disturbance from drill and blast despite that the effect of this is lower in bad rock mass quality.

The four-step-model (Figure 52) represents a worst-placed cross-section, and if the cross-section was considered out-of-the-plane, such as a 3D model would have, the development of the yielded zone would be significantly reduced when moving the cross-section along the tunnel axis towards better Q-values or GSI. This reasoning is illustrated by a quick-sketch in Figure

64, whereas it can be seen an increase in the yielded zone towards origin which represents the lowest Q-value, and the y-axis represents an increase in the Q-value in both directions, along the tunnel axis. This explains why the rock mass in the tunnel did not fully collapse, and only a focused area failed and led to the sink hole.
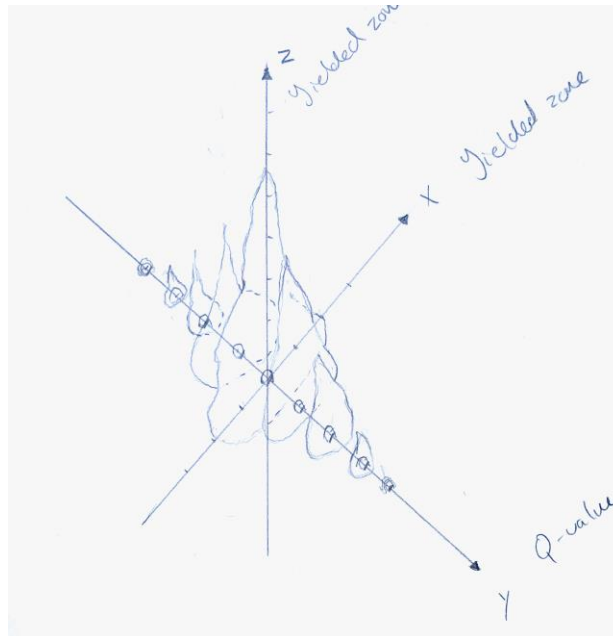
Figure 64. Quick-sketch to illustrate the decrease in yielded zone as the modelled 2D cross-section is moved along the tunnel axis towards higher quality rocks.

Regarding the model quality, it is stated by Palmstrøm and Stille (2007) that numerical modelling works best for blocky ground. Therefore, it could be of interest to simulate a model considering the actual joint sets with their measured spacing, and not superimposing the weakness zone by low GSI value.

Also, complex methods for estimating the underground stability such as numerical modelling does not necessary present a precise model, as stated by many, since the model itself is based on the input parameters. It is therefore in this thesis laid much emphasise on the field investigation, laboratory testing and selecting suitable rock mass parameters.

7.4.4 Final remark

The cast concrete was probably constructed as it was because of the difficulties with supporting the crown. It is assumed that the cast concrete was considered sufficient enough to stabilise the

walls, and that the braced beams and shotcrete in the invert were significant enough to protect the rock mass from erosion caused by flowing water.

The approach for inducing a failure reaching the surface requires very low rock mass parameters, which compared to the realistic rock mass properties might be considered too low, hence, that the rock mass is of higher quality and that water have had a more significant role as triggering factor. The cave-in is therefore considered as a water-influenced gravity-driven failure.

8 Final remarks on the case

8.1 Introduction

The discussions related to the work conducted are carried out respectively in chapter 5, 6 and 7, regarding field investigations, laboratory testing and the stability assessment. From this it is understood the challenges with linking laboratory testing with rock mass in general, and especially weakness zones. This uncertainty is the basis for and follows the analysis, underlining the importance of the input parameters. Many of the uncertain factors, such as rock stresses and rock mass quality in the weakness zone, are critical for the output of the model. To investigate these factors further will enhance stability assessment and enable an analysis of the failure development. Final remarks on the case are carried out subsequently.

8.2 Field, laboratory testing and numerical analysis

The field investigation reveals a complex geology with deformation zones, joint sets, folding and faulting, most of them most likely formed by the over-thrusted nappes characterising the area. This has made it challenging to get an overview of the area in the limited time, and clearly shows the challenge one is faced in the field.

Since the weakness zone area consists of mostly lose rock fragments, direct measurements of the weakness zone of interest could not be conducted. However, a parallel weakness zone was found and at this location it was possible to conduct mapping and sampling, which laid the basis for the understanding of the weakness zone that caused the collapse in Stutakvelven shaft. Naturally, this is not an optimal situation and may not give sufficient information to conclude on the triggering factors of the cave-in. However, the measurements and sampling gave valuable information about the transition zone and surrounding rock. This information was the basis for the assumed rock mass parameters used in the numerical analysis in an attempt to simulate the cave-in. In addition, the laboratory testing of the rocks found at Stutakvelven are supposed to be used for further research with the ongoing FME HydroCen study on long-term stability and has therefore an academic value as well.

It would be of interest to conduct core-drilling of the weakness zone material to verify the condition and/or extract clay from the weakness zone in order to test the potentially swelling properties. This together, would present valuable information regarding the failure, as well as

laying the basis for a representative 3D model. Optimally, it would be of use to have more information about the rock stresses.

8.3 Design principles and operational consequences

Hydropower tunnels have to withstand flowing water with regard to erosion and weathering, as well as operational consequences such as water hammer and mass oscillation. Building in rocks therefor put some requirements on the building material. Norwegian rocks are typically of high quality and this has led to the Norwegian unlined design philosophy where water is in direct contact with the rock masses, meaning, no comprehensive lining is necessary. However, it is evident that some special cases need rock support to maintain operational. Stutakvelven shaft is one of these cases where the surrounding complex geology required special precautions.

Stutakvelven is mainly unlined in accordance with the Norwegian design philosophy. The encountered weakness zone is supported with the cast concrete which must be regarded as a significant precaution. This should have been sufficient, which 30 years of operation indicates. Berdal underlined the importance of thorough casting of concrete especially towards to walls, most likely to ensure that the existing clay zones were supported. Whether or not these specifications were met is uncertain.

In addition, Stutakvelven shaft functions as a pressure shaft which has its consequences for the load applied on the rock mass. Dynamic running of the hydropower plant leads to fluctuating water levels which may have contributed to the weakening of the rock support and contributed to weakening of the rock mass by weathering and erosion. This is supported by measurements and calculations conducted by Neupane and Panthi (2018) where it is shown that the static water level varies both below, at and above the concrete structure, in addition to mass oscillation occurring at the levels leading to more frequent fluctuating in the water level past the concrete structure. During construction the design was probably not attended for the frequent start-stop sequences and varying load of the power plant, meaning, for instance that the rock support was not dimensioned for this phenomenon ongoing throughout a life cycle of the waterway system.

8.4 Rock support

The empty space above the concrete construction, which was left unsupported, may have given water the possibility to flow freely above the construction if the water could enter the area either

Final remarks on the case

from underneath through the hatch, from the several joints sets in the overlaying rock mass or in between the cast concrete and the rock mass. It is unclear why the hatch was place where it was and which functions it had, and why the crown was left unsupported. This makes stability considerations difficult. It might have been because of cost savings, challenges with applying the concrete in the crown or that it may have been considered not necessary to fully cast the periphery based on the assumption that the rectangular concrete structures would protect the clay zones. In this regard, it is important to remember that during the time of construction the operational regime was different, with significantly lower water fluctuations.

The Dacon photos (Figure 22) show possible outwash in the invert, which indicate inadequate rock support, either too weak, bad executed or not covering the sensitive zones sufficiently. This cause is one of the exceptions mentioned in Bruland and Thidemann (1991), representing time dependent factors which influence stability conditions. The abovementioned suspected cause at Stutakvelven was in fact exactly what occurred at Nedre Vinstra (1991), and the same mechanism for triggering the cave-in also took place at both Mauranger and Sundsbarm HPP, where outwash could occur in weakness zones because of insufficient rock support in these areas.

Regarding the Stutakvelven case, in the short term, the rock support was sufficient giving adequately support, but in the long term the construction collapsed and led to a cave-in all the way to the topographical surface.

Compared to joint infill, where the aperture of the joints is significantly smaller than the thickness of weakness zones, weakness zones material is most likely affected by water in a much larger extent, which may be explained by the lesser normal stress acting on thicker discontinuity planes. This makes the rock support even more important to maintain the natural self-supporting abilities of the rock mass, by giving confining pressure. This is one of the reasons why cave-in occurs over time, since the rock mass weight is not carried by the rock mass itself but is inflicted gradually on the rock support which yields in time. This underlines the importance of the contact between the intact rock mass and the rock support, which must hinder the water to enter the weaker rock mass thus hinder erosion.

It is believed through this study that the failure at Stutakvelven initiated as erosion of weakness zone material leading to build-up of support pressure, eventually causing the collapse in 2008.

Final remarks on the case

9 General considerations

A common denominator of the cases examined, including Stutakvelven, is that the weakness zones are not sufficiently supported. That is, the support is either not covering the invert adequately, is not overlapping the solid rock mass or is underestimated strength-wise. This is an observation of great interest, keeping in mind the limited information regarding support of weakness zones. Especially interesting is that no classification system considers or give guidance on how to adequately cover and protect failure-triggering zones such as clay zones and zones consisting of heavily jointing and infill material, as also mentioned in Palmstrøm (2018). Furthermore, and in accordance with the considerations of Palmstrøm, the lack of information about the conditions in weakness zones is a great challenge for engineering geologist.

Throughout this thesis it may be concluded that one of the most prominent causes of failures and larger cave-ins is underestimation or misjudging of the conditions in weakness zones. This is in accordance with the considerations of Panthi (2014), whom states that several collapses in recent times "may either be due to compromises made on the applied support system during construction or may be due to uncareful judgement (mapping) of the geological and stability conditions". It is revealed that in many cases, the support is not overlapping sufficiently enough the high-quality surrounding rock mass. This is assumed to be valid for the Stutakvelven case, as it appears that the reason for the cave-in was scouring in the edge of the support construction invert. A natural eminent though is to over-support the weakness zones, since the consequences may be enormous. This is most likely practiced in many projects, however, the back-side of this is high costs for supporting areas that might not need that extensive rock support. It might therefore be of interest of many to gather empirical data in order to present recommendations on how extensively weakness zones should be covered without exaggerating. This would contribute to securing zones from water entering sensitive areas, thus, destabilizing the situation. In the end, this may prevent periods of long downtime associated with income loss and high repair costs, as well as ensuring a safer environment. Therefore, it should be aspired to gain more accurate knowledge on securing weakness zones.

Lastly, the change in operational regime of the hydropower plants affects the long-term stability, making the considerations of supporting weakness zones even more challenging. In what degree this affects the stability is one of the main research projects of FME HydroCen.

General considerations

Norway, holding almost 50 percent of the total European reservoir capacity, is in a unique position and needs to keep operational at all times so that energy is available when demanded. Caretaking of hydropower tunnels is an important link in achieving this in a sustainable manner.

10 Further work

10.1 On the case

To improve the assessment conducted, some further work is suggested below:

- If possible, conduct an inspection in the tunnel to inspect the rock mass
- Extraction of weakness zone material, especially clay from the weakness zone in order to conduct a swelling test
- Research on the in-situ stresses
- 2D-model-simulation using the actual joint sets and potentially including water pressure
- Continue research on the effect of water fluctuations
- 3D model of the inclined shaft to account for the geometry

10.2 On the general considerations

During the final work in this thesis, it was unveiled that more research on weakness zones may contribute to the public benefit. This may be achieved by initiating a feasibility study on general guidance for securing weakness zones adequately, especially with regard to how meticulously weakness zones are covered.

Further work

References

ALLMENDINGER, R. W., CARDOZO, N. & FISHER, D. M. 2011. *Structural geology algorithms: Vectors and tensors*, Cambridge University Press.

BARTON, N. 2002. Some new Q-value correlations to assist in site characterisation and tunnel design. *International journal of rock mechanics and mining sciences,* 39**,** 185-216.

BARTON, N. & GRIMSTAD, E. 2014. Forty years with the Q-system in Norway and abroad. *Fjellsprengnings, Bergmekanikkdagen, and Geoteknikkdagen, Oslo, Norway,* 27**,** 28.

BARTON, N., LIEN, R. & LUNDE, J. 1974. Engineering classification of rock masses for the design of tunnel support. *Rock mechanics,* 6**,** 189-236.

BASNET, C. B. & PANTHI, K. K. 2018. Analysis of unlined pressure shafts and tunnels of selected Norwegian hydropower projects. *Journal of Rock Mechanics and Geotechnical Engineering,* 10**,** 486-512.

BERDAL AS 1978a. Construction drawings for Svandalsflona hydropower project. Drawing No. 051. *Bekkinntak / svingesjakt - sprengning og graving.*

BERDAL AS 1978b. Construction drawings for Svandalsflona hydropower project. Drawing No. 129. *Bekkinntak / svingesjakt - sikringsstøp.*

BERDAL AS 1978c. Construction drawings for Svandalsflona hydropower project. Drawing No. 140. *Geologi og sikringsarbeider - tilløpstunnel.*

BERGH, S. G. 2003. *Strukturgeologi og berggrunnskart (kompendium),* Tromsø, Fakultet for naturvitenskap og teknologi, UiT.

BIENIAWSKI, Z. T. & BERNEDE, M. J. 1979. Suggested methods for determining the uniaxial compressive strength and deformability of rock materials. *International Journal of Rock Mechanics and Mining Sciences & Geomechanics Abstracts,* 16**,** 137-140.

BRENDE, H., LIA, L. & NILSEN, B. 2018. FME HydroCen - NORSK STORSATSNING PÅ VANNKRAFT. *Fjellsprengningsdagen* Oslo: Norsk Forening for Fjellsprengingsteknikk (NFF).

BROCH, E. 1983. Estimation of strength anisotropy using the point-load test. *Int J Rock Mech Min Sci Geomech Abstr,* 20**,** 181-7.

BROCH, E. 2016. Planning and utilisation of rock caverns and tunnels in Norway. *Tunnelling and Underground Space Technology,* 55**,** 329-338.

BRULAND, A. & THIDEMANN, A. 1991. Sikring av vanntunneler. *Vassdragsregulantenes forening (VR),* 88.

BRÅTVEIT, K., BRULAND, A. & BREVIK, O. 2016. Rock falls in selected Norwegian hydropower tunnels subjected to hydropeaking. *Tunnelling and Underground space technology,* 52**,** 202-207.

References

CAI, M., KAISER, P., UNO, H., TASAKA, Y. & MINAMI, M. 2004. Estimation of rock mass deformation modulus and strength of jointed hard rock masses using the GSI system. *International Journal of Rock Mechanics and Mining Sciences,* 41**,** 3-19.

CARDOZO, N., ALLMENDINGER, R. W. J. C. & GEOSCIENCES 2013. Spherical projections with OSXStereonet. 51**,** 193-205.

CHAUDHRY, M. H. 1979. Applied hydraulic transients. Springer.

FOSSEN, H. 2016. *Structural geology*, Cambridge University Press.

FOSSEN, H., PEDERSEN, R.-B., BERGH, S. & ANDRESEN, A. 2013. *En fjellkjede blir til - Oppbygningen av kaledonidene; ca. 500-405 Ma*, I: Ramberg, I.B. Bryhni, I., Nøttvedt, A. og Ragnes, K. (red). Landet blir til - Norges geologi. 2. utg. Trondheim. Norsk geologisk forening.

HOEK, E. 2000. Practical rock engineering.

HOEK, E. & BROWN, E. T. 1997. Practical estimates of rock mass strength. *International journal of rock mechanics and mining sciences,* 34**,** 1165-1186.

HOEK, E., CARRANZA-TORRES, C. & CORKUM, B. 2002. Hoek-Brown failure criterion-2002 edition. *Proceedings of NARMS-Tac,* 1**,** 267-273.

HOEK, E. & DIEDERICHS, M. S. 2006. Empirical estimation of rock mass modulus. *International journal of rock mechanics and mining sciences,* 43**,** 203-215.

HUDSON, J. A. & HARRISON, J. P. 2000. *Engineering rock mechanics: an introduction to the principles*, Elsevier.

HØIEN, A., NILSEN, B. & OLSSON, R. 2019. Main aspects of deformation and rock support in Norwegian road tunnels. *Tunnelling and Underground Space Technology,* 86**,** 262-278.

ISRM 1978a. Suggested Methods for Determining Tensile Strength of Rock Materials Part 2: Suggested Method for determining indirect tensile strength by the Brazil test. *International journal of rock mechanics and mining sciences,* 15**,** 99-103.

ISRM 1978b. Suggested methods for the quantitative description of discontinuities in rock masses. *International Journal of Rock Mechanics Mining Sciences & Geomechanics Abstracts,* 15.

ISRM 1979. Suggested methods for determining water-content, porosity, density, absorption and related properties and swelling and slake-durability index properties. 1. Suggested methods for determining water-content, porosity, density, absorption and related properties. *International Journal of Rock Mechanics,* 16**,** 143-151.

ISRM 1985. Suggested method for determining point load strength. *International Journal of Rock Mechanics and Mining Sciences & Geomechanics Abstracts,* 22**,** 51-60.

JORDE, K. 1977. *RØLDAL, berggrunnskart 1314 I - M. 1:50 000*. Norges geologiske undersøkelse.

References

LI, C., ZHANG, N. & RUIZ, J. 2017. Measurement of the basic friction angle of planar rock discontinuities with three rock cores. *Bulletin of Engineering Geology*, 1-10.

LI, C. C. 2018. *TGB4210 Rock mechanics (compendium),* Trondheim, Norges teknisk-naturvitenskapelige universitet, Institutt for geologi og bergteknikk.

MAO, D., NILSEN, B. & LU, M. 2012. Numerical analysis of rock fall at Hanekleiv road tunnel. *Bulletin of Engineering Geology and the Environment,* 71**,** 783-790.

MARINOS, P., MARINOS, V. & HOEK, E. Geological Strength Index (GSI). A characterization tool for assessing engineering properties for rock masses. Proceedings International Workshop on Rock Mass Classification for Underground Mining, Mark, Pakalnis and Tuchman (editors), Information Circular, 2007. 87-94.

MARINOS, V. 2019. A revised, geotechnical classification GSI system for tectonically disturbed heterogeneous rock masses, such as flysch. *Bulletin of Engineering Geology and the Environment,* 78**,** 899-912.

MYRVANG, A. Surface indicators of high, near surface rock stresses. 9th ISRM Congress, 1999. International Society for Rock Mechanics and Rock Engineering.

NATERSTAD, J. 1988. *HAUKELISÆTER 1414 IV. Berggrunnskart M 1:50 000*. Norges geologiske undersøkelse.

NEUPANE, B. & PANTHI, K. Effect of Pressure Fluctuations in Long-term Stability of Unlined Pressure Shaft at Svandalsflona Hydropower Project, Norway. ISRM International Symposium-10th Asian Rock Mechanics Symposium, 2018. International Society for Rock Mechanics and Rock Engineering.

NGI 2015. Using the Q-system. *Rock mass classification and support design.* Oslo: NGI.

NGU. 2015. *E39 Krysning av Romsdalsfjorden. Berggrunnsgeologi, strukturgeologi og undersøkelse av ustabile fjellpart* [Online]. Available: https://www.ngu.no/upload/Publikasjoner/Rapporter/2015/2015_039.pdf [Accessed 1 April 2019].

NILSEN, B. & BROCH, E. 2016. *Ingeniørgeologi-berg grunnkurskompendium,* Trondheim, Institutt for geologi og bergteknikk, NTNU.

NILSEN, B., PALMSTRÖM, A. & NORSK, B. 2000. *Engineering geology and rock engineering : handbook. No. 2 No. 2,* Oslo, Norwegian Group for Rock Mechanics.

NILSEN, B. & THIDEMANN, A. 1993. *Rock Engineering*, Norwegian Institute of Technology, Division of Hydraulic Engineering.

NVE. Undated. *Vannkraftverk* [Online]. Available: https://www.nve.no/energiforsyning/vannkraftpotensialet/vannkraftdatabase/ [Accessed 18 march 2019].

PALMSTRØM, A. 1995. *RMI–a rock mass characterization system for rock engineering purposes [Ph. D. Thesis]* [Online]. Oslo, Norway: University of Oslo. Available:

References

http://www.rockmass.net/articles/rmi/phd_thesis_on_rmi.html [Accessed 20 march 2019].

PALMSTRØM, A. 2003. Ras i vanntunneler - et vedlikeholdsproblem? *Norconsult AS*.

PALMSTRØM, A. Ras i tunneler. Hva kan vi lære? Fjellsprengningsteknikk / Bergmekanikk / Geoteknikk, 2018 Oslo.

PALMSTRØM, A. & BERTHELSEN, O. The significance of weakness zones in rock tunnelling. ISRM International Symposium, 1988. International Society for Rock Mechanics and Rock Engineering.

PALMSTRØM, A. & BROCH, E. 2017. The design of unlined hydropower tunnels and shafts: 100 years of Norwegian experience. *International journal on hydropower and dams,* 3**,** 1-9.

PALMSTRØM, A. & SINGH, R. 2001. The deformation modulus of rock masses — comparisons between in situ tests and indirect estimates. *Tunnelling Underground Space Technology,* 16**,** 115-131.

PALMSTRØM, A. & STILLE, H. 2007. Ground behaviour and rock engineering tools for underground excavations. *Tunnelling and Underground Space Technology,* 22**,** 363-376.

PANTHI, K. K. 2006. *Analysis of engineering geological uncertainties related to tunnelling in Himalayan rock mass conditions.* Doctoral thesis, NTNU.

PANTHI, K. K. 2014. Analysis on the Dynamics of Burst Debris Flood at the Inclined Pressure-Shaft of Svandalsflona Hydropower Project, Norway. *Rock mechanics and rock engineering,* 47**,** 923-932.

RUMMEL, F. & VANHEERDEN, W. L. 1978. Suggested methods for determining sound-velocity. *International Journal of Rock Mechanics and Mining Sciences,* 15**,** 53-58.

STATENS VEGVESEN 2016. Laboratorieundersøkelser - Håndbok R210.

STRECKEISEN, A. 1980. Classification and nomenclature of volcanic rocks, lamprophyres, carbonatites and melilitic rocks IUGS Subcommission on the systematics of igneous rocks. *Geologische Rundschau,* 69**,** 194-207.

TRINH, N. & JONSSON, K. 2013. Design considerations for an underground room in a hard rock subjected to a high horizontal stress field at Rana Gruber, Norway. *Tunnelling and Underground Space Technology,* 38**,** 205-212.

VIK ØRSTA. Undated. *CT-bolt M22* [Online]. https://www.vikorsta.no/globalassets/vik-orsta/berg/produktark/ct-bolt-m22.pdf. [Accessed 4 May 2019].

Appendices

Appendix A

Compilation of the Q-system parameters and the ESR table from NGI (2015).

Table 1   RQD-values and volumetric jointing.

1	RQD (Rock Quality Designation)		RQD
A	Very poor	(> 27 joints per m³)	0-25
B	Poor	(20-27 joints per m³)	25-50
C	Fair	(13-19 joints per m³)	50-75
D	Good	(8-12 joints per m³)	75-90
E	Excellent	(0-7 joints per m³)	90-100

Note: i) Where RQD is reported or measured as ≤ 10 (including 0) the value 10 is used to evaluate the Q-value
ii) RQD-intervals of 5, i.e. 100, 95, 90, etc., are sufficiently accurate

Table 2 J_n – values.

2	Joint set number	J_n
A	Massive, no or few joints	0.5-1.0
B	One joint set	2
C	One joint set plus random joints	3
D	Two joint sets	4
E	Two joint sets plus random joints	6
F	Three joint sets	9
G	Three joint sets plus random joints	12
H	Four or more joint sets, random heavily jointed "sugar cube", etc	15
J	Crushed rock, earth like	20

Note: i) For tunnel intersections, use 3 x J_n
ii) For portals, use 2 x J_n

Table 3 J_r – values.

3	Joint Roughness Number	J_r
a) Rock-wall contact, and b) Rock-wall contact before 10 cm of shear movement		
A	Discontinuous joints	4
B	Rough or irregular, undulating	3
C	Smooth, undulating	2
D	Slickensided, undulating	1.5
E	Rough, irregular, planar	1.5
F	Smooth, planar	1
G	Slickensided, planar	0.5
Note: i) Description refers to small scale features and intermediate scale features, in that order		
c) No rock-wall contact when sheared		
H	Zone containing clay minerals thick enough to prevent rock-wall contact when sheared	1

Note: ii) Add 1 if the mean spacing of the relevant joint set is greater than 3 m (dependent on the size of the underground opening)
iii) J_r = 0.5 can be used for planar slickensided joints having lineations, provided the lineations are oriented in the estimated sliding direction

Table 4 J_a – values.

4	Joint Alteration Number	Φ_r approx.	J_a
a) Rock-wall contact (no mineral fillings, only coatings)			
A	Tightly healed, hard, non-softening, impermeable filling, i.e., quartz or epidote.		0.75
B	Unaltered joint walls, surface staining only.	25-35°	1
C	Slightly altered joint walls. Non-softening mineral coatings; sandy particles, clay-free disintegrated rock, etc.	25-30°	2
D	Silty or sandy clay coatings, small clay fraction (non-softening).	20-25°	3
E	Softening or low friction clay mineral coatings, i.e., kaolinite or mica. Also chlorite, talc gypsum, graphite, etc., and small quantities of swelling clays.	8-16°	4
b) Rock-wall contact before 10 cm shear (thin mineral fillings)			
F	Sandy particles, clay-free disintegrated rock, etc.	25-30°	4
G	Strongly over-consolidated, non-softening, clay mineral fillings (continuous, but <5 mm thickness).	16-24°	6
H	Medium or low over-consolidation, softening, clay mineral fillings (continuous, but <5 mm thickness).	12-16°	8
J	Swelling-clay fillings, i.e., montmorillonite (continuous, but <5 mm thickness). Value of J_a depends on percent of swelling clay-size particles.	6-12°	8-12
c) No rock-wall contact when sheared (thick mineral fillings)			
K	Zones or bands of disintegrated or crushed rock. Strongly over-consolidated.	16-24°	6
L	Zones or bands of clay, disintegrated or crushed rock. Medium or low over-consolidation or softening fillings.	12-16°	8
M	Zones or bands of clay, disintegrated or crushed rock. Swelling clay. J_a depends on percent of swelling clay-size particles.	6-12°	8-12
N	Thick continuous zones or bands of clay. Strongly over-consolidated.	12-16°	10
O	Thick, continuous zones or bands of clay. Medium to low over-consolidation.	12-16°	13
P	Thick, continuous zones or bands with clay. Swelling clay. J_a depends on percent of swelling clay-size particles.	6-12°	13-20

Table 5 J_w – values.

5	Joint Water Reduction Factor	J_w
A	Dry excavations or minor inflow (humid or a few drips)	1.0
B	Medium inflow, occasional outwash of joint fillings (many drips/"rain")	0.66
C	Jet inflow or high pressure in competent rock with unfilled joints	0.5
D	Large inflow or high pressure, considerable outwash of joint fillings	0.33
E	Exceptionally high inflow or water pressure decaying with time. Causes outwash of material and perhaps cave in	0.2-0.1
F	Exceptionally high inflow or water pressure continuing without noticeable decay. Causes outwash of material and perhaps cave in	0.1-0.05

Note: i) Factors C to F are crude estimates. Increase J_w if the rock is drained or grouting is carried out
ii) Special problems caused by ice formation are not considered

Table 6   SRF-values.

6	Stress Reduction Factor			SRF
a) Weak zones intersecting the underground opening, which may cause loosening of rock mass				
A	Multiple occurrences of weak zones within a short section containing clay or chemically disintegrated, very loose surrounding rock (any depth), or long sections with incompetent (weak) rock (any depth). For squeezing, see 6L and 6M			10
B	Multiple shear zones within a short section in competent clay-free rock with loose surrounding rock (any depth)			7.5
C	Single weak zones with or without clay or chemical disintegrated rock (depth ≤ 50m)			5
D	Loose, open joints, heavily jointed or "sugar cube", etc. (any depth)			5
E	Single weak zones with or without clay or chemical disintegrated rock (depth > 50m)			2.5

Note: i) Reduce these values of SRF by 25-50% if the weak zones only influence but do not intersect the underground opening

b) Competent, mainly massive rock, stress problems	σ_c/σ_1	σ_θ/σ_c	SRF
F	Low stress, near surface, open joints	>200	<0.01	2.5
G	Medium stress, favourable stress condition	200-10	0.01-0.3	1
H	High stress, very tight structure. Usually favourable to stability. May also be unfavourable to stability dependent on the orientation of stresses compared to jointing/weakness planes*	10-5	0.3-0.4	0.5-2 / 2-5*
J	Moderate spalling and/or slabbing after > 1 hour in massive rock	5-3	0.5-0.65	5-50
K	Spalling or rock burst after a few minutes in massive rock	3-2	0.65-1	50-200
L	Heavy rock burst and immediate dynamic deformation in massive rock	<2	>1	200-400

Note: i) For strongly anisotropic virgin stress field (if measured): when 5 ≤ σ_1 /σ_3 ≤ 10, reduce σ_c to 0.75 σ_c. When σ_1 /σ_3 > 10, reduce σ_c to 0.5 σ_c, where σ_c = unconfined compression strength, σ_1 and σ_3 are the major and minor principal stresses, and σ_θ = maximum tangential stress (estimated from elastic theory)
ii) When the depth of the crown below the surface is less than the span; suggest SRF increase from 2.5 to 5 for such cases (see F)

c) Squeezing rock: plastic deformation in incompetent rock under the influence of high pressure	σ_θ/σ_c	SRF
M	Mild squeezing rock pressure	1-5	5-10
N	Heavy squeezing rock pressure	>5	10-20

Note: iv) Determination of squeezing rock conditions must be made according to relevant literature (i.e. Singh et al., 1992 and Bhasin and Grimstad, 1996)

d) Swelling rock: chemical swelling activity depending on the presence of water	SRF
O	Mild swelling rock pressure	5-10
P	Heavy swelling rock pressure	10-15

Table 7   ESR-values.

7	Type of excavation	ESR
A	Temporary mine openings, etc.	ca. 3-5
B	Vertical shafts*: i) circular sections / ii) rectangular/square section / * Dependant of purpose. May be lower than given values.	ca. 2.5 / ca. 2.0
C	Permanent mine openings, water tunnels for hydro power (exclude high pressure penstocks) water supply tunnels, pilot tunnels, drifts and headings for large openings.	1.6
D	Minor road and railway tunnels, surge chambers, access tunnels, sewage tunnels, etc.	1.3
E	Power houses, storage rooms, water treatment plants, major road and railway tunnels, civil defence chambers, portals, intersections, etc.	1.0
F	Underground nuclear power stations, railways stations, sports and public facilities, factories, etc.	0.8
G	Very important caverns and underground openings with a long lifetime, ≈ 100 years, or without access for maintenance.	0.5

Appendix B

The rock mass quality and rock support chart from NGI (2015). The green circle indicates support category 7 for the weakness zone 17, the green lines indicates mainly support class 4 for the adjacent rock mass and support class 1 for the surrounding rock mass.
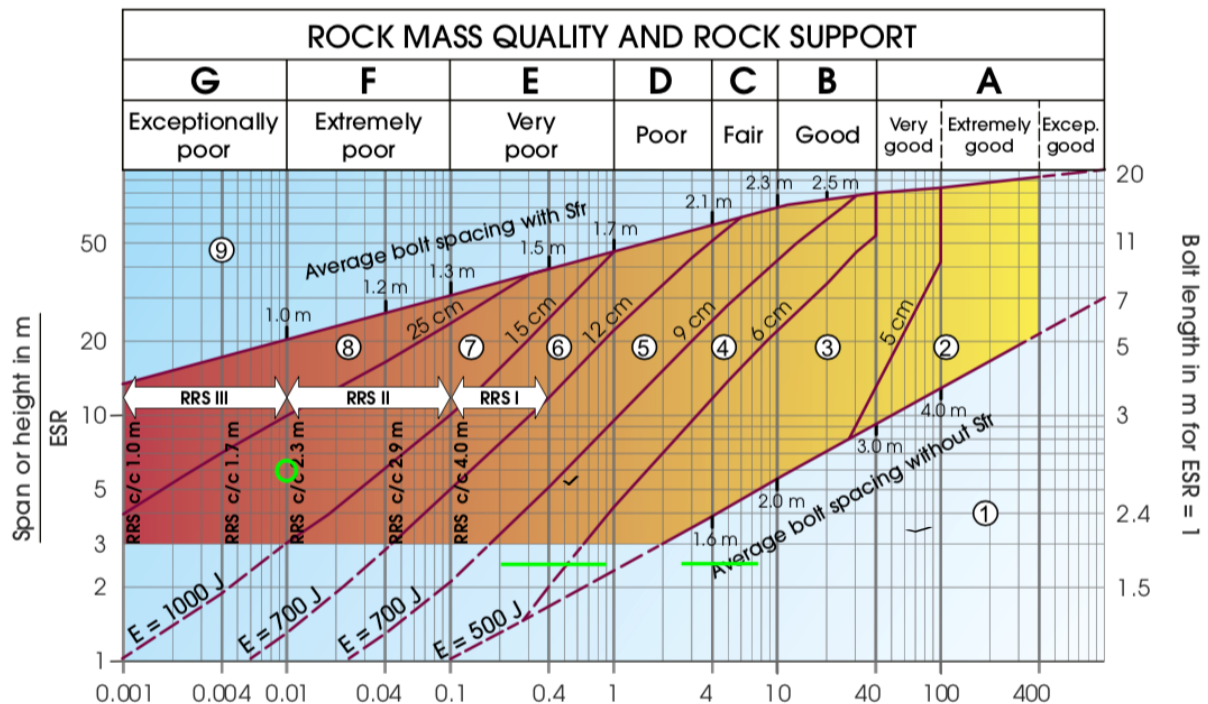
$$\text{Rock mass quality} \quad Q = \frac{RQD}{J_n} \times \frac{J_r}{J_a} \times \frac{J_w}{SRF}$$

Support categories

① Unsupported or spot bolting
② Spot bolting, **SB**
③ Systematic bolting, fibre reinforced sprayed concrete, 5-6 cm, **B+Sfr**
④ Fibre reinforced sprayed concrete and bolting, 6-9 cm, **Sfr (E500)+B**
⑤ Fibre reinforced sprayed concrete and bolting, 9-12 cm, **Sfr (E700)+B**
⑥ Fibre reinforced sprayed concrete and bolting, 12-15 cm + reinforced ribs of sprayed concrete and bolting, **Sfr (E700)+RRS I +B**
⑦ Fibre reinforced sprayed concrete >15 cm + reinforced ribs of sprayed concrete and bolting, **Sfr (E1000)+RRS II+B**
⑧ Cast concrete lining, **CCA** or **Sfr (E1000)+RRS III+B**
⑨ Special evaluation

Bolts spacing is mainly based on Ø20 mm
E = Energy absorbtion in fibre reinforced sprayed concrete
ESR = Excavation Support Ratio
Areas with dashed lines have no empirical data

RRS - spacing related to Q-value

Si30/6 Ø16 - Ø20 (span 10m)
D40/6+2 Ø16-20 (span 20m)

Si35/6 Ø16-20 (span 5m)
D45/6+2 Ø16-20 (span 10m)
D55/6+4 Ø20 (span 20m)

D40/6+4 Ø16-20 (span 5 m)
D55/6+4 Ø20 (span 10 m)
Special evaluation (span 20 m)

Si30/6 = Single layer of 6 rebars,
          30 cm thickness of sprayed concrete
D = Double layer of rebars
Ø16 = Rebar diameter is 16 mm
c/c = RSS spacing, centre - centre

Appendix C.1

Uniaxial compressive test results, density and p-wave velocity (for information about stress-strain curves is found in Appendix C.2).

Sample	Diameter dry (mm)						Avg. dia. (mm)	Dia. /w stocking (mm)	Std.dev. (mm)	Length (mm)	Mass dry (g)	Mass wet (g)	Mass diff (%)	Density wet (g/cm3)	Traveltime (µs)	P-wave vel. (m/s)	UCS (MPa)	Youngs mod. (GPa)	Poisson's
1.1.1	34,29	34,29	34,28	34,28	34,28	34,28	34,28	36,03	0,01	91,41	221,91	222,23	0,14	2,63	16,4	5574	47,3	65,6	0,44
1.1.2	34,28	34,29	34,28	34,28	34,28	34,28	34,28	36,03	0,00	91,40	221,76	222,13	0,17	2,63	16,4	5573	71,6	37,6	0,65
1.2.1	34,29	34,29	34,29	34,28	34,29	34,28	34,29	36,04	0,01	91,04	221,54	221,74	0,09	2,64	16,4	5551	87,8	40,6	0,31
1.2.2	34,29	34,28	34,28	34,28	34,28	34,28	34,28	36,03	0,00	91,03	221,78	221,98	0,09	2,64		5551	56,8	45,8	0,29
															Series 1 avg.	5562	65,9	47,4	0,42
2.1	34,26	34,25	34,26	34,25	34,25	34,25	34,25	36,00	0,01	91,00	221,19	221,41	0,10	2,64	16,4	5549	193,0	50,1	0,46
2.2	34,25	34,25	34,25	34,25	34,25	34,26	34,25	36,00	0,00	90,90	220,66	220,88	0,10	2,64	16,4	5543	239,5	49,4	0,40
2.3	34,25	34,26	34,26	34,26	34,25	34,25	34,26	36,01	0,01	91,52	222,79	223,06	0,12	2,64	16,9	5415	233,8	48,4	0,38
															Series 2 avg.	5502	222,1	49,3	0,41
3.1	34,26	34,26	34,25	34,27	34,26	34,26	34,26	36,01	0,01	91,98	225,91	226,37	0,20	2,67	29,9	3076	195,9	39,6	0,27
3.2	34,27	34,28	34,28	34,27	34,27	34,28	34,28	36,03	0,01	92,42	226,92	227,36	0,19	2,67	29,9	3091	198,5	42,7	0,30
3.3	34,27	34,27	34,28	34,31	34,29	34,3	34,29	36,04	0,02	72,65	178,16	178,57	0,23	2,66	24,1	3015	-	-	-
													All series avg.	2,65	Series 3 avg.	3061	197,2	41,2	0,29

Appendix C.2

Stress-strain curve sample 1.1.1 and 1.1.2 (series 1)

Stress-strain curve sample 1.2.1 and 1.2.2 (series 1)

Stress-strain curve sample 2.1, 2.2 and 2.3 (series 2)

Stress-strain curve sample 3.1, 3.2 and 3.3 (series 3)
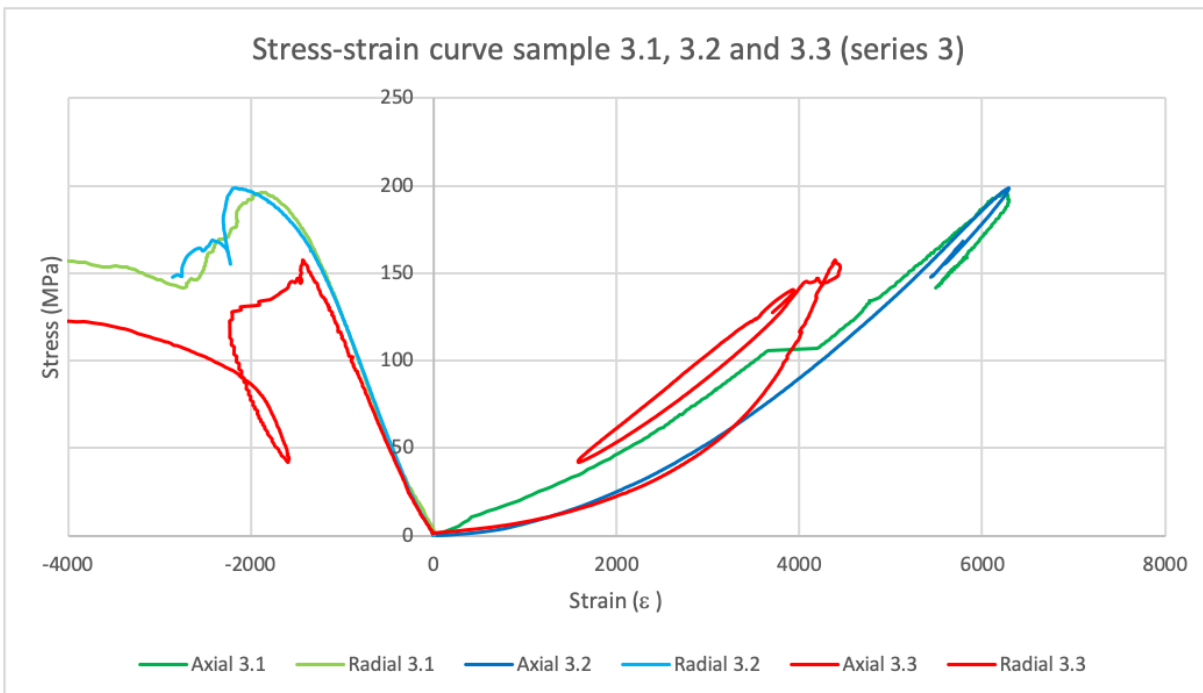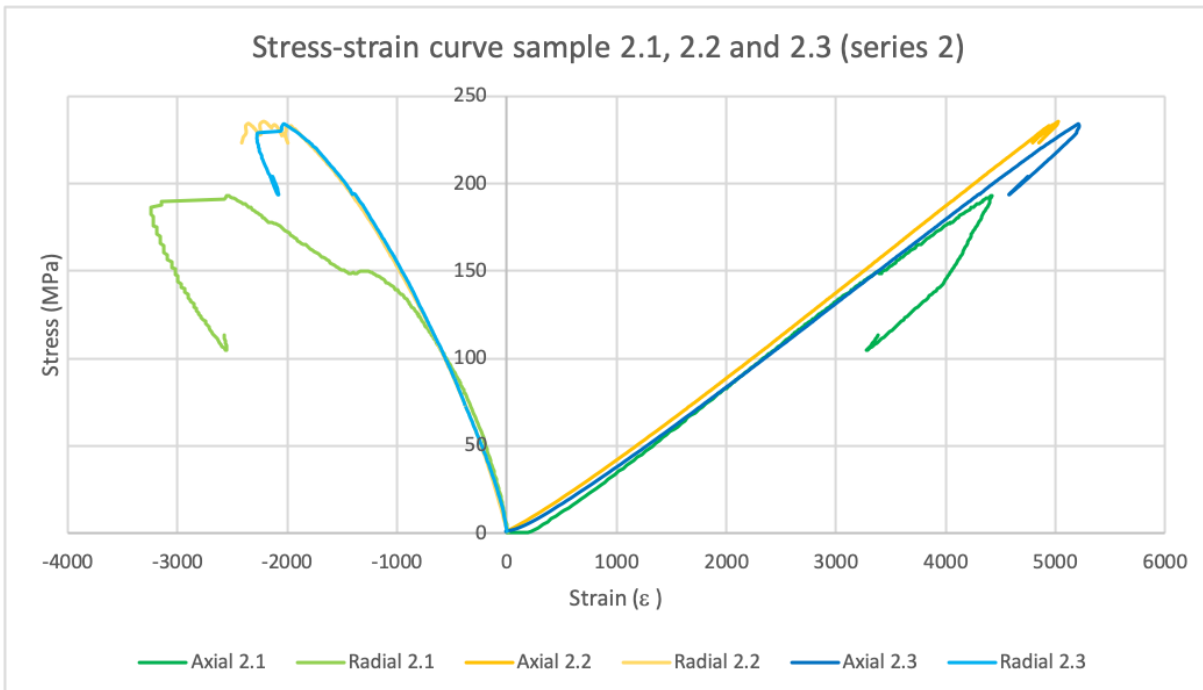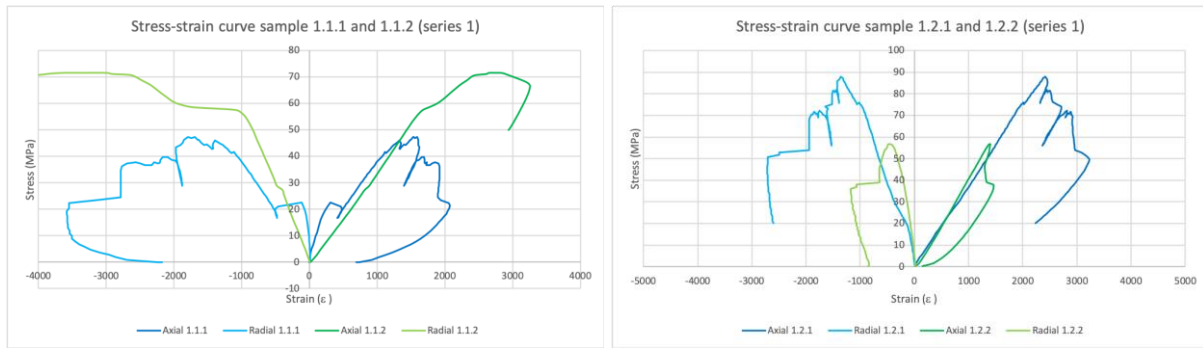
Appendix D

Brazil test results.

Sample	Load direction	Diameter (mm)	Thickness (mm)	Max load (kN)	Tensile str. (MPa)	STD.DEV
1.1.1	Normal	50,2	25,3	33,19	16,6	
1.1.2	Normal	50,2	25,0	36,16	18,3	
1.1.3	Normal	50,2	24,0	44,97	23,7	
1.1.4	Normal	50,2	25,6	52,28	25,8	
1.1.5	Normal	50,2	24,0	47,86	25,2	
1.1.6	Normal	50,2	24,7	24,61	-	
1.2.1	Normal	50,2	24,2	32,54	17,0	
1.2.2	Normal	50,2	26,1	40,74	19,8	
1.2.3	Normal	50,2	24,8	31,2	15,9	
1.2.4	Normal	50,2	24,8	28,7	14,6	
1.2.5	Normal	50,2	24,3	22,61	11,8	
1.2.6	Normal	50,2	23,9	37,72	20,0	
1.2.7	Normal	50,2	25,6	39,46	19,5	
1.2.8	Normal	50,2	24,5	18,31	-	
				Avg.:	19,0	4,3
2.1	Normal	50,2	24,6	36,7	18,9	
2.2	Normal	50,2	25,3	26,46	13,3	
2.3	Normal	50,2	24,9	39,24	20,0	
2.4	Normal	50,2	24,6	29,62	15,2	
2.5	Normal	50,2	24,7	35,9	18,4	
2.6	Normal	50,2	24,5	34,74	18,0	
				Avg.:	17,3	2,5

Appendix E

Point-load test results.

Sample	Type	D (mm)	L/W (mm)	P (kN)	A=(W*D) (mm^2)	D_e (mm)	I(s)	F	I_s(50)	Mean	STD.DEV
1.1	d (II)	34,28	22,1	5,59	757,59	34,28	4,8	0,84	4,0		
1.2	d (II)	34,27	20,7	9,17	709,39	34,27	7,8	0,84	6,6		
1.3	d (II)	34,28	failed	-	-	-	-	-	-		
1.4	d (II)	34,29	27,4	14,16	939,55	34,29	12,0	0,84	10,2		
1.5	d (II)	34,30	21,4	13,92	734,02	34,30	11,8	0,84	10,0		
1.6	d (II)	34,27	21,9	15,98	750,51	34,27	13,6	0,84	11,5		
1.7	d (II)	34,27	18,0	14,82	616,86	34,27	12,6	0,84	10,6	9,3	1,9
1.8	a (⊥)	24,45	34,27	24,76	837,90	32,66	23,2	0,83	19,2		
1.9	a (⊥)	24,56	34,27	20,12	841,67	32,74	18,8	0,83	15,5		
1.10	a (⊥)	13,93	34,26	9,65	477,24	24,65	15,9	0,73	11,6		
1.11	a (⊥)	14,45	34,28	13,69	495,35	25,11	21,7	0,73	15,9		
1.12	a (⊥)	21,01	34,29	16,93	720,43	30,29	18,5	0,80	14,7		
1.13	a (⊥)	25,79	34,26	23,44	883,57	33,54	20,8	0,84	17,4		
1.14	a (⊥)	23,84	34,28	18,49	817,24	32,26	17,8	0,82	14,6		
1.15	a (⊥)	21,87	34,27	12,77	749,48	30,89	13,4	0,81	10,8	15,0	2,0
2.1	d (II)	34,25	20,0	11,00	685,00	34,25	9,4	0,84	7,91		
2.2	d (II)	34,26	20,1	12,44	687,26	34,26	10,6	0,84	8,94		
2.3	d (II)	34,26	19,6	13,70	670,47	34,26	11,7	0,84	9,85		
2.4	d (II)	34,26	20,7	13,62	709,18	34,26	11,6	0,84	9,79		
2.5	d (II)	34,26	22,7	12,75	777,70	34,26	10,9	0,84	9,16		
2.6	d (II)	34,26	26,2	11,45	895,90	34,26	9,8	0,84	8,23		
2.7	d (II)	34,26	21,0	12,08	719,46	34,26	10,3	0,84	8,68		
2.8	d (II)	34,26	20,0	9,47	685,20	34,26	8,1	0,84	6,81		
2.9	d (II)	34,26	failed	-	-	-	-	-	-		
2.10	d (II)	34,25	28,9	5,44	988,80	34,25	4,6	0,84	3,91		
2.11	d (II)	34,25	24,3	11,54	831,93	34,25	9,8	0,84	8,30		
2.12	d (II)	34,24	22,7	10,87	777,25	34,24	9,3	0,84	7,82		
2.13	d (II)	34,25	25,36	11,24	868,58	34,25	9,6	0,84	8,08		
2.14	d (II)	34,26	24,56	9,45	841,43	34,26	8,1	0,84	6,79		
2.15	d (II)	34,25	24,47	12,92	838,10	34,25	11,0	0,84	9,29		
2.16	d (II)	34,26	21,94	11,66	751,66	34,26	9,9	0,84	8,38		
2.17	d (II)	34,25	22,19	11,77	760,01	34,25	10,0	0,84	8,46	8,3	0,6
2.18	a (⊥)	27,89	34,26	21,36	955,51	34,88	17,6	0,85	14,9		
2.19	a (⊥)	28,00	34,26	23,49	959,28	34,95	19,2	0,85	16,4		
2.20	a (⊥)	23,29	34,25	8,57	797,68	31,87	8,4	0,82	6,9		
2.21	a (⊥)	25,88	34,25	20,90	886,39	33,59	18,5	0,84	15,5		
2.22	a (⊥)	28,66	34,25	23,09	981,61	35,35	18,5	0,86	15,8		
2.23	a (⊥)	22,17	34,25	19,55	759,32	31,09	20,2	0,81	16,3		
2.24	a (⊥)	29,05	34,25	27,59	994,96	35,59	21,8	0,86	18,7		
2.25	a (⊥)	25,21	34,25	21,16	863,44	33,16	19,2	0,83	16,0		
2.26	a (⊥)	22,90	34,25	17,23	784,33	31,60	17,3	0,81	14,0		
2.27	a (⊥)	20,33	34,25	16,90	696,30	29,78	19,1	0,79	15,1		
2.28	a (⊥)	23,63	34,24	10,98	809,09	32,10	10,7	0,82	8,7		
2.29	a (⊥)	28,88	failed	-	-	-	-	-	-		
2.30	a (⊥)	29,12	34,25	18,26	997,36	35,64	14,4	0,86	12,3		
2.31	a (⊥)	16,41	34,26	10,48	562,21	26,75	14,6	0,75	11,0		
2.32	a (⊥)	21,16	34,26	16,51	724,94	30,38	17,9	0,80	14,3	14,5	1,7
3.1	d (II)	34,27	21,09	3,58	722,75	30,34	3,9	0,80	3,1		
3.2	d (II)	34,27	18,92	3,08	648,39	28,73	3,7	0,78	2,9		
3.3	d (II)	34,27	17,55	4,41	601,44	27,67	5,8	0,77	4,4		
3.4	d (II)	34,28	22,48	3,47	770,61	31,32	3,5	0,81	2,9		
3.5	d (II)	34,28	20,75	4,40	711,31	30,09	4,9	0,80	3,9		
3.6	d (II)	34,30	22,90	2,22	785,47	31,62	2,2	0,81	1,8		
3.7	d (II)	34,29	25,74	4,19	882,62	33,52	3,7	0,84	3,1		
3.8	d (II)	34,27	23,08	2,29	790,95	31,73	2,3	0,81	1,9		
3.9	d (II)	34,27	19,41	3,16	665,18	29,10	3,7	0,78	2,9		
3.10	d (II)	34,26	19,81	4,82	678,69	29,40	5,6	0,79	4,4		
3.11	d (II)	34,26	24,07	3,00	824,68	32,40	2,9	0,82	2,4	3,0	0,5
3.12	a (⊥)	22,26	34,26	11,55	762,63	31,16	11,9	0,81	9,6		
3.13	a (⊥)	34,28	23,32	12,41	799,41	31,90	12,2	0,82	10,0		
3.14	a (⊥)	34,28	20,64	11,15	707,54	30,01	12,4	0,79	9,8		
3.15	a (⊥)	34,27	20,88	12,00	715,56	30,18	13,2	0,80	10,5		
3.16	a (⊥)	34,28	failed	-	-	-	-	-	-		
3.17	a (⊥)	34,27	21,05	15,14	721,38	30,31	16,5	0,80	13,2		
3.18	a (⊥)	34,26	18,42	12,12	631,07	28,35	15,1	0,77	11,7		
3.19	a (⊥)	34,27	failed	-	-	-	-	-	-		
3.20	a (⊥)	34,25	22,08	15,60	756,24	31,03	16,2	0,81	13,1		
3.21	a (⊥)	34,29	19,75	12,30	677,23	29,36	14,3	0,79	11,2		
3.22	a (⊥)	34,27	21,22	13,16	727,21	30,43	14,2	0,80	11,4		
3.23	a (⊥)	34,26	23,32	11,07	798,94	31,89	10,9	0,82	8,9		
3.24	a (⊥)	34,27	22,42	11,65	768,33	31,28	11,9	0,81	9,6	10,6	0,8

D = distance between platens contact points, d = diametric, a = axial, ⊥ = normal, II = parallel

	Series 1	Series 2	Series 3
I_s(50)_d	9,3	8,3	10,6
I_s(50)_a	15,0	14,5	3,0
I_a(50)	1,6	1,7	3,5

Appendix F

Tilt test results.

Dry test #	Series 1*	Series 2	Series 3	Wet test #	Series 1	Series 2	Series 3
1	33,5	35,7	34,4	1	34,6	36,2	36,7
2	33	34,5	38,2	2	31,3	36,3	36,6
3	31,6	37,6	32,8	3	33,9	35,6	34,4
4	30,8	34,6	38,6	4	34,4	35,8	34,3
5	30,6	36,4	35,0	5	34,1	36,5	34,7
6	32,3	36,7	32,3	6	34,9	37,0	34,6
7	29,5	37,5	36,3	7	33,2	35,6	35,2
8	30,3	37,3	36,0	8	32,9	34,7	36,1
9	33,2	34,7	35,3	9	34,0	34,1	37,0
10	32,9	34,0	33,4	10	33,1	35,6	34,5
Avg.:	31,8	35,9	35,2		33,6	35,7	35,4
Std.dev.:	1,4	1,4	2,1		1,1	0,9	1,1
Tilt rate (deg/s)	0,43						

Appendix G

XRD analysis for series 1, 2 and 3, by Laurentius Tijhuis at the NTNU mineralogical laboratories.

180975: Prøve 1

Microcline maximum	30.55 %
Chlorite IIb	1.23 %
Quartz	42.49 %
Albite	21.11 %
Phlogopite 1M Mica	4.63 %

180976: Prøve 2

Microcline maximum	28.02 %
Chlorite IIb	0.84 %
Quartz	35.46 %
Albite	29.73 %
Phlogopite 1M Mica	5.95 %

Appendices

180977: Prøve 3

Microcline maximum	15.43 %
Chlorite IIb	1.91 %
Quartz	62.03 %
Muscovite 2M1	14.70 %
Albite	5.92 %
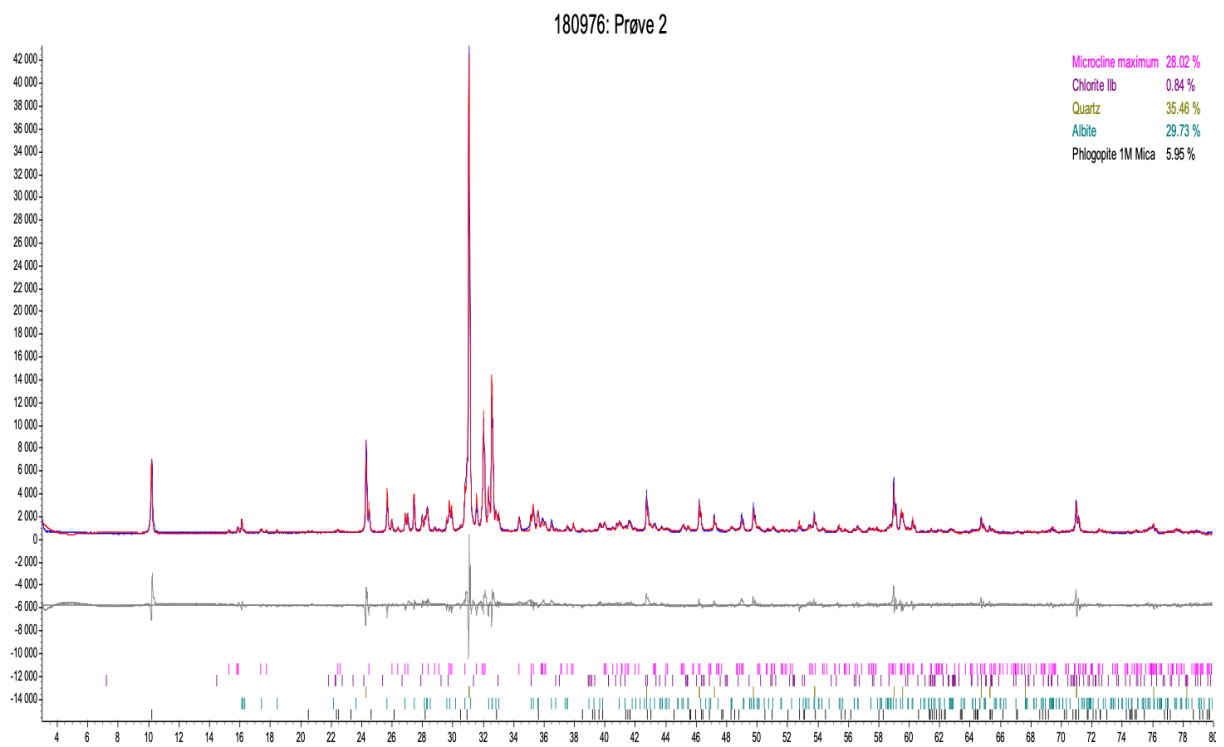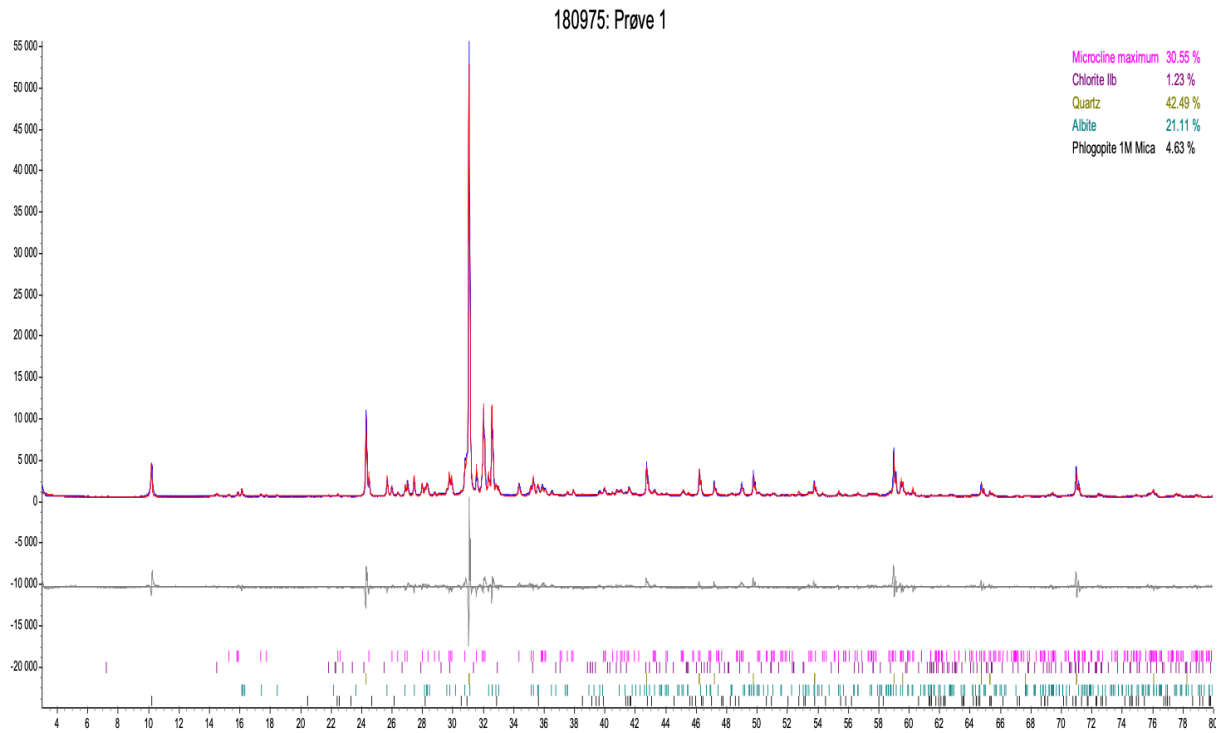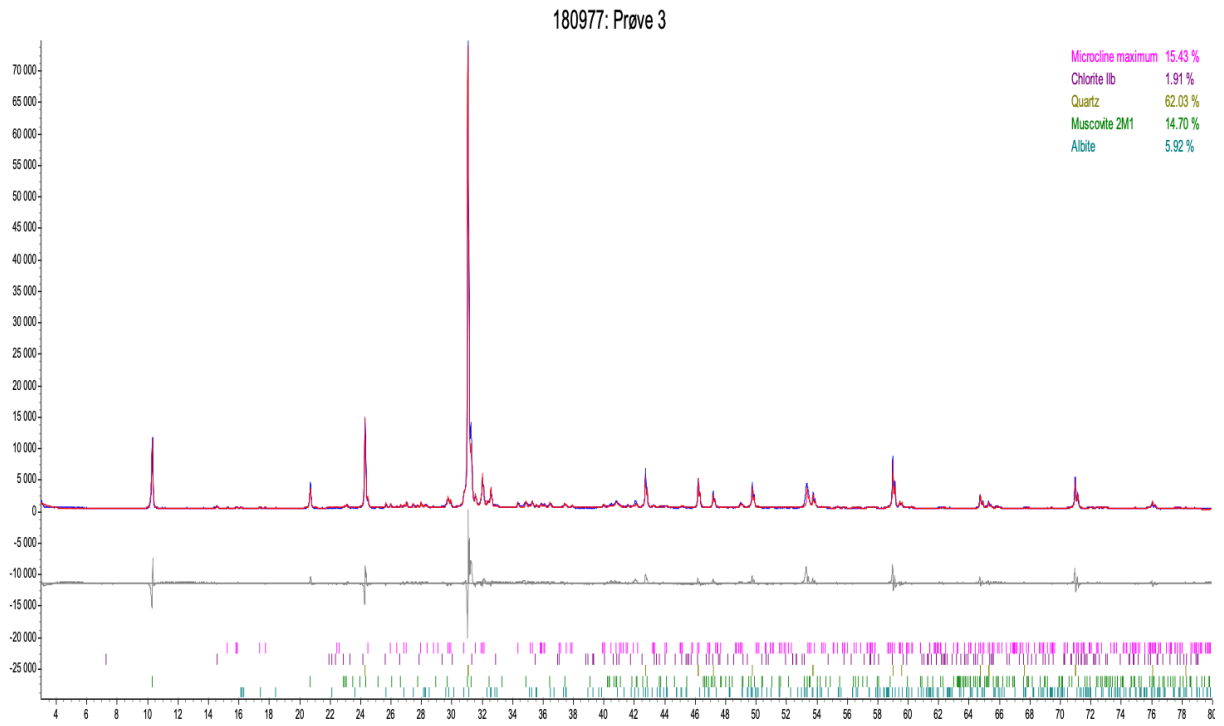
Appendix H

Material constants in the generalised Hoek-Brown failure criterion by Hoek et al. found in Li (2018).

GENERALISED HOEK-BROWN CRITERION

$$\sigma_1' = \sigma_3' + \sigma_c \left(m_b \frac{\sigma_3'}{\sigma_c} + s \right)^a$$

σ_1' = major principal effective stress at failure

σ_3' = minor principal effective stress at failure

σ_c = uniaxial compressive strength of *intact* pieces of rock

m_b, s and a are constants which depend on the composition, structure and surface conditions of the rock mass

STRUCTURE	SURFACE CONDITION	VERY GOOD — Very rough, unweathered surfaces	GOOD — Rough, slightly weathered, iron stained surfaces	FAIR — Smooth, moderately weathered or altered surfaces	POOR — Slickensided, highly weathered surfaces with compact coatings or fillings containing angular rock fragments	VERY POOR — Slickensided, highly weathered surfaces with soft clay coatings or fillings
BLOCKY -very well interlocked undisturbed rock mass consisting of cubical blocks formed by three orthogonal discontinuity sets	m_b/m_i	0.60	0.40	0.26	0.16	0.08
	s	0.190	0.062	0.015	0.003	0.0004
	a	0.5	0.5	0.5	0.5	0.5
	E_m	75,000	40,000	20,000	9,000	3,000
	v	0.2	0.2	0.25	0.25	0.25
	GSI	85	75	62	48	34
VERY BLOCKY-interlocked, partially disturbed rock mass with multifaceted angular blocks formed by four or more discontinuity sets	m_b/m_i	0.40	0.29	0.16	0.11	0.07
	s	0.062	0.021	0.003	0.001	0
	a	0.5	0.5	0.5	0.5	0.53
	E_m	40,000	24,000	9,000	5,000	2,500
	v	0.2	0.25	0.25	0.25	0.3
	GSI	75	65	48	38	25
BLOCKY/SEAMY-folded and faulted with many intersecting discontinuities forming angular blocks	m_b/m_i	0.24	0.17	0.12	0.08	0.06
	s	0.012	0.004	0.001	0	0
	a	0.5	0.5	0.5	0.5	0.55
	E_m	18,000	10,000	6,000	3,000	2,000
	v	0.25	0.25	0.25	0.3	0.3
	GSI	60	50	40	30	20
CRUSHED-poorly interlocked, heavily broken rock mass with a mixture of angular and rounded blocks	m_b/m_i	0.17	0.12	0.08	0.06	0.04
	s	0.004	0.001	0	0	0
	a	0.5	0.5	0.5	0.55	0.60
	E_m	10,000	6,000	3,000	2,000	1,000
	v	0.25	0.25	0.3	0.3	0.3
	GSI	50	40	30	20	10

Aleksander Olvik Thorbergsen

NTNU

Norwegian University of
Science and Technology